1-1-2017

Quantum Dragon Solutions for Electron Transport through Single-Layer Planar Rectangular

Godfred Inkoom

Quantum dragon solutions for electron transport through single-layer planar rectangular crystals

By

Godfred Inkoom

A Dissertation
Submitted to the Faculty of
Mississippi State University
in Partial Fulfillment of the Requirements
for the Degree of Doctor of Philosophy
in Physics
in the Department of Physics and Astronomy

Mississippi State, Mississippi

December 2017

Quantum dragon solutions for electron transport through single-layer planar rectangular crystals

By

Godfred Inkoom

Approved:

Mark A. Novotny
(Major Professor)

Vivien G. Miller
(Committee Member)

Seong-Gon Kim
(Committee Member)

R.Torsten Clay
(Committee Member)

Hendrik F. Arnoldus
(Committee Member/Graduate Coordinator)

Rick Travis
Dean
College of Arts & Sciences

Name: Godfred Inkoom

Date of Degree: December 11, 2017

Institution: Mississippi State University

Major Field: Physics

Major Professor: Dr. Mark A. Novotny

Title of Study: Quantum dragon solutions for electron transport through single-layer planar rectangular crystals

Pages of Study: 188

Candidate for Degree of Doctor of Philosophy

When a nanostructure is coupled between two leads, the electron transmission probability as a function of energy, E, is used in the Landauer formula to obtain the electrical conductance of the nanodevice. The electron transmission probability as a function of energy, $\mathcal{T}(E)$, is calculated from the appropriate solution of the time independent Schrödinger equation. Recently, a large class of nanostructures called quantum dragons have been discovered. Quantum dragons are nanodevices with correlated disorder but still can have electron transmission probability unity for all energies when connected to appropraite (idealized) leads. Hence for a single channel setup, the electrical conductivity is $\mathcal{G}_o = \frac{2e^2}{h}$ where e is the charge of an electron and h is Planck's constant. Thus quantum dragons have the minimum electrical conductance allowed by quantum mechanics. These quantum dragons have potential applications in nanoelectronics.

It is shown that for dimerized leads coupled to a simple two-slice ($l = 2$, $m = 1$) device, the matrix method gives the same expression for the electron transmission probability

as renormalization group methods and as the well known Green's function method. If a nanodevice has m atoms per slice, with l slices to calculate the electron transmission probability as a function of energy via the matrix method requires the solution of the inverse of a $(2 + ml) \times (2 + ml)$ matrix. This matrix to invert is of large dimensions for large m and l. Taking the inverse of such a matrix could be done numerically, but getting an exact solution may not be possible. By using the mapping technique, this reduces this large matrix to invert into a simple $(l + 2) \times (l + 2)$ matrix to invert, which is easier to handle but has the same solution. By using the map-and-tune approach, quantum dragon solutions are shown to exist for single-layer planar rectangular crystals with different boundary conditions. Each chapter provides two different ways on how to find quantum dragons. This work has experimental relevance, since this could pave the way for planar rectangular nanodevices with zero electrical resistance to be found. In the presence of randomness of the single-band tight-binding parameters in the nanodevice, an interesting quantum mechanical phenomenon called Fano resonance of the electron transmission probability is shown to be observed.

Key words: Quantum dragons, single-layer planar rectangular crystals, electron transmission probability, Fano resonances, Perron Frobenius theorem, nanodevices, single-band tight-binding model

DEDICATION

To the memory of my late father, Mr. Raymond Inkoom, my dearest wife, Barbara Addo and my sweet daughter, Deborah Marjorie Afua Amofa Inkoom.

ACKNOWLEDGEMENTS

I am very grateful to God Almighty for His strength and favor and all the people who have contibuted in diverse ways to make this work a success.

First and foremost I wish to thank my advisor Dr. M.A. Novotny for giving me an invaluable opportunity to work with him as a student over the past years. He has been my mentor, a friend with whom I can always confide and he has always made himself available for help and advice. There has never been an occasion when I've knocked on his door that he hasn't given me time for personal and academic discussions. On one occasion I went to his office and he was about to leave for a meeting. He said we can walk and discuss whiles he was on his way to the meeting. He gave me the opportunity to take hold of my research under his guidance and inspired me to its conclusion. I appreciate his vast knowledge, skills and demeanor with which he guided me through this project. I am gratefully indebted to him for my successful completion of my doctoral program. Thanks to Dr. Seong-Gon Kim, Dr. R. Torsten Clay, Dr. Vivien Miller, and Dr. Henk F. Arnoldus for consenting to be members of the dissertation committee and their valuable suggestions to making of this documents. Their patience and advice is appreciated. In addition, I would like to thank the Department of Physics and Astronomy at Mississippi State University for the financial support, as well as partial support from grants from the National Science Foundation. I am also thankful for all faculty and staff who helped me during my stay here especially

Dr. David Monts and Susan Galloway. I would like to thank Nathan Drake, admissions assistant, office of the graduate school for his immense role he played in getting this Ph.D degree.

To Akshay Vaghani, Victor Otu Hayford, Justice Archer, Stephen Addo, Ababa Abdulai Abdul Karim, Jehan Seneviratne and Mr Evans Asare Bediako, I say thank you for your encouragement. I am most thankful to the Buckner family (Johnny Buckner and his wonderful wife Debbie Hearn Buckner) for their constant support and prayers. I would like to thank all New Horizon family members in Starkville especially James Hamilton, Scott Morgan, Pete Hayes, the Copeland family, the Bates family and Tim Boden for their special love they have shown my family. We are forever grateful.

I owe my deepest thanks to my family members especially my sister, Mrs. Ivy Asare Bediako, and my brothers, Theophilus Incoom and Samuel Adutwum and my mother, Miss Janet Nyame for their sacrifices in life for my education and long patience during my PhD.

Lastly, I owe it all to my wonderful wife Barbara Addo who has been a constant support without which I could not have come thus far. Thanks to my lovely daughter Deborah Marjorie Afua Amofa Inkoom who is always a source of joy. It is impossible to remember all, and I apologize to those I've inadventently left out. The findings and opinions in this thesis belong solely to the author, and are not necessarily those of the sponsor.

TABLE OF CONTENTS

LIST OF FIGURES

LIST OF SYMBOLS, ABBREVIATIONS, AND NOMENCLATURE

e: Charge of an electron.

h: Planck's constant.

k_B: Boltzmann's constant.

l: Number of slices in the nanodevice.

m: Number of atoms per slice.

nn: Nearest neighbor.

nnn: Next nearest neighbor.

t_a: Intra-slice hopping strength at slice $j = a$.

t_b: Intra-slice hopping strength at slice $j = b$.

t_{eo}: Hopping interaction for the even-odd lead sites.

t_{oe}: Hopping interaction for the odd-even lead sites.

$\vec{u}$: Connection vector for the outgoing lead.

$\vec{w}$: Connection vector for the incoming lead.

$\mathbf{A}_a$: Intra-slice coupling matrix.

$\mathbf{B}$: Inter-slice coupling matrix.

E: Energy of electron.

F: Fano factor

G: Electrical conductance.

I: Current.

$\mathbf{I}$: Identity matrix.

P: Power.

R: Electrical resistance.

V: Voltage.

$\mathbf{X}$: Matrix of transformation.

$\mathbf{\Gamma_{1,2}}$: Coupling matrices in Green's function method.

ϵ: On-site energy.

$\mathbf{\Sigma_{1,2}}$: Self energy matrices in Green's function method.

χ: Parameter for Bloch wavefunctions.

$\mathcal{H}$: Hamiltonian.

Tr: Trace of matrix

$\mathcal{T}(E)$: Electron transmission probability.

$\mathcal{R}(E)$: Electron reflection probability.

$\mathcal{I}$: Integral for transmission.

CHAPTER 1

INTRODUCTION

1.1 Classical Ohm's law

In the macroscopic regime, when considering a metallic wire (conductor), the electrical conductance of a wire is simply expressed by Ohm's law. Ohm's law is the assertion that the current, I, flowing through a wire (conductor) is proportional to the electric potential difference, V, across the conductor. The constant of proportionality is called the electrical resistance, R. The electrical conductance, G, is the inverse of the electrical resistance and can be expressed as

$$G = R^{-1} = \frac{I}{V}. \tag{1.1}$$

The existence of electrical resistance in daily life has a lot of practical applications. For instance, the electrical resistance of a wire in a light bulb results in lighting, or as used in heating systems including electric stoves and electric heaters. The electrical resistance also describes device losses, including in laptop computers and mobile devices, as described by the Joule heating law $P = I^2R$ for the power dissipated P. Ohm's law is just an empirical law, built from numerous measurements. It is not a fundamental law such as Newton's law of gravity. For a uniform wire of length, l, and cross-sectional area, A, the electrical resistance, R, is given by

$$R = \frac{\rho l}{A} \tag{1.2}$$

where ρ is the resistivity. See Fig. 1.1

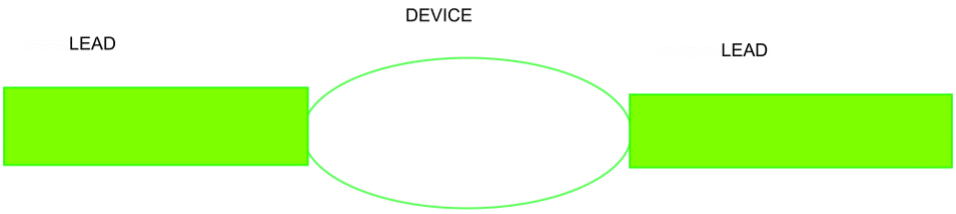

Figure 1.1

A device connected to input (incoming) and output (outgoing) leads.

1.2 Conductance from transmission

When the dimensions of a conductor becomes small enough, Ohm's law is no longer valid. Hence to study the transport properties of a nanoscale conductor, such as the electrical conductance, we apply quantum mechanics. As argued by Todorov [1], when a nanostructure is coupled between two leads (incoming and outgoing, as in Fig. 1.1), the quantum transport properties of the electron moving through the nanodevice can be measured. In his seminal work in 1957, Landauer [2] showed that the transmission probability, as a function of energy E, $\mathcal{T}(E)$, plays an important role in determining the electrical conductance, G, of a conductor. The electrical conductance G can be expressed as [2, 3]

$$G = \frac{2e^2}{h}\Big(\mathcal{I}_1 + \mathcal{I}_2 + \mathcal{I}_3 + \mathcal{I}_4 + \cdots\Big) \tag{1.3}$$

where e is the charge of an electron and h is Planck's constant. The transmisison probability, $\mathcal{T}$, is calculated from the appropriate solution of the time independent Schrödinger equation [2, 3, 4, 5].

The Fermi function, $f(E)$, is defined as

$$f(E) = \frac{1}{1 + e^{\frac{(E-\mu)}{k_B T}}} \tag{1.4}$$

where μ is the chemical potential, k_B is Boltmann's constant and T is the temperature. Consider the simplest case of the Fermi function at zero temperature, $T = 0$ K, and from Eq. (1.4) it can be observed that

$$f(E) = \begin{cases} 1 & E < \mu \\ \\ 0 & E > \mu \end{cases}. \tag{1.5}$$

Eq. (1.5) means that at zero temperature, all states with energy below μ are fully occupied. All states with energy above μ are empty. The plot for the Fermi function as a function of energy, E, is shown in Fig. 1.2.

Fig. 1.2, shows a plot of the Fermi function vs $\frac{E}{k_B}$ in units of Kelvin. The parameters used are $\frac{\mu}{k_B} = 1$. Here, different colors show different temperatures. The minimum temperature used was $T = 0.002$ K and the maximum temperature was $T = 0.02$ K with an increment of 0.002 K.

The shape of the Fermi function for different temperatures is shown in Fig. 1.2, indicating that the energy levels are mostly occupied below a certain energy and mostly unoccupied above that. A plot of the derivative of the Fermi function is shown in Fig.

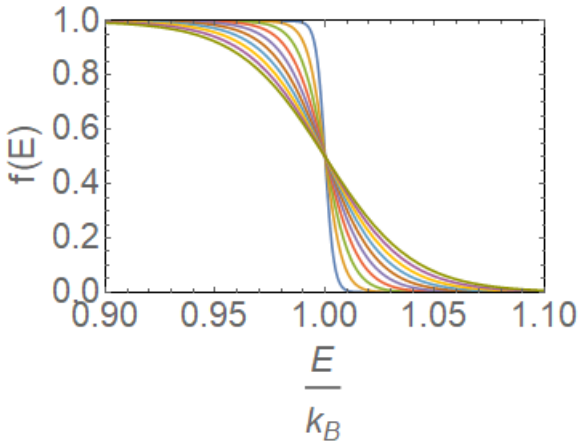

Figure 1.2

A plot of the Fermi function vs $\frac{E}{k_B}$ for some temperatures.

1.3. The derivative of the Fermi function approaches a delta function as the temperature approaches zero.

Fig. 1.3, shows a plot of the derivative of the Fermi function vs $\frac{E}{k_B}$. The parameters used are $\frac{\mu}{k_B} = 1$. Here, different colors show different temperatures. The minimum temperature used was $T = 0.002$ K and the maximum temperaure was $T = 0.02$ K with an increment of 0.002 K. Room temperature corresponds to about $\frac{k_B T}{\mu} = 0.01$.

Each integral $\mathcal{I}_k$ in Eq. (1.3) contains the derivative of the Fermi function and the transmission probability $\mathcal{T}_k$ of the kth conduction channel for an incoming electron of energy E. For each channel, the integral $\mathcal{I}$ can be expressed as

$$\mathcal{I}_k = \int \mathcal{T}_k(E)\Big(\frac{\partial f}{\partial E}\Big)dE \approx \mathcal{T}_k(E_F)\,. \tag{1.6}$$

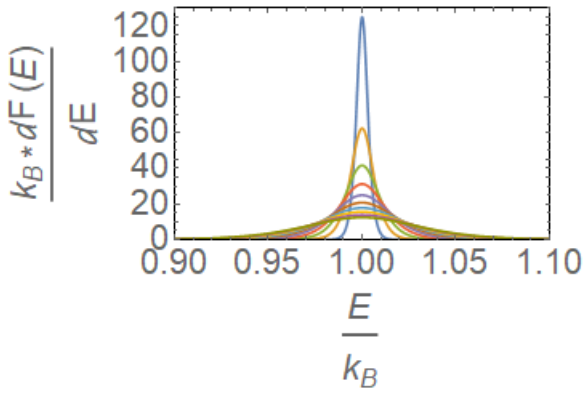

Figure 1.3

A plot of the derivative of the Fermi function vs $\frac{E}{k_B}$.

Since the partial derivative of the Fermi Dirac function, $f(E)$, is approximately a delta function at the Fermi energy, the integral in Eq. (1.6) is approximately the integral evaluated at the Fermi energy, E_F, as shown in Fig. 1.3. Eq. (1.3) simply suggests that in order to calculate the electrical conductance, G, of a nanodevice one must calculate the transmission probability as a function of energy, $\mathcal{T}(E)$, from the appropiate solution of the time independent Schrödinger equation with the attached long (semi-infinite) leads as described in detail in section 1.4 and shown in Fig. 1.1.

Consider the case, where the first mode has $\mathcal{I}_1 = 1$ and invoke a Taylor expansion in Eq. (1.3). This gives

$$G = \frac{2e^2}{h}\mathcal{I}_1\Big(1 + \frac{\mathcal{I}_2}{\mathcal{I}_1} + \frac{\mathcal{I}_3}{\mathcal{I}_1} + \frac{\mathcal{I}_4}{\mathcal{I}_1} + \cdots\Big)\,. \tag{1.7}$$

Hence the electrical conductance of the quantum device is well approximated by $G = \frac{2e^2}{h}$. The electrical conductance, $G_o = \frac{2e^2}{h} = 7.74 \times 10^{-5} S$ is called the conductance quantum.

As argued by [6], in theoretical and simulation studies, the linear conductance as a function of energy, E is plotted at zero temperature. This can seen from the Landauer expression, in Eq. (1.3). The concept of electron transmission probability, $\mathcal{T}$, for electrical conductance for one-dimenional (1D) systems such as nanowires and nanoribbons was first introduced by Landauer [2, 7]. It was later extended by Büttiker et. al [8] to multichannel and multi-lead systems, including planar conductors and nanotubes [6].

It is known that in the absence of scattering mechanisms, electrons of all energies which impinge on the nanodevice are fully transmitted, and hence $\mathcal{T}(E) = 1$. In this case, electron transport is said to be ballistic [2, 5, 9, 10, 11]. Ballistic electron transport has been observed experimentally in high purity semiconducting wires [12] as well as graphene nanoribbons and metallic single-walled carbon nanotubes [13, 14].

1.3 Anderson localization

The Anderson model [15, 16] is most often used to study wavefunction localization in disordered systems. It is based on the single-band tight-binding model. The Hamiltonian of such a system is expressed as

$$\mathcal{H} = \sum_i \epsilon_i \mid i\rangle\langle i \mid -t \sum_{<ij>} \mid i\rangle\langle j \mid \tag{1.8}$$

where $\mid i\rangle$ denotes the localized state of the lattice at site i, ϵ_i is the on-site energy at site i and $\mid i\rangle\langle j \mid$ indicates the nearest neighbor hopping interaction. The hopping strength, t, is related to the lattice spacing, a, and the mass of the electron, m, by the equation

$$t = \frac{\hbar^2}{2ma^2} \tag{1.9}$$

where $\hbar = \frac{h}{2\pi}$ and h is the Planck's constant.

Anderson [15], showed that random disorder in 1D of any system will localize the electron wavefunction, and hence $\mathcal{T}_k(E)$ is small at almost all energies. Anderson localization simply suggests that $\mathcal{T}(E)$ of any nanostructure which has disorder will have a very small G and consequently very large electrical resistance, R. This simply means that any 1D device with random disorder should act as an insulator. Fig. 1.4 through Fig. 1.6 shows the plot of $\mathcal{T}(E)$ showing Anderson localization. As it can be seen from Fig. 1.4 through Fig. 1.6, as the length of the device increases, there are distinct features in the electron transmission probability as a function of energy. The result of the random disorder of the tight-binding parameters in all three plots shows the appearance of wavefunction localization effects. In other words, the wavefunction becomes localized, meaning that the electron transmission probability decreases at long distances as a result of interference effects. It can also be seen from Fig. 1.4 through Fig. 1.6 that a small degree of disorder leads to localization of quantum states even for devices not very large. Note in particular the logarithmic scale for $\mathcal{T}(E)$ and how small it is for almost all energies.

Fig. 1.4, shows a plot of $\mathcal{T}$ vs E. Here, $m = 1$, and $l = 2, 4, 6, 8$. It should be noted that m is the number of atoms per slice and l is the number of slices. The red thick curve shows $l = 2$. The blue dotted thick curve shows $l = 4$, the green dashed show $l = 6$, and the magenta, thick dashed curve shows $l = 8$. The interslice parameters used are randomly uniformly distributed $t_{ij} = [-0.5, 0.5]$ and the on-site energy used are randomly distributed as $\epsilon_i = [-0.1, 0.1]$.

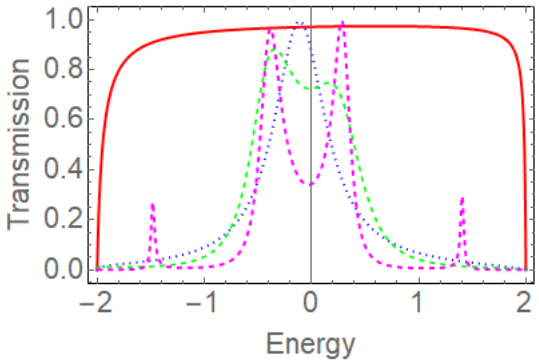

Figure 1.4

A plot of transmission vs E which shows Anderson localization.

Fig. 1.5, shows a plot of $\mathcal{T}(E)$. The same as Fig. 1.4, except on a logarithmic scale and with different choices for the random parameters.

Fig. 1.6, shows a plot transmission vs energy. The device sites are the same as in Fig. 1.4, but the random values of t_{ij} and ϵ_i are different.

Furthermore, Anderson localization has also been extended to two dimensional (2D) as well as three dimensional (3D) systems. In the case of two dimensions (2D), Lee and Fisher [17], observed that all systems in 2D with on-site disorder with uncorrelated randomness show Anderson localization. This implies that all 2D systems with on-site disorder will have a very large electrical resistance, R (very small electrical conductance, G). However, in this work it will be shown that the presence of correlated disorder will not localize the

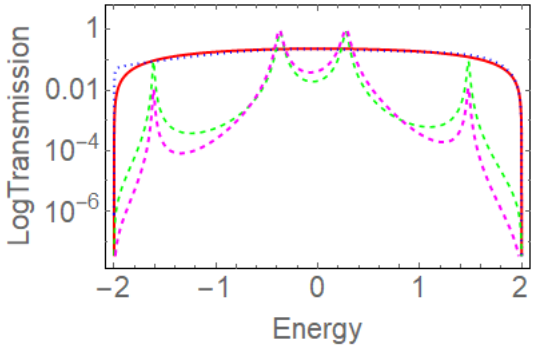

Figure 1.5

A plot of transmission vs E which shows Anderson localization, log scale.

wavefunction of certain classes of 1D and 2D nanostructures. These nanostructures, may have an even-odd structure. In fact all electrons which impinge on these nanostructures through the incoming lead have full electron transmission probability, $\mathcal{T}_k(E) = 1$, at all energies. Earlier in 2014, Novotny named these classes of nanostucture which have full transmission probability, $\mathcal{T}(E) = 1$ quantum dragons [18]. Each of the nanostructures (nanodevices) studied in this dissertation will be connected to single channel conducting 1D leads (incoming and outgoing).

1.4 $\mathcal{T}(E)$ from solution of time independent Schrödinger equation

In most cases, the tight-binding model is solved using the Green's function method [3, 4, 5, 6], however the matrix method can also be used [18, 19, 20, 21, 22, 23, 24, 25, 26].

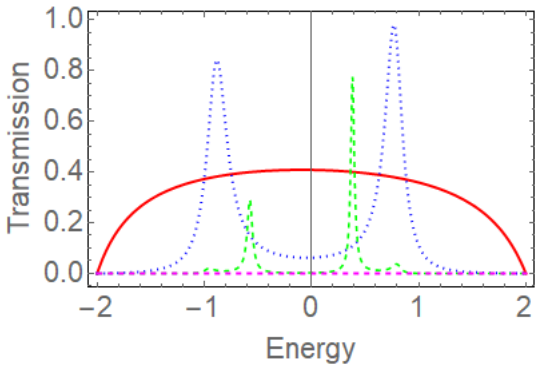

Figure 1.6

A plot of transmission vs E which shows Anderson localization.

In this study, the matrix method will be used because it allows the electron transmission probability to be calculated for a small number of atoms such as a single atom in the device as well as in situations where there are large number of atoms in the nanodevice. Also, in finding quantum dragons, the matrix method is easy to use since the algebra is easier to handle. Using the matrix method, one can easily modify the model parameters, such as the on-site energies of the atoms in the lead as well as the nanodevices, the connection hopping strengths $\vec{w}$ and $\vec{u}$ or the intra-slice and inter-slice coupling matrices in the nanodevice.

1.5 Method of finite differences

Several techniques can be used to obtain a numerical solution of the time independent Schrödinger equation. One such method is the method of finite differences. This technique

can be used to study transport properties in the quantum realm. A detailed derivation of the method of finite differences can be found on pp 141-144 of Ref [3]. To set the tone for the single-channel approach for quantum electron transport, a re-derivation of the method of finite differences for a 1D linear chain is presented here. The approach leads to a single band tight binding model.

Let the Hamiltonian, $\mathcal{H}(r)$ for an arbitrary shaped conductor in the absence of magnetic field be expressed as

$$\mathcal{H}(r) = \frac{-\hbar^2\nabla^2}{2m} + U(r) \tag{1.10}$$

where $\hbar = \frac{h}{2\pi}$ and h is Planck's constant, m is the mass of the electron and $U(r)$ is the potential. In 1D, Eq. (1.10) can be expressed as

$$\mathcal{H}(x) = \frac{-\hbar^2}{2m}\frac{d^2}{dx^2} + U(x)\ . \tag{1.11}$$

To obtain the matrix representation for the 1D chain, lets consider the quantity $\mathcal{H}(x)\psi(x)$,

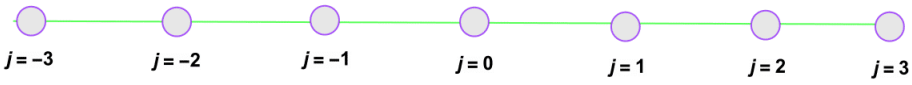

Figure 1.7

An infinite linear chain discretized into a 1D lattice.

where $\psi(x)$ is any function of x. Consider a discrete lattice whose points are located at $x = na$, where n is an integer, as in Fig. 1.7. The matrix equation can be expressed as

$$[\mathcal{H}\psi]_{x=na} = \left[\frac{-\hbar^2}{2m}\frac{d^2\psi}{dx^2}\right]_{x=na} + U_n\psi_n \tag{1.12}$$

where $\psi_n \rightarrow \psi(x = na)$ and $U_n \rightarrow U(x = na)$. The method of finite differences can be used to approximate the operator $\frac{d^2\psi}{dx^2}$ as

$$\frac{d^2\psi}{dx^2} = \frac{1}{a^2}[\psi_{n-1} - 2\psi_n + \psi_{n+1}]\,. \tag{1.13}$$

This means that Eq. (1.12) can be expressed as

$$[\mathcal{H}\psi]_{x=na} = -t_o\psi_{j-1} + (U_j + 2t_o)\psi_j - t_o\psi_{j+1} \tag{1.14}$$

where $t_o = \frac{\hbar^2}{2ma^2}$.

Thus the Hamiltonian operator for the 1D linear chain can be expressed as

$$\mathcal{H} = \begin{pmatrix} \cdots & -t_o & 0 & 0 & 0 \\ -t_o & U_{-1} + 2t_o & -t_o & 0 & 0 \\ 0 & -t_o & U_o + 2t_o & -t_o & 0 \\ 0 & 0 & -t_o & U_1 + 2t_o & -t_0 \\ 0 & 0 & 0 & -t_0 & \cdots \end{pmatrix}. \tag{1.15}$$

Assume a constant potential at every site, U_o. Eq. (1.15) simply suggests that each site is connected to its nearest neighbor by the hopping term t_o while the diagonal elements are expressed as $U_o + 2t_o$ (i.e potential energy plus $2t_o$). From Eq. (1.14), this means that for a uniform discrete wire, the time independent Schrödinger equation can be expressed as

$$E\psi_j = (U_o + 2t_o)\psi_j - t_o\psi_{j-1} - t_o\psi_{j+1}\,. \tag{1.16}$$

To solve Eq. (1.16) assume an $ansatz$ in the form of Bloch wave, $\psi_j = e^{ikja}$ of wavevector k. Substitute the $ansatz$ back into Eq. (1.16) and upon further simplification this gives

$$E = (U_o + 2t_o) - 2t_o \cos(ka) \tag{1.17}$$

and therefore

$$\cos(ka) = \frac{(U_o + 2t_o) - E}{2t_o}. \tag{1.18}$$

Since propagating waves require $-1 \leq \cos(ka) \leq 1$ one has

$$U_o \leq E \leq U_o + 4t_o \,. \tag{1.19}$$

Eq. (1.19) is the condition which is imposed on the energy of the incoming electron, E, in the 1D limit. It leads to a tight binding model, where continuous space has been replaced by discretized points. The Hamiltonian operator in Eq. (1.15) is a typical example of a tridiagonal matrix.

1.6 Tight binding model

The single-band tight-binding model has several applications. For instance it can be used to describe the electronic interactions for 1D or almost 1D systems such as single crystals with one orbital per site [27]. The single-band tight-binding model can also be used to describe the electronic interactions for 2D systems such as planar rectangular crystals with more than 1 atom per slice. For these systems, the Hamiltonian assumes a tridiagonal or block-tridiagonal form.

Assume an incident wave (an electron of energy E) impinges from $z = -\infty$ on a potential well (nanodevice) which is located at the origin ($z = 0$) and scatters off to $z =$

$\pm\infty$. For this incident electron of energy E the probability that it gets transmitted to $z = +\infty$ or gets reflected to $z = -\infty$ are respectively $\mathcal{T}(E)$ and $\mathcal{R}(E)$. The transmission and reflection probabilities, $\mathcal{T}(E)$ and $\mathcal{R}(E)$ are calculated from the appropriate solution of the time-independent Schrödinger equation [2, 3, 4, 5].

In the single-band tight-binding model, the inter-slice coupling matrix is taken to contain both the hopping terms of the nearest neighbor (nn) and next-nearest neighbor (nnn) hopping interactions t_x and t_y respectively. These hopping interaction terms are the result of the overlap of the wavefunction between two atoms. The intra-slice coupling matrix contains the on-site energy at site j, ϵ_j, for each slice as well as the intra-slice hopping term t_j. The on-site energy is a result of the discretization of the time independent Schrödinger equation as well as the electrical potential at site j, U_j. The inter-slice and intra-slice coupling matrices are Hermitian matrices since they come from the Hamiltonian of the time-independent Schrödinger equation. These are square matrices of the correct dimensions. Hopping terms between sites within the same slice are referred to as intra-slice. See Fig. 1.8. Because we connect semi-infinite leads, the matrix is of infinite dimension. Fig. 1.8, is an example of a nanodevice connected to input and output leads. There are three atoms shown in the incoming and the outgoing semi-infinite leads. The atoms in the leads are shown in light green color. The vertical lines show the division into slices for the device. There are four slices in the nanodevice, and the intra-slice hopping in the device are shown in red color. The atoms in the device are shown in a forest green color. The inter-slice hopping terms are nn (violet) and nnn (light green).

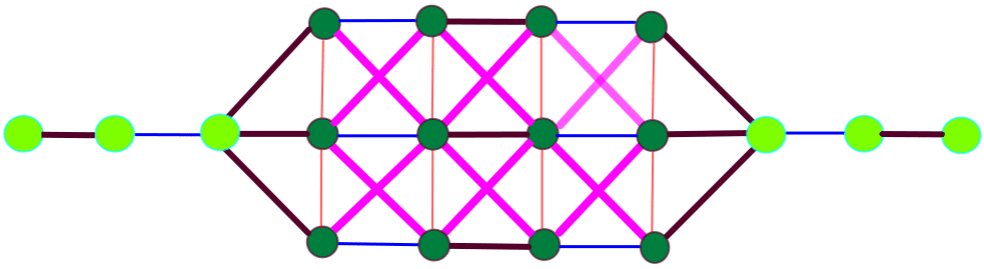

Figure 1.8

An example of a $m = 3$, $l = 4$ nanodevice coupled to input (incoming) and output (outgoing) leads.

The nanodevice is connected to a 1D infinite chain of lead sites from the left (incoming) and the right (outgoing). The lattice spacing, a, between the lead sites is set to unity for simplicity. The on-site energy of the atoms in the lead site is set to zero, $\epsilon_L = 0$, since the atoms in the incoming lead sites as well as the outgoing lead sites are assumed identical. Therefore, we have chosen our zero for the energy. The nanodevice studied in Fig. 1.8 consists of 4 slices ($l = 4$) for simplicity, though the number of slices can be increased to any even integer so that the even-odd interactions are maintained through the incoming (outgoing) lead as well as the nanodevice. Appendix A.1, shows how to go from an infinite matrix to a finite matrix.

For the nanodevice with 4 slices ($l = 4$) in Fig. 1.8, the matrix equation to solve to calculate the electron transmission probability as a function of energy, E, can be expressed as [18]

$$\begin{pmatrix} \xi(E) & -\vec{w}^{\dagger} & \vec{0}^{\dagger} & \vec{0}^{\dagger} & \vec{0}^{\dagger} & 0 \\ -\vec{w} & \mathbf{F_1} & -\mathbf{B}_{oe} & \mathbf{0} & \mathbf{0} & \vec{0} \\ \vec{0} & -\mathbf{B}_{oe}^{\dagger} & \mathbf{F_2} & -\mathbf{B}_{eo} & \mathbf{0} & \vec{0} \\ \vec{0} & \mathbf{0} & -\mathbf{B}_{eo}^{\dagger} & \mathbf{F_1} & -\mathbf{B}_{oe} & \vec{0} \\ \vec{0} & \mathbf{0} & \mathbf{0} & -\mathbf{B}_{oe}^{\dagger} & \mathbf{F_2} & -\vec{u} \\ 0 & \vec{0}^{\dagger} & \vec{0}^{\dagger} & \vec{0}^{\dagger} & -\vec{u}^{\dagger} & \xi(E) \end{pmatrix} \begin{pmatrix} \chi + r\chi^{*} \\ \vec{\psi}_a \\ \vec{\psi}_b \\ \vec{\psi}_c \\ \vec{\psi}_d \\ t_T \end{pmatrix} = \begin{pmatrix} \Lambda \\ \vec{0} \\ \vec{0} \\ \vec{0} \\ \vec{0} \\ 0 \end{pmatrix} \tag{1.20}$$

with the definitions $\xi(E) = \frac{-Et_{eo}e^{-iq}}{t_{eo}e^{-iq}+t_{oe}e^{iq}}$, $\Lambda = \frac{-t_{oe}}{\chi^{*}}(\chi e^{iq} - \chi^{*}e^{-iq})$, $\chi = \frac{-E}{t_{eo}e^{-iq}+t_{oe}e^{iq}}$ and $\mathbf{F}_i = \mathbf{A}_i - E\mathbf{I}$. The vector $\vec{w}$ connects the left (incoming) lead to the nanodevice and the vector $\vec{u}$ connects the right (outgoing) lead to the nanodevice. For l nanodevice slices, each of size m, the dimension of the matrix that needs to be inverted to calculate the quantum transmission probability is $(2 + lm) \times (2 + lm)$ Using Eq. (1.20) and solving for the transmission amplitude, t_T, the electron transmission probability, as a function of energy, E, can be calculated since $\mathcal{T} = |t_T|^2$. Furthermore, from the conservation of the number of electrons, the equation $|t_T|^2 + |r|^2 = \mathcal{T} + \mathcal{R} = 1$ must always be valid. In Eq. (1.20), the energy, E, of the incoming electron is only in the diagonal elements.

1.7 Definitions for quantum dragons

Recently, the theoretical discovery of a large class of nanostructures called quantum dragons for the case of a single conduction channel has been published [18]. Quantum

dragons are nanodevices that when connected to appropriate leads have unity transmission probability for all energies [18]. Quantum dragons have unity transmission probability as a result of the interplay between the leads and the nanodevice. Since quantum dragons have unity transmission probability, $\mathcal{T}(E) = 1$, this means that in the case of two-probe and four-probe measurements, G is quantized, $G = G_o$ and infinite, $G = \infty$ ($R = 0$) respectively. This can be seen from the Landauer formula for a single conduction channel at low temperatures for the two-probe measurement and four-probe measurement cases [5, 28]

$$G = \begin{cases} G_0 \mathcal{T}(E_F) & \text{two} - \text{probe} \\ \\ G_0 \frac{\mathcal{T}(E_F)}{1-\mathcal{T}(E_F)} & \text{four} - \text{probe} \end{cases} . \tag{1.21}$$

Furthermore, since quantum dragons have unity transmission probability, this means that quantum dragons do not exhibit shot noise power ($P = 0$). This can be seen from the zero temperature expression for shot power noise for a 2-terminal coherent device [9]

$$P = \frac{4e^3}{h} \mathcal{T}(1 - \mathcal{T})V \tag{1.22}$$

where V is the applied voltage. Typical examples of quantum dragons include single-walled carbon nanotubes (SWCNTs) in armchair or zigzag configurations, and cojoined Bethe lattices [18]. Novotny in 2015 [24], has shown theoretically how a weighted undirected graph can be turned into a quantum dragon by adjusting the vertex weights. This study concentrates on single channel quantum dragons from single-layer planar rectangular crystals, trying to answer the question what kind of single-layer planar rectangular crystals can be turned into quantum dragons. However some background on single-walled carbon nanotubes and single layer systems is desired.

1.8 Experimental and theoretical background for nanotubes and single-atom layer systems

Atomically thin 2D materials are one of the most researched classes of materials [29, 30]. This is because of their exceptional properties which makes them interesting materials suitable for electronics and optoelectronics applications [30, 31, 32, 33]. A typical example of a two dimensional crystal is graphene [34]. Graphene was first isolated in [35] and has a hexagonal honeycomb lattice.

In recent times, all kinds of nanotubes have been fabricated using different techniques. Examples include carbon nanotubes [36, 37], MoS_2 [38], SnO_2 [39], and BN nanotubes [40]. Most of these nanotubes which have been fabricated have cylindrical symmetry and therefore this suggests a circular cross-sectional area. There are other known 2D nanostructures which have different crystal structure apart from the ones with a hexagonal lattice. Typical examples include metallic single-walled silicon nanotubes and silver metallic nanotubes which have a square lattice [41, 42] and PbTe nanotubes which have a rectangular lattice [43]. The hexagonal honeycomb lattice, square lattice and rectangular lattice are three of the five known 2D Bravais lattice types.

Generally, the position vector $\mathbf{R}$ of a 2D Bravais lattice can be expressed as

$$\mathbf{R} = n_1\mathbf{a}_1 + n_2\mathbf{a}_2 \tag{1.23}$$

where n_i are any integers and $\mathbf{a}_i$ are the primitive vectors that span the lattice. Since the discovery of 2D materials, many research works have been reported. An excellent review of the properties of 2D crystals has been conducted [44]. Experimental work has also been

reported for 2D crystals [45, 46]. In [45], the method of micromechanical cleavage was successsfully used to synthesize some 2D crystals such as complex oxides.

With recent rapid progress in nanotechnology, some single-atom layer systems have been reported [43, 47, 48, 49]. For example, free-standing single-atom thick rectangular lattices of Fe have been fabricated [47] which have a rectangular lattice structure. Also, single-crystal PbTe nanotubes with rectangular cross section have been synthesized using a vertical induction furnace [43]. Theoretically, the structural and electronic properties of carbon nanotubes with square lattice structures have been reported [50].

Many interesting phenomena can occur in classical and quantum systems. One such phenomenon is Fano resonance (FR). Fano resonance occurs as a result of quantum intereference between a resonant state and a continuum of non-resonant states [51]. Fano resonance can occur in the coherent regime of an electrical resistance measurement when a finite nanostructure is coupled between two semi-infinite leads [51]. Theoretically, Fano resonances have been reported in molecular wires, and in both three-terminal and two-terminal nanodevices [52, 53]. Experimentally, the first observation of Fano resonance to be reported in mesoscopic devices is credited to Göres et. al [54]. In their experimental work in electron transport, they observed Fano resonance in the electrical conductance when parameters such as gate voltage were varied in a single-electron transistor [54]. Furthermore, other experimental works on Fano resonance have also been reported. These include metallic single-walled carbon nanotubes, electron waveguides and crossed carbon nanotubes [51, 55, 56]. Recently, Stanssi et. al in 2017, have reported experimentally Fano resonances in nanomechanical resonators [57]. The phonemenon of Fano resonances have

also been observed in classical systems including prism-coupled square micropillars, photonic crystals, waveguide cavity systems, whispering-gallery microresonators and classical coupled oscillators [58, 59, 60, 61, 62]. An excellent discussion of the classical analogy of Fano resonances has been reported [63]. For a single conducting channel, the quantum electron transport property, such as Fano factor, F, is related to the transmission probability by [64]

$$F = 1 - \mathcal{T}(E). \tag{1.24}$$

In the slices of rectangular crystals, atoms in different slices may have different hopping strengths. For these rectangular crystals, the matrices $\mathbf{A}$ are symmetric tridiagonal matrices [65]. A symmetric tridiagonal matrix of dimension $N \times N$ can be expressed in the form [65]

$$\mathbf{A} = \begin{pmatrix} a \pm \beta & b & 0 & \cdots & 0 & 0 \\ b & a & b & \cdots & 0 & 0 \\ 0 & b & a & \cdots & 0 & 0 \\ \vdots & \vdots & \vdots & \ddots & \vdots & \vdots \\ 0 & 0 & 0 & \cdots & a & b \\ 0 & 0 & 0 & \cdots & b & a \pm \gamma \end{pmatrix} = a\mathbf{I} \pm b\mathbf{Z} \tag{1.25}$$

where a and b are real numbers. In Eq. (1.25), the matrix $\mathbf{Z}$ is defined as

$$\mathbf{Z} = \begin{pmatrix} \frac{\beta}{b} & 1 & 0 & \cdots & 0 & 0 \\ 1 & 0 & 1 & \cdots & 0 & 0 \\ 0 & 1 & 0 & \cdots & 0 & 0 \\ \vdots & \vdots & \vdots & \ddots & \vdots & \vdots \\ 0 & 0 & 0 & \cdots & 0 & 1 \\ 0 & 0 & 0 & \cdots & 1 & \frac{\gamma}{b} \end{pmatrix}. \tag{1.26}$$

These types of matrices will be used in our analysis to obtain quantum dragons.

1.9 Motivation and Outline

Quantum transport in nanosystems is currently a subject of major interest both experimentally and theoretically as a result of the possible applications in electronic devices. In this light, recently, a theoretical discovery of a large class of nanostructures called quantum dragons has been reported. Quantum dragons are nanodevices which have full electron transmission probability when coupled to the appropiate leads. Quantum dragons have potential applications in nanoelectronics [18]. The quantum dragons published previously had cylindrical symmetry, but this raises the interesting question whether other forms of quantum dragons with different symmetry could also exist. If these quantum dragons exist, how can such nanodevices with unity electron transmission probability be found? If these quantum dragons exist and we are lucky to find them, could they have applications in the future? These and many more questions form the basis of the quest to look for quantum dragons in this study.

The outline for the dissertation is as follows. As a way of warm-up or appetizer on how to find quantum dragons in single-layer planar crystals, Chapter 2 discusses and shows how to find quantum dragons for a two site device ($m = 1, l = 2$). These types of quantum dragons may be trivial since there is no disorder and consequently electron transmission is ballistic. However, it is also interesting to see how such two site devices have full transmission probability. For such linear nanodevices, the transmission probability for the dimerized leads for two site devices is presented. Here, the matrix method, the matrix RG method and the Green's function method will be used to calculate the electron transmission probability. Chapters 3, 4, 5 and 6 show how to find quantum dragons with different boundary conditions and even-odd symmetry using the map-and-tune approach. Each chapter provides specific details of the technique or details of the calculations on how to find quantum dragons from single-layer planar rectangular crystals with different boundary conditions. In each chapter, two different ways are provided on how to find quantum dragons. Explicitly the boundary conditions are noted as 00 (Chap. 3), $--$ (Chap. 4), $++$ (Chap. 5) and $-+$ (Chap. 6). Chapter 7 contains discussion and conclusions.

In appendix A.1, a complete derivation of the transmission for the dimerized leads is presented. The dimerized leads have on-site energies as ϵ_o and ϵ_e for the odd and even lead sites. This is followed by the mathematics of how to find quantum dragons for a 2 site ($l = 2, m = 1$) device in appendix A.2. In appendix A.3, numerical results for quantum dragon solutions are presented for $m = 1$, $l = 2, 4, 8, 16$. In appendix B.1, the decimation renormalization group (RG) calculation is presented. Here, the quantum transmission solution for two site ($l = 2, m = 1$) devices is presented. The RG method

parallels the transmission probability expression using the matrix method and the standard Green's function method.

The electron transmission probability as a function of energy E, $\mathcal{T}(E)$, is of central importance in this study because not only does one calculate the electron transmission probability, $\mathcal{T}(E)$, of a nanodevice to find quantum dragons but also to show that indeed the nanodevice is a quantum dragon. The picture provided in this study is valid as long as it is reasonable to think in terms of the single-band tight-binding model.

CHAPTER 2

TRANSMISSION FOR DIMERIZED LEADS COUPLED TO 2 SITE DEVICES

Three solution methods for electron transport for a two site device are presented using the single-band tight-binding model. The goals of this chapter are two fold: (1) to provide the motivation necessary for the analysis of the electron transport using the single-band tight-binding model and (2) to show that a solution of the matrix method is identical to the commonly used Green's function method. In each calculational method, the electron transmission probability is calculated for two slices ($l = 2$) in the nanodevice coupled to single channel incoming and outgoing dimerized leads.

2.1 Matrix Method: Model and approach

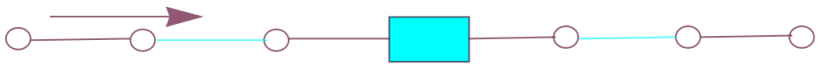

Figure 2.1

A device (blue rectangle) connected to input (incoming) and output (outgoing) leads.

Fig. 2.1, shows a device connected to input and output leads. The direction of the incident electron is shown with an arrow. Here the leads are uniform (not dimerized). Consider a nanodevice consisting of a certain number of atoms. The device is connected to a 1D infinite chain of lead sites from the left (incoming) and the right (outgoing). See Fig. 2.1 for the problem set-up. The lattice spacing a between the sites is set to unity for simplicity. To simplify the calculations lets make the following two assumptions: (1) the distance between the sites are close so that an electron can hop between nearest neighbor sites and next nearest neighbor sites and (2) the nanodevice consists of slices of sites where each slice has m sites. We further assume all lead sites have zero on-site energy. This sets our zero of energy. See Appendix A.1, for the case with dimerized values of the lead on-site energies. The leads could also have dimerized inter-slice hopping parameters even-odd, t_{eo}, and odd-even, t_{oe}. A slice may correspond to atoms in the same plane. The Hamiltonian for such a system is infinite since we have an infinite chain of sites for the leads. With the help of an $ansatz$ (physical guess) of the solution, such an infinite dimensional matrix can be reduced to a finite matrix. With this reduced finite matrix the transport properties of an electron traversing the nanodevice can easily be determined. Therefore, the time independent Schrödinger equation can be expressed as

$$(\mathcal{H} - E\mathbf{I}_\infty)\,\vec{\Psi} = \vec{0}\,, \tag{2.1}$$

where $\mathcal{H}$ is the Hamiltonian of the incoming electron, E is the energy of the incoming electron, and $\vec{\Psi}$ the infinite vector containing as the elements the wavefunction ψ_j for site j. $\mathbf{I}_\infty$ is the infinite-dimensional identity matrix. Some transport quantities include the

electrical conductance, G in Eq. (1.3), and the Fano factor, F in Eq. (1.24). In the rest of section 2.1, the uniform leads as well as the dimerized leads are presented. The uniform leads follow Daboul et. al [19] and the dimerized leads follow Novotny [18].

Daboul et. al [19] proposed to reduce this infinite uniform lead problem into a finite dimensional one that includes only the nanodevice and the closest points on the input (incoming) and output (outgoing) lead. The form of the lattice written for two sites (labeled a and b) in the nanodevice which is placed between lead sites $n = 0$ and $n = 1$ is shown in Fig. 2.2. $\mathcal{T}(E)$ through the nanostructure can be calculated from the solution of the time-independent Schrödinger equation. Here, the inter-slice hopping terms are uniform. See Fig. 2.2

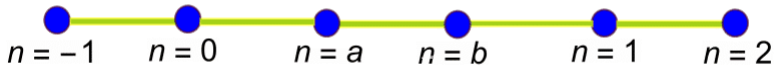

Figure 2.2

A uniform wire connected to a two site device. The device is located between site $n = 0$ and site $n = 1$.

The infinite matrix which is the time independent Schrödinger equation Eq. (2.1) then is

$$\begin{pmatrix}
\ddots & \vdots & \vdots & \vdots & \vdots & \vdots & \vdots & \vdots & \vdots & \\
\cdots & \kappa_o & -t_0 & 0 & 0 & 0 & 0 & 0 & 0 & \cdots \\
\cdots & -t_0 & \kappa_o & -t_0 & 0 & 0 & 0 & 0 & \cdots & \\
\cdots & 0 & -t_0 & \kappa_o & -t_w & 0 & 0 & 0 & 0 & \cdots \\
\cdots & 0 & 0 & -t_w & \epsilon_a - E & -t_{ab} & 0 & 0 & 0 & \cdots \\
\cdots & 0 & 0 & 0 & -t_{ab} & \epsilon_b - E & -t_u & 0 & 0 & \cdots \\
\cdots & 0 & 0 & 0 & 0 & -t_u & \kappa_o & -t_0 & 0 & \cdots \\
\cdots & 0 & 0 & 0 & 0 & 0 & -t_0 & \kappa_o & -t_0 & \cdots \\
\cdots & 0 & 0 & 0 & 0 & 0 & 0 & -t_0 & \kappa_o & \cdots \\
\vdots & \vdots & \vdots & \vdots & \vdots & \vdots & \vdots & \vdots & \vdots & \ddots
\end{pmatrix} \times \begin{pmatrix} \vdots \\ \psi_{-2} \\ \psi_{-1} \\ \psi_0 \\ \psi_a \\ \psi_b \\ \psi_{+1} \\ \psi_{+2} \\ \psi_{+3} \\ \vdots \end{pmatrix} = \begin{pmatrix} \vdots \\ 0 \\ 0 \\ 0 \\ 0 \\ 0 \\ 0 \\ 0 \\ 0 \\ \vdots \end{pmatrix} . \tag{2.2}$$

where $\kappa_o = \epsilon_o - E$. The $ansatz$ from [19] is the slice wave function of the leads can be written as

$$\psi_n = \begin{cases} e^{iqna} + re^{-iqna} & n \leq 0 \\ \\ t_T e^{iq(n-1)a} & n \geq 1 \end{cases} . \tag{2.3}$$

Substitute the $ansatz$ of Eq. (2.3) in the tight-binding equation Eq. (2.2) for the outgoing lead $(n \geq 1)$ to give

$$\begin{aligned} -t_0 t_T e^{i(n-2)qa} + (\epsilon_0 - E) t_T e^{i(n-1)qa} - t_0 t_T e^{inqa} &= 0 \\ -t_0 e^{-iqa} + (\epsilon_0 - E) - t_0 e^{iqa} &= 0 \\ \epsilon_0 - E &= 2t_0 \cos qa \, . \end{aligned} \tag{2.4}$$

Since, here the leads are uniform, this means that we can choose $t_0 = 1$. This sets our unit of energy. Assume that the on-site energy is set to zero, thus $\epsilon_0 = 0$, setting our zero of energy. This means that the energy, E, of incoming electron is related to the wavevector q by

$$\cos(q) = \frac{-E}{2}. \tag{2.5}$$

Substitute the $ansatz$ of Eq. (2.3) in the tight-binding equation Eq. (2.2) for the incoming lead $(n \leq 0)$. This gives

$$\begin{aligned} -t_0(e^{iq(n-1)a} + re^{-iq(n-1)a}) + (\epsilon_0 - E)(e^{iqna} + re^{-iqna}) - t_0(e^{iq(n+1)a} + re^{-iq(n+1)a}) &= 0 \\ e^{inqa}[-t_0 e^{-iqa} + (\epsilon_0 - E) - t_0 e^{iqa}] + re^{-inqa}[-t_0 e^{iqa} + (\epsilon_0 - E) - t_0 e^{-iqa}] &= 0 \\ e^{inqa}[-2t_0 \cos(qa) + (\epsilon_0 - E)] + re^{-inqa}[-2t_0 \cos(qa) + (\epsilon_0 - E)] &= 0 \\ [(\epsilon_0 - E) - 2t_0 \cos(qa)][e^{inqa} + re^{-iqna}] &= 0 \, . \end{aligned} \tag{2.6}$$

This equation can also be satisfied by the last equation in Eq. (2.6). Furthermore, Novotny [18] extended this approach to the case of dimerized lead sites. Here the form of the lattice is written for two sites (labeled a and b) in the nanodevice which is placed between lead sites $j = 0$ and $j = 1$ as shown in Fig. 2.3.

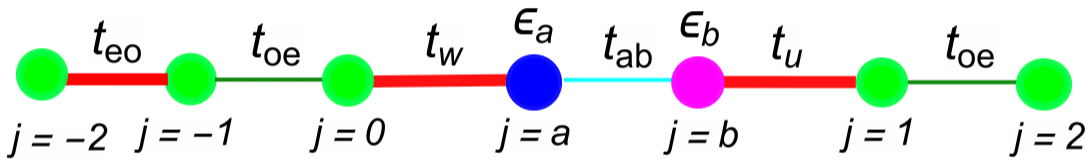

Figure 2.3

A two site device coupled to dimerized leads.

Fig. 2.3 shows an example of two site device. The device is located between site $j = 0$ and $j = 1$. The hopping strength between the device is denoted by t_{ab}. The atoms in the incoming and outgoing leads are identical and are shown by a green color.

The inter-slice hopping interaction between the lead sites, even-odd and odd-even, are designated as t_{eo} and t_{oe} respectively. For instance, interactions between lead sites $j = 2$ and $j = 3$ is denoted by $-t_{eo}$, with $t_{eo} > 0$ and interactions between lead sites $j = 3$ and

$j = 4$ is labeled t_{oe}. The hopping parameters t_{eo} and t_{oe} come from the discretization of the time independent Schrödinger equation. The negative sign is inserted so t_{eo} and t_{oe} are positive after discretizing the time independent Schrödinger equation. By multiplying the matrix and vector in Eq. (2.1) to the sites that are not connected directly to the 2-site device, this results in the set of infinite equations expressed as [18]

$$\begin{aligned}
-t_{oe}\psi_{j-1} - E\psi_j - t_{eo}\psi_{j+1} &= 0 \qquad j = \cdots, -6, -4, -2 \\
-t_{eo}\psi_{j-1} - E\psi_j - t_{oe}\psi_{j+1} &= 0 \qquad j = \cdots, -5, -3, -1 \\
-t_{oe}\psi_{j-1} - E\psi_j - t_{eo}\psi_{j+1} &= 0 \qquad j = 2, 4, 6, \cdots \\
-t_{eo}\psi_{j-1} - E\psi_j - t_{oe}\psi_{j+1} &= 0 \qquad j = 3, 5, 7, \cdots .
\end{aligned} \tag{2.7}$$

It should be noted that in Eq. (2.7), the sites numbered 0 and 1 are not included since they couple to the device sites. Introduce the $ansatz$ [18] for the propagating waves in the incoming and outgoing leads. The wavefunction have the form

$$\begin{aligned}
\psi_j &= \chi e^{iqj} + r\,\chi^* e^{-iqj} \qquad j = -\infty, \cdots, -4, -2, 0 \\
\psi_j &= e^{iqj} + r\, e^{-iqj} \qquad j = -\infty, \cdots, -5, -3, -1 \\
\psi_j &= t_T\, \chi e^{iq(j-1)} \qquad j = 2, 4, \cdots, +\infty \\
\psi_j &= t_T\, e^{iq(j-1)} \qquad j = 1, 3, 5, 7, 9 \cdots, +\infty
\end{aligned} \tag{2.8}$$

where the *ansatz* also is valid for the sites numbered 0 and 1 which connect to the device. This is a plane wave with wavevector q from $-\infty$ impinging on the device and being partially transmitted to ∞ and partially reflected to $-\infty$. In other words, the *ansatz* takes into account Bloch's theorem in the parameter χ. Substitute the $ansatz$ in Eq. (2.8) back into Eq. (2.7) to give an infinite set of equations

$$
\begin{aligned}
e^{iqj}\left(-t_{oe}e^{-iq}-E\chi-t_{eo}e^{iq}\right)+re^{-iqj}\left(-t_{oe}e^{iq}-E\chi^{*}-t_{eo}e^{-iq}\right) &= 0 \qquad j1\\
e^{iqj}\left(-t_{eo}\chi e^{-iq}-E-t_{oe}\chi e^{iq}\right)+re^{-iqj}\left(-t_{eo}\chi^{*}e^{iq}-E-t_{oe}\chi^{*}e^{-iq}\right) &= 0 \qquad j2\\
t_{T}e^{iq(j-1)}\left(-t_{oe}e^{-iq}-E\chi-t_{eo}e^{iq}\right) &= 0 \qquad j3\\
t_{T}e^{iq(j-1)}\left(-t_{eo}\chi e^{-iq}-E-t_{oe}\chi e^{iq}\right) &= 0 \qquad j4
\end{aligned}
\tag{2.9}
$$

where we have defined for convenience

$$j1=\cdots,-6,-4,-2 \tag{2.10}$$

$$j2=\cdots,-3,-1 \tag{2.11}$$

$$j3=2,4,6,\cdots \tag{2.12}$$

and

$$j4=3,5,7,\cdots. \tag{2.13}$$

The two equations for the output lead in Eq. (2.9) can be manipulated to eliminate the phase factor χ. The Bloch structure of the even-odd dimerized leads is captured by χ. The solution of χ gives

$$\chi=-\frac{t_{eo}e^{iq}+t_{oe}e^{-iq}}{E}=-\frac{E}{t_{eo}e^{-iq}+t_{oe}e^{iq}}\,. \tag{2.14}$$

This resulting equation for χ is satisfied provided

$$\cos\left(2q\right)=\frac{E^{2}-t_{eo}^{2}-t_{oe}^{2}}{2t_{eo}t_{oe}}\,, \tag{2.15}$$

or with the double-angle formula for $\cos(2q)$ gives

$$\cos(q)=\pm\sqrt{\frac{E^{2}-\left(t_{eo}-t_{oe}\right)^{2}}{4t_{eo}t_{oe}}}\,. \tag{2.16}$$

From trigonometry, since $\cos(q)^2 + \sin(q)^2 = 1$, this means that from Eq. (2.16)

$$\sin q = \pm\sqrt{\frac{4t_{eo}t_{oe} - [E^2 - (t_{eo} - t_{oe})^2]}{4t_{eo}t_{oe}}} \,. \tag{2.17}$$

Using Eq. (2.16), the energy range of propagation of moving electrons can be calculated since for traveling waves one requires

$$-1 \leq \cos q \leq 1 \,. \tag{2.18}$$

In the limiting case when $t_{eo} = t_{oe} = 1$, using Eq. (2.16) and Eq. (2.18), the energy of the incident electron in the leads is restricted to be $-2 \leq E \leq 2$ [4, 19, 23]. Also, when $t_{eo} \neq t_{oe}$, Eq. (2.16) allows propagation modes in the leads for [18]

$$-|t_{eo} + t_{oe}| \leq E \leq -|t_{eo} - t_{oe}| \qquad \text{and} \qquad |t_{eo} - t_{oe}| \leq E \leq |t_{eo} + t_{oe}| \,. \tag{2.19}$$

The two solutions are due to the two signs in front of the expression in the square root in Eq. (2.16). Fig. 2.3, shows a typical example of an infinite chain of lead sites which is connected to a two site device. Here, the leads are dimerized.

2.2 Matrix Method : Solution for $l = 2$ via (4×4) matrix method

The finite matrix equation to solve to calculate $\mathcal{T}(E)$ for the single channel dimerized lead coupled to two site device can be expressed as [18]

$$\begin{pmatrix} \xi(E) & -t_w & 0 & 0 \\ -t_w & \kappa_a & -t_{ab} & 0 \\ 0 & -t_{ab} & \kappa_b & -t_u \\ 0 & 0 & -t_u & \xi(E) \end{pmatrix} \begin{pmatrix} \psi_o \\ \psi_a \\ \psi_b \\ \psi_1 \end{pmatrix} = \begin{pmatrix} \Lambda \\ 0 \\ 0 \\ 0 \end{pmatrix} \tag{2.20}$$

with the definitions $\Lambda = \frac{-t_{oe}}{\chi^*}(\chi e^{iq} - \chi^* e^{-iq})$, $\chi = \frac{-E}{t_{eo}e^{-iq}+t_{oe}e^{iq}}$, $\xi(E) = \frac{-Et_{eo}e^{-iq}}{t_{eo}e^{-iq}+t_{oe}e^{iq}} = \chi t_{eo}e^{-iq}$, $\kappa_a = \epsilon_a - E$, $\kappa_b = \epsilon_b - E$ and t_w and t_u connects the incoming and the outgoing leads to the nanodevice. This is derived for more general dimerized leads in Appendix A.1. Using the *ansatz* [18] of Eq. (2.8) for the propagating waves in the leads, the wavefunction for the lead sites $j = 0$ and $j = 1$ can respectively be expressed as $\psi_o = \chi + r\chi^*$ and $\psi_1 = t_T$. From Eq. (2.20), the matrix to invert to calculate the electron transmission probability for the 2 site device is :

$$\mathbf{N}_2 = \begin{pmatrix} \xi & -t_w & 0 & 0 \\ -t_w & \kappa_a & -t_{ab} & 0 \\ 0 & -t_{ab} & \kappa_b & -t_u \\ 0 & 0 & -t_u & \xi \end{pmatrix} \tag{2.21}$$

which has the inverse

$$\mathbf{N}_2^{-1} = \frac{1}{(t_w^2 - \kappa_a\xi)(t_u^2 - \kappa_b\xi) - \xi^2 t_{ab}^2}\mathbf{S} \tag{2.22}$$

where

$$\mathbf{S} = \begin{pmatrix} \xi(\kappa_a\kappa_b - t_{ab}^2) - t_u^2\kappa_a & t_w(\kappa_b\xi - t_u^2) & t_{ab}t_w\xi & t_{ab}t_wt_u \\ t_w(\kappa_b\xi - t_u^2) & \kappa_b\xi^2 - t_u^2\xi & t_{ab}\xi^2 & t_{ab}t_u\xi \\ t_{ab}t_u\xi & t_{ab}\xi^2 & \kappa_a\xi^2 - t_w^2\xi & t_u(\kappa_a\xi - t_w^2) \\ t_{ab}t_wt_u & t_{ab}t_u\xi & t_u(\kappa_a\xi - t_w^2) & \xi(\kappa_a\kappa_b - t_{ab}^2) - t_w^2\kappa_a \end{pmatrix}. \tag{2.23}$$

From Eq. (2.20), Eq. (2.22) and Eq. (2.23) only the lower-left element of $\mathbf{N}_2^{-1}$ is needed to calculate the electron transmission probability. One finds the transmission amplitude, t_T can be expressed as

$$t_T = \frac{t_w t_u t_{ab} \Lambda}{(t_w^2 - \kappa_a \xi)(t_u^2 - \kappa_b \xi) - t_{ab}^2 \xi^2} \tag{2.24}$$

and

$$t_T^* = \frac{t_w t_u t_{ab} \Lambda^*}{(t_w^2 - \kappa_a \xi^*)(t_u^2 - \kappa_b \xi^*) - t_{ab}^2 \xi^{*2}}. \tag{2.25}$$

Therefore the electron transmission probability $\mathcal{T} = |t_T|^2$ gives

$$\mathcal{T}(E) = \frac{t_w^2 t_u^2 t_{ab}^2 \Lambda^* \Lambda}{[(t_w^2 - \kappa_a \xi)(t_u^2 - \kappa_b \xi) - t_{ab}^2 \xi^2][(t_w^2 - \kappa_a \xi^*)(t_u^2 - \kappa_b \xi^*) - t_{ab}^2 \xi^{*2}]}. \tag{2.26}$$

It should be noted that both t_w and t_u are real positive numbers, but the quantities ξ and Λ are complex numbers. Eq. (2.26) is one of the equations plotted in Fig. 2.6 and Fig. 2.7.

In general, the dimensions of the matrix to invert to calculate $\mathcal{T}(E)$ for a two slice ($l = 2$) device at $j = a$ and $j = b$ can be expressed as $(2m_L + m_a + m_b) \times (2m_L + m_a + m_b)$ where m_L is the number of channels in the incoming (outgoing) leads, m_a is the number of site(s) in the device at $m = a$ and m_b is the number of site(s) in the device at $m = b$. In Eq. (2.20), the dimensions of the matrix to invert to calculate $\mathcal{T}(E)$ is 4×4 since there is a single channel in the incoming and outgoing leads coupled to the two sites of the device at $j = a$ and $j = b$.

2.3 General matrix renormalization group formulation for two site device

In this section, the renormalization group (RG) approach will be used to reduce the 4×4 matrix in Eq. (2.20), to a 2×2 matrix which can easily be used to calculate $\mathcal{T}(E)$.

A 4×4 matrix has already been used to calculate $\mathcal{T}(E)$, Eq. (2.26). The type of RG used is decimation RG. It is important to note that no approximations are made, our RG is exact. The main purpose of this section is to introduce the concepts of the RG group and to show that the electron transmission probability for the 2 site device can be calculated in two ways using the matrix method. Thus either by inverting the 4×4 matrix in Eq. (2.20) or by inverting the 2×2 matrix in Eq. (2.46)

2.3.1 Theory

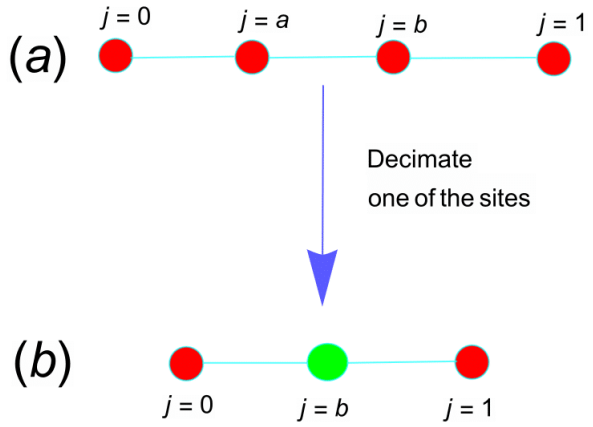

Figure 2.4

Schematic representation of the decimation procedure for the atomic site labeled a.

Fig. 2.4, shows the decimation procedure. (a) 2 atom device before decimation. The nanodevice is located between site $j = 0$ and $j = 1$. Eliminating the atom at site $j = a$ we obtain the renormalized chain in (b).

The finite matrix equation to solve to calculate $\mathcal{T}(E)$, through the nanodevice at $j = a$ and $j = b$ can be expressed as Eq. (2.20). Multiply the four rows of Eq. (2.20), this gives the four equations

$$\xi\psi_o - t_w\psi_a = \Lambda \tag{2.27}$$

$$-t_w\psi_o + \kappa_a\psi_a - t_{ab}\psi_b = 0 \tag{2.28}$$

$$-t_{ab}\psi_a + \kappa_b\psi_b - t_u\psi_1 = 0 \tag{2.29}$$

$$-t_u\psi_b + \xi\psi_1 = 0. \tag{2.30}$$

From Eq. (2.28), solving for ψ_a gives

$$\psi_a = \kappa_a^{-1}t_{ab}\psi_b + \kappa_a^{-1}t_w\psi_o. \tag{2.31}$$

Substitute Eq. (2.31) back into Eq. (2.27) and upon grouping the like terms gives

$$(\xi - t_w^2\kappa_a^{-1})\psi_o - t_w\kappa_a^{-1}t_{ab}\psi_b = \Lambda. \tag{2.32}$$

Similarly, put Eq. (2.31) back into Eq. (2.29) and upon grouping like terms yields

$$-t_{ab}\kappa_a^{-1}t_w\psi_o + (\kappa_b - \kappa_a^{-1}t_{ab}^2)\psi_b - t_u\psi_1 = 0. \tag{2.33}$$

Now rewriting Eq. (2.32), Eq. (2.33) and Eq. (2.30) into matrix form gives

$$\begin{pmatrix} (\xi - t_w^2\kappa_a^{-1}) & -t_w\kappa_a^{-1}t_{ab} & 0 \\ -t_{ab}\kappa_a^{-1}t_w & (\kappa_b - \kappa_a^{-1}t_{ab}^2) & -t_u \\ 0 & -t_u & \xi \end{pmatrix} \begin{pmatrix} \psi_o \\ \psi_b \\ \psi_1 \end{pmatrix} = \begin{pmatrix} \Lambda \\ 0 \\ 0 \end{pmatrix}. \tag{2.34}$$

Therefore we have reduced our 4×4 matrix equation to a 3×3 matrix equation. See Fig. 2.4. Now for simplicity, from the L.H.S of Eq. (2.34), let $G = \xi - t_w^2 \kappa_a^{-1}$, $B = t_w \kappa_a^{-1} t_{ab}$, $Q = t_{ab} \kappa_a^{-1} t_w$ and $P = \kappa_b - \kappa_a^{-1} t_{ab}^2$. This means that Eq. (2.34) can be expressed as

$$\begin{pmatrix} G & -B & 0 \\ -Q & P & -t_u \\ 0 & -t_u & \xi \end{pmatrix} \begin{pmatrix} \psi_o \\ \psi_b \\ \psi_1 \end{pmatrix} = \begin{pmatrix} \Lambda \\ 0 \\ 0 \end{pmatrix} . \tag{2.35}$$

Multiply the three rows of Eq. (2.35) to give the three equations

$$G\psi_o - B\psi_b = \Lambda \tag{2.36}$$

$$-Q\psi_o + P\psi_b - t_u\psi_1 = 0 \tag{2.37}$$

and

$$-t_u\psi_b + \xi\psi_1 = 0. \tag{2.38}$$

Solving for ψ_b from Eq. (2.37) gives

$$\psi_b = P^{-1}t_u\psi_1 + P^{-1}Q\psi_0. \tag{2.39}$$

Substitute Eq. (2.39) back into Eq. (2.36) and upon grouping like terms yields

$$(G - BP^{-1}Q)\psi_o - BP^{-1}t_u\psi_1 = \Lambda. \tag{2.40}$$

Similarly, substitute Eq. (2.39) into Eq. (2.38) and upon grouping like terms results in

$$-t_uP^{-1}Q\psi_o + (\xi - t_u^2P^{-1})\psi_1 = 0\,. \tag{2.41}$$

Rewrite Eq. (2.40) and Eq. (2.41) into matrix form to give

$$\begin{pmatrix} G - BP^{-1}Q & -BP^{-1}t_u \\ -t_uP^{-1}Q & \xi - t_u^2P^{-1} \end{pmatrix} \begin{pmatrix} \psi_o \\ \psi_1 \end{pmatrix} = \begin{pmatrix} \Lambda \\ 0 \end{pmatrix} . \tag{2.42}$$

For simplicity, from the LHS of Eq. (2.42) let $\alpha = G - BP^{-1}Q$ which means that Eq. (2.42) can be re-expressed as

$$\begin{pmatrix} \alpha & -BP^{-1}t_u \\ -t_u P^{-1}Q & \xi - t_u^2 P^{-1} \end{pmatrix} \begin{pmatrix} \psi_o \\ \psi_1 \end{pmatrix} = \begin{pmatrix} \Lambda \\ 0 \end{pmatrix} . \tag{2.43}$$

Now substitute the expressions for G, B, Q and P in the above back into α and upon simplification results in a simple expression for α which can be expressed as

$$\alpha = \xi - \frac{t_w^2}{\kappa_a} - \frac{t_w^2 t_{ab}^2}{\kappa_a(\kappa_a\kappa_b - t_{ab}^2)} . \tag{2.44}$$

Put α and the rest of the definitions of G, B, Q and P back into Eq. (2.43). This gives

$$\begin{pmatrix} \xi - \frac{t_w^2}{\kappa_a} - \frac{t_w^2 t_{ab}^2}{\kappa_a(\kappa_a\kappa_b - t_{ab}^2)} & \frac{-t_w t_u t_{ab}}{(\kappa_a\kappa_b - t_{ab}^2)} \\ \frac{-t_w t_u t_{ab}}{(\kappa_a\kappa_b - t_{ab}^2)} & \xi - \frac{t_u^2\kappa_a}{(\kappa_a\kappa_b - t_{ab}^2)} \end{pmatrix} \begin{pmatrix} \psi_o \\ \psi_1 \end{pmatrix} = \begin{pmatrix} \Lambda \\ 0 \end{pmatrix} . \tag{2.45}$$

See Fig. 2.5. From the *ansatz* of the propagating waves in the leads, the wavefunctions [18] , $\psi_o = \chi + r\chi^*$ and $\psi_1 = t_T$. Therefore, Eq. (2.45) can be rewritten as

$$\begin{pmatrix} \xi - \frac{t_w^2}{\kappa_a} - \frac{t_w^2 t_{ab}^2}{\kappa_a(\kappa_a\kappa_b - t_{ab}^2)} & \frac{-t_w t_u t_{ab}}{(\kappa_a\kappa_b - t_{ab}^2)} \\ \frac{-t_w t_u t_{ab}}{(\kappa_a\kappa_b - t_{ab}^2)} & \xi - \frac{t_u^2\kappa_a}{(\kappa_a\kappa_b - t_{ab}^2)} \end{pmatrix} \begin{pmatrix} \chi + r\chi^* \\ t_T \end{pmatrix} = \begin{pmatrix} \Lambda \\ 0 \end{pmatrix} . \tag{2.46}$$

Using Eq. (2.46), solving for t_T gives

$$t_T = \frac{t_w t_u t_{ab}\Lambda}{(t_w^2 - \xi\kappa_a)(t_u^2 - \xi\kappa_b) - \xi^2 t_{ab}^2}. \tag{2.47}$$

Similarly, from Eq. (2.47),

$$t_T^* = \frac{t_w t_u t_{ab}\Lambda^*}{(t_w^2 - \kappa_a\xi^*)(t_u^2 - \kappa_b\xi^*) - t_{ab}^2\xi^{*2}} \tag{2.48}$$

and therefore the transmission probability, $\mathcal{T} = |t_T|^2$ can be expressed as

$$\mathcal{T}(E) = \frac{t_w^2 t_u^2 t_{ab}^2 \Lambda^*\Lambda}{[(t_w^2 - \kappa_a\xi)(t_u^2 - \kappa_b\xi) - t_{ab}^2\xi^2][(t_w^2 - \kappa_a\xi^*)(t_u^2 - \kappa_b\xi^*) - t_{ab}^2\xi^{*2}]}. \tag{2.49}$$

Thus Eq. (2.49) is the same as Eq. (2.26). This simply shows the electron transmission probability can either be found by inverting the 4×4 matrix on the L.H.S of Eq. (2.20) or by inverting 2×2 matrix on the L.H.S of Eq. (2.46). Appendix B.1.1 performs the same decimation RG using a different method. Although the RG method is different, the expression Eq. (2.49) for the transmission is the same.

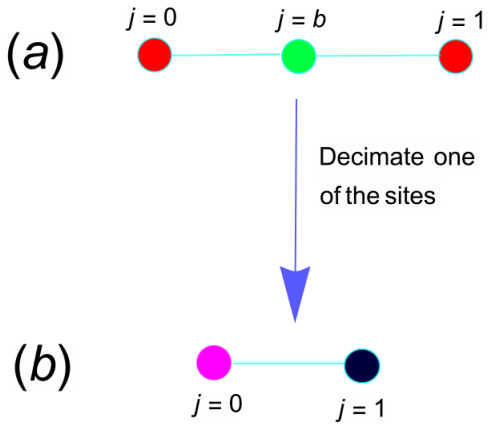

Figure 2.5

Schematic representation of the decimation procedure for the atomic site b.

Fig 2.5 shows decimation procedure. Here, one of the three sites is decimated and this gives two sites both of which are lead sites.

2.4 Quantum transmission solution for a two site device connected to dimerized leads: Green's function method

The Green's function technique is a standard method used to calculate $\mathcal{T}(E)$ through nanostructures [3, 4, 5, 6]. In this section, the Green's function method will be used to calculate the electron transmission probability for a 2 site device connected to 1D dimerized leads (incoming and outgoing). The goal of this section is to show that for the two site device using the Green's function method gives same result as using the matrix method and the matrix RG method for $\mathcal{T}(E)$. See Fig. 2.3 for the problem setup.

Let the Hamiltonian for the two site ($l = 2, m = 1$) be written as

$$\mathcal{H} = \begin{pmatrix} \epsilon_a & -t_{ab} \\ -t_{ab} & \epsilon_b \end{pmatrix} \tag{2.50}$$

where ϵ_a and ϵ_b are the on-site energies for the two atoms and t_{ab} is the hopping strength between the two atoms in the device. The self energy matrices can be expressed as [3, 4, 5, 6]

$$\mathbf{\Sigma_1} = t_w g_L t_w^\dagger = \begin{pmatrix} \frac{-t_w^2}{\xi} & 0 \\ 0 & 0 \end{pmatrix} \tag{2.51}$$

and

$$\mathbf{\Sigma_2} = t_u g_R t_u^\dagger = \begin{pmatrix} 0 & 0 \\ 0 & \frac{-t_u^2}{\xi} \end{pmatrix}. \tag{2.52}$$

Here, g_L and g_R are the Green's function of the left and right leads respectively and t_w and t_u are the incoming and the outgoing hopping strengths which are connected to the device. It should be noted that the quantity ξ is complex but t_w and t_u are real numbers

and are both positive, $t_w > 0$, $t_u > 0$. The complex quantity ξ is different for uniform and dimerized leads, namely

$$\xi(E) = \begin{cases} e^{-iq} & \text{uniform} \\ \\ \frac{-Et_{eo}e^{-iq}}{t_{eo}e^{-iq}+t_{oe}e^{iq}} & \text{dimerized} \end{cases} . \tag{2.53}$$

From Eq. (2.51) and Eq. (2.52) the coupling matrices can be expressed as

$$\mathbf{\Gamma_1} = i[\mathbf{\Sigma_1} - \mathbf{\Sigma_1}^\dagger] = it_w^2 \begin{pmatrix} \frac{1}{\xi^*} - \frac{1}{\xi} & 0 \\ \\ 0 & 0 \end{pmatrix} \tag{2.54}$$

and

$$\mathbf{\Gamma_2} = i[\mathbf{\Sigma_2} - \mathbf{\Sigma_2}^\dagger] = it_u^2 \begin{pmatrix} 0 & 0 \\ \\ 0 & \frac{1}{\xi^*} - \frac{1}{\xi} \end{pmatrix} . \tag{2.55}$$

The coupling matrices may be seen as matrices which connect the incoming and outgoing leads to the device. In quantum electron transport calculations, the Green's function, $\mathcal{G}$, can be expressed in terms of the energy of the incident electron, E, the Hamiltonian for the device, $\mathcal{H}$, and the self-energy matrices $\mathbf{\Sigma_1}$ and $\mathbf{\Sigma_2}$. The Green's function is [3, 4, 5, 6]

$$\mathcal{G} = [E\mathbf{I} - \mathcal{H} - \mathbf{\Sigma_1} - \mathbf{\Sigma_2}]^{-1} = \begin{pmatrix} \frac{t_w^2}{\xi} - \kappa_a & t_{ab} \\ \\ t_{ab} & \frac{t_u^2}{\xi} - \kappa_b \end{pmatrix}^{-1} . \tag{2.56}$$

From Eq. (2.56), the Green's function $\mathcal{G}^\dagger$ can be expressed as

$$\mathcal{G}^\dagger = [E\mathbf{I} - \mathcal{H} - \mathbf{\Sigma_1}^\dagger - \mathbf{\Sigma_2}^\dagger]^{-1} = \begin{pmatrix} \frac{t_w^2}{\xi^*} - \kappa_a & t_{ab} \\ \\ t_{ab} & \frac{t_u^2}{\xi^*} - \kappa_b \end{pmatrix}^{-1} . \tag{2.57}$$

$\mathcal{T}(E)$ can be defined in terms of the Green's function ($\mathcal{G}$) and the coupling matrices $\mathbf{\Gamma_1}$ and $\mathbf{\Gamma_2}$ as

$$\mathcal{T}(E) = \mathrm{Tr}[\mathbf{\Gamma_1}\mathcal{G}\mathbf{\Gamma_2}\mathcal{G}^\dagger] \tag{2.58}$$

where Tr is the trace of the matrix. Now put Eq. (2.54), Eq. (2.55), Eq. (2.56) and Eq. (2.57) back into Eq. (2.58). This yields the electron transmission probability as

$$\mathcal{T}(E) = \frac{t_w^2 t_u^2 t_{ab}^2 \Lambda^* \Lambda}{[(t_w^2 - \kappa_a\xi)(t_u^2 - \kappa_b\xi) - t_{ab}^2\xi^2][(t_w^2 - \kappa_a\xi^*)(t_u^2 - \kappa_b\xi^*) - t_{ab}^2\xi^{*2}]}. \tag{2.59}$$

It should be noted that Λ is a complex quantity and is different for uniform and dimerized leads, namely

$$\Lambda(E) = \begin{cases} -2i\sin q & \text{uniform} \\ \\ \frac{-t_{oe}}{\chi^*}(\chi e^{iq} - \chi^* e^{-iq}) & \text{dimerized} \end{cases}. \tag{2.60}$$

Eq. (2.59) is one of the equations plotted in Fig. 2.6 and Fig. 2.7. Fig. 2.6 shows a plot of transmission vs E for a 2 site dimerized device. If $t_w = t_u = t_{eo} = 2$, $t_{oe} = t_{ab} = 1$ and $\epsilon_a = \epsilon_b = \epsilon_l = 0$, the $(l = 2, m = 1)$ device is a quantum dragon with $\mathcal{T}(E) = 1$ for all three calculation methods used.

Fig. 2.7, shows curves plotted for all three calculational procedure. All results for the three different methods of solution lie on top of each other. The values plotted have $t_w = t_u = t_{eo} = 2$, $t_{oe} = t_{ab} = 1$ and $\epsilon_a = \epsilon_b = 0.5$ for the $(l = 2, m = 1)$ device.

2.5 Summary

In this chapter, a compact and explicit expression for $\mathcal{T}(E)$, of spinless electrons through a 2 site nanodevice is provided using the matrix method, the matrix renormal-

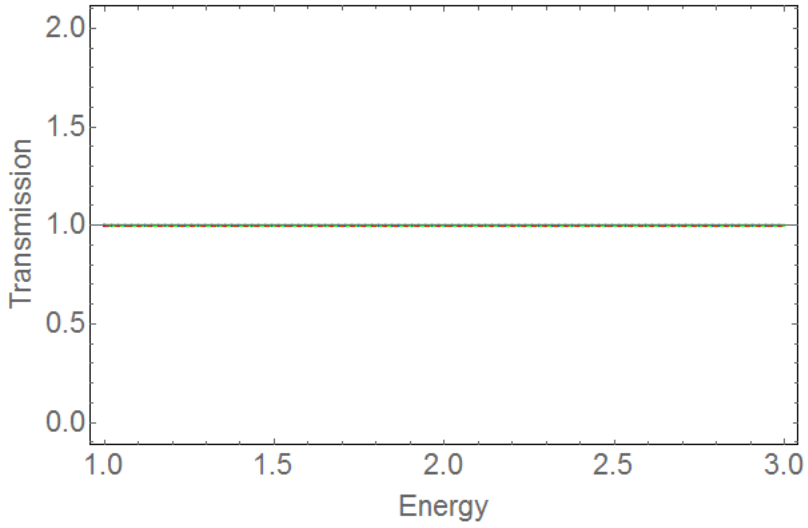

Figure 2.6

$\mathcal{T}$ is plotted as a function of E for the 2 site dimerized device.

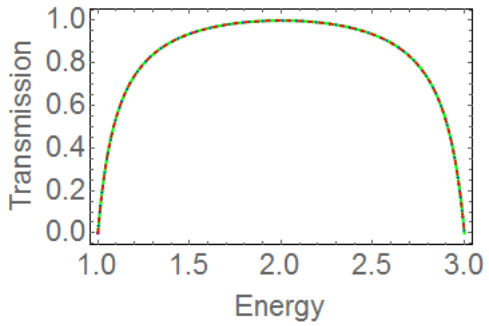

Figure 2.7

The curves plotted correspond to the final results of section 2.2 (matrix method), section 2.3 (matrix RG method) and section 2.4 (Green's function method).

ization group method, and the Green's function method. It is apparent from Eq. (2.26), Eq. (2.49) and Eq. (2.59) that for a two site ($l = 2$, $m = 1$) nanodevice, the matrix method yields the same expression as the matrix RG method and the traditional Green's function method. Also, it can be seen that there are certain tight binding parameters where $\mathcal{T}(E)$ gives full transmission, $\mathcal{T}(E) = 1$. This can be seen in Fig. 2.6. The equivalence of the three methods makes sense because these three techniques all solve the time independent Schrödinger equation for the semi-infinite leads attached to the nanodevice. In the rest of the chapters that follow, the technique of how to find quantum dragons for single-layer planar systems is presented.

CHAPTER 3

QUANTUM DRAGON SOLUTIONS FOR RECTANGULAR CRYSTALS : CASE 1: BOUNDARY CONDITION 00

There are an infinite number of possible connections between leads and the device. The busbar (all strengths equal) and the point-to-point (for a chosen point on the device) are only two. These two are the ones used in the study of percolation [66]. Experimentally, one type of connection is about as easy to make as another, but this also depends on the experimental system. There is another type of connection between leads and the device called the modified busbar connection. The busbar and modified busbar connection will be used in this study to find quantum dragons.

It is shown in this section of the dissertation how to find quantum dragons for single-layer planar rectangular crystals using boundary conditions which we label as 00. We call the boundary conditions 00 because in Eq. (1.25), we set ($\beta = \gamma = 0$). The connections used in this chapter are the modified busbar. There are two ways to find quantum dragons: (1) we assume the inter-slice coupling matrices for the nanodevice has nearest neighbor (nn) and next nearest neighbor (nnn) interactions and (2) we assume the inter-slice coupling matrices is proportional to the identity matrix. In other words, the device has only nn interactions. In the absence of nnn interactions this gives results in [24].

From Eq. (1.25), by setting ($\beta = \gamma = 0$), the matrix of dimension $m \times m$ is a Toeplitz matrix which has the form

$$\mathbf{A} = \begin{pmatrix} a & b & 0 & \cdots & 0 & 0 \\ b & a & b & \cdots & 0 & 0 \\ 0 & b & a & \cdots & 0 & 0 \\ \vdots & \vdots & \vdots & \ddots & \vdots & \vdots \\ 0 & 0 & 0 & \cdots & a & b \\ 0 & 0 & 0 & \cdots & b & a \end{pmatrix} = a\mathbf{I} + b\mathbf{Q} \tag{3.1}$$

where a and b are real numbers. The Toeplitz matrix, which is sometimes also called a diagonal-constant matrix, was named after the German mathematician Otto Toeplitz. In Eq. (3.1), $\mathbf{I}$ is an identity matrix of the correct dimension and the matrix $\mathbf{Q}$ is defined as

$$\mathbf{Q} = \begin{pmatrix} 0 & 1 & 0 & \cdots & 0 & 0 \\ 1 & 0 & 1 & \cdots & 0 & 0 \\ 0 & 1 & 0 & \cdots & 0 & 0 \\ \vdots & \vdots & \vdots & \ddots & \vdots & \vdots \\ 0 & 0 & 0 & \cdots & 0 & 1 \\ 0 & 0 & 0 & \cdots & 1 & 0 \end{pmatrix} . \tag{3.2}$$

Our nanodevice has an intra-slice coupling matrix of the form (written for $m = 8$)

$$\mathbf{A} = \begin{pmatrix} \epsilon & -t & 0 & 0 & 0 & 0 & 0 & 0 \\ -t & \epsilon & -t & 0 & 0 & 0 & 0 & 0 \\ 0 & -t & \epsilon & -t & 0 & 0 & 0 & 0 \\ 0 & 0 & -t & \epsilon & -t & 0 & 0 & 0 \\ 0 & 0 & 0 & -t & \epsilon & -t & 0 & 0 \\ 0 & 0 & 0 & 0 & -t & \epsilon & -t & 0 \\ 0 & 0 & 0 & 0 & 0 & -t & \epsilon & -t \\ 0 & 0 & 0 & 0 & 0 & 0 & -t & \epsilon \end{pmatrix} = \epsilon\mathbf{I} - t\mathbf{Q} \tag{3.3}$$

and an inter-slice coupling matrix of the form (written for $m = 8$)

$$\mathbf{B} = \begin{pmatrix} -t_x & -t_y & 0 & 0 & 0 & 0 & 0 & 0 \\ -t_y & -t_x & -t_y & 0 & 0 & 0 & 0 & 0 \\ 0 & -t_y & -t_x & -t_y & 0 & 0 & 0 & 0 \\ 0 & 0 & -t_y & -t_x & -t_y & 0 & 0 & 0 \\ 0 & 0 & 0 & -t_y & -t_x & -t_y & 0 & 0 \\ 0 & 0 & 0 & 0 & -t_y & -t_x & -t_y & 0 \\ 0 & 0 & 0 & 0 & 0 & -t_y & -t_x & -t_y \\ 0 & 0 & 0 & 0 & 0 & 0 & -t_y & -t_x \end{pmatrix} = -t_x\mathbf{I} - t_y\mathbf{Q} \tag{3.4}$$

where t's are the hopping strengths which are non-negative real numbers and ϵ is the on-site energy of the atom which is a real number. The Toeplitz matrix in Eq. (3.1) has eigenvalues expressed as [67, 68]

$$\lambda_s = a + 2b\cos\left(\frac{\pi s}{m+1}\right) \tag{3.5}$$

for $s = 1, ...m$ and eigenvectors expressed as

$$x_j^{(s)} = \sqrt{\frac{2}{m+1}} \sin\left(\frac{\pi s j}{m+1}\right) \tag{3.6}$$

where $j = 1....., m$ and $s = 1, ...m$. In Eq. (3.3) and Eq. (3.4), the matrix $\mathbf{Q}$ is shown in Eq. (3.2). To find quantum dragons for nanostructures, the transformation matrix, $\mathbf{X}$ for a successful mapping needs to be found first. Without this mapping, it would be very difficult to find quantum dragons. The outline for this chapter is as follows. In section 3.1 and section 3.2, we will show how to find quantum dragons for $m = 3$, $l = 4$ and $m = 5$, $l = 4$ respectively. The main objective of these sections are to show how to find quantum dragons for a small number of atoms per slice and a small number of slices in the device. However, this same analysis can be applied to any number of atoms per slice and any number of even slices, l, in the device. In section 3.3, we will introduce the general mapping method and this will be followed by section 3.3.1 which shows the general case mapping. In section 3.3, we will introduce the matrix to invert to calculate the electron transmission probability, for three atoms per slice with two slices in the device. However, for a large l and m such a matrix to invert could be large, and therefore we will use the general mapping technique to reduce the dimensionality of the matrix. This section will then be followed by the general method for 2D system mapping. In section 3.3.3, the mapping technique is applied to 2D systems, where a six site device will be used as an example. In section 3.4, we will show the general tuning to obtain a quantum dragon. This section will be followed by specific tuning of how to obtain quantum dragons as applied to the six site device. Section 3.5, puts all the results into perspective. Here all plots obtained

will be shown and discussed. The summary of results for our boundary condition 00 are given in section 3.6.

3.1 Quantum dragons for $m = 3$, $l = 4$ with nn and nnn interactions

Assume the nanodevice has three atoms per slice at slice $j = \nu$. See Fig. 3.1.

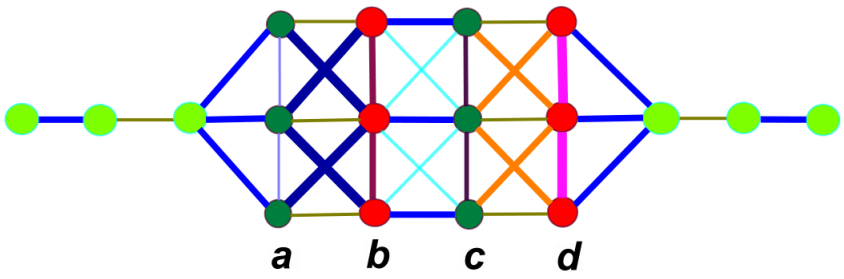

Figure 3.1

An example of the case of dimerized leads, and a rectangular nanodevice, for 00 boundary conditions.

In Fig. 3.1, the vertical lines show the intra-slice hopping. The device has $m = 3$, $l = 4$ and therefore $ml = 12$ atoms. The device has non-uniform intra-slice hopping parameters. Only three atoms in the incoming lead as well as the outgoing lead are shown. The lead atoms are shown by a green color. The connections between leads and the device are shown by line segments (blue). The inter-slice coupling matrices are for nn shown by the horizontal line (blue and brown color) and the nnn (coolblack, cyan and pink color)

shown by line segments which form an X-shape. Appropriate choices of the tight-binding parameters makes this disordered nanodevice into a quantum dragon.

The intra-slice coupling matrices have the form

$$\mathbf{A}_\nu = \begin{pmatrix} \epsilon_\nu & -t_\nu & 0 \\ -t_\nu & \epsilon_\nu & -t_\nu \\ 0 & -t_\nu & \epsilon_\nu \end{pmatrix} = \epsilon_\nu \mathbf{I} - t_\nu \mathbf{Q} \tag{3.7}$$

where $\nu = a, b, c, d$ for the $l = 4$ slices and ϵ_ν are the on-site energies for the atoms in the slice $j = \nu$ and t_ν are the intra-slice hopping parameters between atoms. Using Eq. (3.5), the eigenvalues of Eq. (3.7) are $\lambda_{\nu,1} = \epsilon_\nu - t_\nu\sqrt{2}$, $\lambda_{\nu,2} = \epsilon_\nu$, and $\lambda_{\nu,3} = \epsilon_\nu + t_\nu\sqrt{2}$. Now assume the device inter-slice coupling matrices have the form

$$\mathbf{B}_{\omega,\omega+1} = \begin{pmatrix} -t_{x,\omega} & -t_{y,\omega} & 0 \\ -t_{y,\omega} & -t_{x,\omega} & -t_{y,\omega} \\ 0 & -t_{y,\omega} & -t_{x,\omega} \end{pmatrix} = -t_{x,\omega}\mathbf{I} - t_{y,\omega}\mathbf{Q} \tag{3.8}$$

where we will let $\mathbf{B}_{\omega,\omega+1}$ with ω even be $\mathbf{B}_{eo}$ and with ω odd be $\mathbf{B}_{oe}$. In Eq. (3.7) and Eq. (3.8), the matrix $\mathbf{Q}$ is explicitly for $m = 3$

$$\mathbf{Q} = \begin{pmatrix} 0 & 1 & 0 \\ 1 & 0 & 1 \\ 0 & 1 & 0 \end{pmatrix} . \tag{3.9}$$

In this example, only a single incoming lead atom is coupled to three atoms in the nanodevice at $j = 1$. The incoming connection vector $\vec{w}$ can be expressed as

$$\vec{w}^\dagger = \begin{pmatrix} w_{11} & w_{12} & w_{13} \end{pmatrix} \tag{3.10}$$

where w_{ij} are hopping terms between a lead slice and a device slice. The i index is for the atom in the lead. Since there is a single atom in a lead slice, i is 1. The j index is for the atoms in the device, and j can be 1, 2 or 3 since there are 3 atoms in each device slice. For instance, w_{11} connects the first site (atom) in the lead to the first atom in the first slice of the device and w_{12} connects the first site (atom) in the lead to the second atom in the first slice of the device. Fig. 3.2, shows a typical connection between the first atom in the lead coupled to the first 3 atoms in the nanodevice. Furthermore, assume that $\vec{w}$ is equal to $\vec{u}$, this means that the connection between the last slice in the incoming lead to the first slice of the device and the connection between the last slice in the device to the first slice in the outgoing lead are the same.

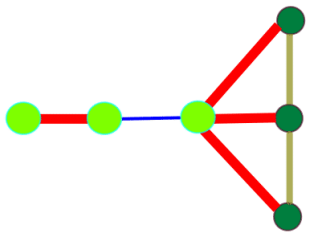

Figure 3.2

An example of connection between lead sites and the device where the first atom in the lead is connected to all three atoms in the first slice of the device.

Fig. 3.2, is an example of the connection between leads and device. The forest green color shows the atom in the device and the green color shows atoms in the lead. There

are only three atoms shown in the incoming lead. Note the even-odd bond structure in the lead.

After making these assumptions, the set of successful mapping equations become

$$\vec{w}^{\dagger}\mathbf{X} = \begin{pmatrix} -\tilde{w} & \mathbf{0} \end{pmatrix} \tag{3.11}$$

$$\mathbf{X}\vec{u} = \begin{pmatrix} -\tilde{u} \\ \\ \mathbf{0} \end{pmatrix} \tag{3.12}$$

$$\mathbf{X}_j\mathbf{A}_j\mathbf{X}_j^{\dagger} = \begin{pmatrix} \tilde{\epsilon}_j & \mathbf{0} \\ \\ \mathbf{0} & \hat{\mathbf{A}}_j \end{pmatrix} \tag{3.13}$$

and

$$\mathbf{X}_j\mathbf{B}_{j,j+1}\mathbf{X}_{j+1}^{\dagger} = \begin{pmatrix} -\tilde{s}_b & \mathbf{0} \\ \\ \mathbf{0} & \hat{\mathbf{B}}_{j,j+1} \end{pmatrix} \tag{3.14}$$

where j is the device slice index. Using Eq. (3.6), the normalized eigenvectors for the intra-slice and inter-slice coupling matrices are

$$\vec{v}_3^{3\dagger} = \begin{pmatrix} \frac{1}{2} & \frac{1}{\sqrt{2}} & \frac{1}{2} \end{pmatrix} \tag{3.15}$$

$$\vec{v}_2^{3\dagger} = \begin{pmatrix} \frac{1}{\sqrt{2}} & 0 & \frac{-1}{\sqrt{2}} \end{pmatrix} \tag{3.16}$$

and

$$\vec{v}_1^{3\dagger} = \begin{pmatrix} \frac{1}{2} & \frac{-1}{\sqrt{2}} & \frac{1}{2} \end{pmatrix} . \tag{3.17}$$

Now let the matrix of transformation, $\mathbf{X}$ be defined as

$$\mathbf{X} = \begin{pmatrix} \vec{v}_3^{3\dagger} \\ \\ \vec{v}_2^{3\dagger} \\ \\ \vec{v}_1^{3\dagger} \end{pmatrix} . \tag{3.18}$$

Note that from Eq. (3.18),

$$\mathbf{X}\mathbf{X}^{\dagger} = \mathbf{I}. \tag{3.19}$$

This means that the device intra-slice matrix at site $j = \nu$ has been transformed to

$$\mathbf{X}\mathbf{A}_{\nu}\mathbf{X}^{\dagger} = \begin{pmatrix} \epsilon_{\nu} - t_{\nu}\sqrt{2} & 0 & 0 \\ 0 & \epsilon_{\nu} & 0 \\ 0 & 0 & \epsilon_{\nu} + t_{\nu}\sqrt{2} \end{pmatrix}. \tag{3.20}$$

From Eq. (3.20) and the mapping Eq. (3.13), tuning for the device and the lead hence requires

$$\epsilon_L = \epsilon_{\nu} - t_{\nu}\sqrt{2} \tag{3.21}$$

where ϵ_L is the on-site energy of the atom in the lead. Since we have set the on-site energy of the atoms in the leads to zero, $\epsilon_L = 0$, this means Eq. (3.21) can be re-expressed as

$$\epsilon_{\nu} = t_{\nu}\sqrt{2}\,. \tag{3.22}$$

Note ϵ_{ν} can be any value, and the tuning only requires t_{ν} and ϵ_{ν} satisfy Eq. (3.22). Furthermore, note Eq. (3.22) allows a different ϵ_{ν} for every device slice ν. Similarly, for the inter-slice coupling matrices, use the same transformation matrix, $\mathbf{X}$ in Eq. (3.18). Upon multiplying through this gives

$$\mathbf{X}\mathbf{B}_{\omega,\omega+1}\mathbf{X}^{\dagger} = \begin{pmatrix} -t_{x,\omega} - t_{y,\omega}\sqrt{2} & 0 & 0 \\ 0 & -t_{x,\omega} & 0 \\ 0 & 0 & -t_{x,\omega} + t_{y,\omega}\sqrt{2} \end{pmatrix} \tag{3.23}$$

and therefore the mapping equation, Eq. (3.14) is satisfied provided $\tilde{s}_{b1} = t_{x,\omega} + t_{y,\omega}\sqrt{2}$. Now the last task to do is to check for the mapping equations for the incoming and outgoing

connection vector, $\vec{w}$ and $\vec{u}$. To do this, use the same transformation matrix, $\mathbf{X}$ in Eq. (3.18) and then define the incoming connection vector, $\vec{w}$ as

$$\vec{w}^{\dagger} = \begin{pmatrix} -\frac{w}{2} & -\frac{w}{\sqrt{2}} & -\frac{w}{2} \end{pmatrix} . \tag{3.24}$$

This means that

$$\vec{w}^{\dagger}\mathbf{X} = \begin{pmatrix} -w & 0 & 0 \end{pmatrix} . \tag{3.25}$$

Similarly define the outgoing connection vector, $\vec{u}$ as

$$\vec{u} = \begin{pmatrix} -\frac{u}{2} \\ -\frac{u}{\sqrt{2}} \\ -\frac{u}{2} \end{pmatrix} . \tag{3.26}$$

This means that

$$\mathbf{X}\vec{u} = \begin{pmatrix} -u \\ 0 \\ 0 \end{pmatrix} . \tag{3.27}$$

Thus in effect the mapping equations, Eq. (3.11) and Eq. (3.12) have been satisfied. Therefore to find quantum dragons, tune the on-site energy of the atom at slice $j = \nu$ to $\epsilon_{\nu} = t_{\nu}\sqrt{2}$, as well as $\tilde{s}_{b1} = t_{x,\omega} + t_{y,\omega}\sqrt{2}$, and $\vec{w} = \vec{u} = \begin{pmatrix} -\frac{t_{eo}}{2} \\ -\frac{t_{eo}}{\sqrt{2}} \\ -\frac{t_{eo}}{2} \end{pmatrix}$. In defining the connection vector for the incoming and outgoing leads coupled to the nanodevice, use the Perron-Frobenius theorem [69, 70, 71]. The inter-slice coupling matrices, $\mathbf{B}_{\omega,\omega+1}$, are all real $m \times m$ matrices with non-positive entries, and therefore each has a largest positive eigenvalue with an eigenvector which has all elements the same sign [69, 70, 71].

Similarly, the intra-slice coupling matrices can undergo a shift procedure to enable use of the Perron-Frobenius theorem [24].

3.1.1 Quantum dragons for $m = 3$, $l = 4$ with nn interactions

In Eq. (3.8), the inter-slice coupling matrices odd-even and even-odd are defined in terms of nearest neighbor and next nearest neighbor. This assumption has already been used to find quantum dragons for the three site device. Quantum dragons can also be found by relaxing this earlier assumption. Here, lets assume that the inter-slice coupling matrices, $\mathbf{B}_{\omega,\omega+1}$ are proportional to the identity matrix. Therefore, the device inter-slice coupling matrices have the simple form $\mathbf{B}_{\omega,\omega+1} = -t_{x,\omega}\mathbf{I}$. Use the same transformation matrix, $\mathbf{X}$ in Eq. (3.18) to satisfy the mapping equations. Therefore the mapping equation, Eq. (3.14) is satisfied provided $\tilde{s}_{b2} = t_{x,\omega}$. Here assume the device intra-slice coupling matrices are the same as Eq. (3.7). This means that to find quantum dragons, tune the on-site energy of the atom at slice $j = \nu$ to $\epsilon_\nu = t_\nu\sqrt{2}$, as well as $\tilde{s}_{b2} = t_{x,\omega}$, and $\vec{w} = \vec{u} = \begin{pmatrix} -\frac{t_{eo}}{2} \\ -\frac{t_{eo}}{\sqrt{2}} \\ -\frac{t_{eo}}{2} \end{pmatrix}$.

3.2 Quantum dragons for $m = 5$, $l = 4$ with nn and nnn interactions

Assume the nanodevice has five atoms per slice at slice $j = \nu$. See Fig. 3.3.

Fig. 3.3, is an example of 20 site device connected to dimerized leads. The vertical lines show the intra-slice hopping. The device has $m = 5$, $l = 4$ and therefore $ml = 20$ atoms. The device has non-uniform intra-slice hopping parameters. Only three atoms in the incoming lead as well as the outgoing leads are shown. The lead atoms are shown by

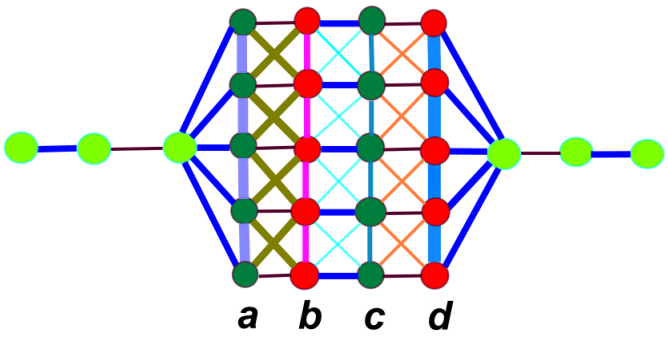

Figure 3.3

An example of the case of dimerized leads, and a $m = 5$ rectangular nanodevice, for 00 boundary conditions.

a green color. The connections between leads and the device are shown by line segments (blue). The inter-slice coupling strengths are for nn shown by a horizontal line (blue and black color) and the nnn shown by (pink, dark yellow and cyan color) line segments which form an X-shape. Appropriate choices of the tight-binding parameters makes this disordered nanodevice into a quantum dragon.

The intra-slice coupling matrices have the form

$$\mathbf{A}_\nu = \begin{pmatrix} \epsilon_\nu & -t_\nu & 0 & 0 & 0 \\ -t_\nu & \epsilon_\nu & -t_\nu & 0 & 0 \\ 0 & -t_\nu & \epsilon_\nu & -t_\nu & 0 \\ 0 & 0 & -t_\nu & \epsilon_\nu & -t_\nu \\ 0 & 0 & 0 & -t_\nu & \epsilon_\nu \end{pmatrix} = \epsilon_\nu \mathbf{I} - t_\nu \mathbf{Q} \tag{3.28}$$

where ϵ_ν are the on-site energies for the atoms at slice $j = \nu$ and t_ν are the intra-slice hopping parameters between the atoms. From Eq. (3.5), the eigenvalues of Eq. (3.28) are $\lambda_{\nu,1} = \epsilon_\nu - t_\nu\sqrt{3}$, $\lambda_{\nu,2} = \epsilon_\nu - t_\nu$, $\lambda_{\nu,3} = \epsilon_\nu$, $\lambda_{\nu,4} = \epsilon_\nu + t_\nu$, and $\lambda_{\nu,5} = \epsilon_\nu + t_\nu\sqrt{3}$.

Now assume the device inter-slice coupling matrices have the forms

$$\mathbf{B}_{\omega,\omega+1} = \begin{pmatrix} -t_{x,\omega} & -t_{y,\omega} & 0 & 0 & 0 \\ -t_{y,\omega} & -t_{x,\omega} & -t_{y,\omega} & 0 & 0 \\ 0 & -t_{y,\omega} & -t_{x,\omega} & -t_{y,\omega} & 0 \\ 0 & 0 & -t_{y,\omega} & -t_{x,\omega} & -t_{y,\omega} \\ 0 & 0 & 0 & -t_{y,\omega} & -t_{x,\omega} \end{pmatrix} = -t_{x,\omega}\mathbf{I} - t_{y,\omega}\mathbf{Q}\,. \tag{3.29}$$

The matrix $\mathbf{Q}$ is explicitly for $m = 5$

$$\mathbf{Q} = \begin{pmatrix} 0 & 1 & 0 & 0 & 0 \\ 1 & 0 & 1 & 0 & 0 \\ 0 & 1 & 0 & 1 & 0 \\ 0 & 0 & 1 & 0 & 1 \\ 0 & 0 & 0 & 1 & 0 \end{pmatrix}. \tag{3.30}$$

Using Eq. (3.6), the normalized eigenvectors for the intra-slice and inter-slice coupling matrices are

$$\vec{v}_5^{5\dagger} = \begin{pmatrix} \frac{1}{2\sqrt{3}} & \frac{1}{2} & \frac{1}{\sqrt{3}} & \frac{1}{2} & \frac{1}{2\sqrt{3}} \end{pmatrix} \tag{3.31}$$

$$\vec{v}_4^{5\dagger} = \begin{pmatrix} \frac{1}{2} & \frac{1}{2} & 0 & \frac{-1}{2} & \frac{-1}{2} \end{pmatrix} \tag{3.32}$$

$$\vec{v}_3^{5\dagger} = \begin{pmatrix} \frac{1}{\sqrt{3}} & 0 & \frac{-1}{\sqrt{3}} & 0 & \frac{1}{\sqrt{3}} \end{pmatrix} \tag{3.33}$$

$$\vec{v}_2^{5\dagger} = \begin{pmatrix} \frac{1}{2} & \frac{-1}{2} & 0 & \frac{1}{2} & \frac{-1}{2} \end{pmatrix} \tag{3.34}$$

and

$$\vec{v}_1^{5\dagger} = \begin{pmatrix} \frac{1}{2\sqrt{3}} & \frac{-1}{2} & \frac{1}{\sqrt{3}} & \frac{-1}{2} & \frac{1}{2\sqrt{3}} \end{pmatrix} . \tag{3.35}$$

Let the transformation matrix $\mathbf{X}$ be defined as

$$\mathbf{X} = \begin{pmatrix} \vec{v}_5^{5\dagger} \\ \vec{v}_4^{5\dagger} \\ \vec{v}_3^{5\dagger} \\ \vec{v}_2^{5\dagger} \\ \vec{v}_1^{5\dagger} \end{pmatrix} . \tag{3.36}$$

From Eq. (3.36),

$$\mathbf{X}\mathbf{X}^{\dagger} = \mathbf{I} . \tag{3.37}$$

This means that the device intra-slice coupling matrix at slice $j = \nu$ has been transformed to

$$\mathbf{X}\mathbf{A}_\nu\mathbf{X}^\dagger = \begin{pmatrix} \epsilon_\nu - t_\nu\sqrt{3} & 0 & 0 & 0 & 0 \\ 0 & \epsilon_\nu - t_\nu & 0 & 0 & 0 \\ 0 & 0 & \epsilon_\nu & 0 & 0 \\ 0 & 0 & 0 & \epsilon_\nu + t_\nu & 0 \\ 0 & 0 & 0 & 0 & \epsilon_\nu + t_\nu\sqrt{3} \end{pmatrix}. \tag{3.38}$$

From Eq. (3.38), and the mapping Eq. (3.13), tuning for the device and the lead hence requires

$$\epsilon_L = \epsilon_\nu - t_\nu\sqrt{3} \tag{3.39}$$

where ϵ_L is the on-site energy of the atom in the lead. Since the on-site energy of the atom in the lead is set to zero, $\epsilon_L = 0$, this means that Eq. (3.39) can be re-expressed as

$$\epsilon_\nu = t_\nu\sqrt{3}. \tag{3.40}$$

Note ϵ_ν can be any value, and the tuning only requires t_ν and ϵ_ν satisfy Eq. (3.40). Furthermore, note Eq. (3.40) allows a different ϵ_ν for every device slice ν. Similarly, for the inter-slice coupling matrices, use the same transformation matrix, $\mathbf{X}$ in Eq. (3.36). Upon multiplying through, this gives

$$\mathbf{X}\mathbf{B}_{\omega,\omega+1}\mathbf{X}^\dagger = \begin{pmatrix} \varrho_1 & 0 & 0 & 0 & 0 \\ 0 & \varrho_2 & 0 & 0 & 0 \\ 0 & 0 & \varrho_3 & 0 & 0 \\ 0 & 0 & 0 & \varrho_4 & 0 \\ 0 & 0 & 0 & 0 & \varrho_5 \end{pmatrix}. \tag{3.41}$$

Here,

$$\varrho_1 = -t_{x,\omega} - t_{y,\omega}\sqrt{3} \tag{3.42}$$

$$\varrho_2 = t_{x,\omega} - t_{y,\omega} \tag{3.43}$$

$$\varrho_3 = -t_{x,\omega} \tag{3.44}$$

$$\varrho_4 = t_{x,\omega} + t_{y,\omega} \tag{3.45}$$

and

$$\varrho_5 = -t_{x,\omega} + t_{y,\omega}\sqrt{3}. \tag{3.46}$$

Therefore the mapping Eq. (3.14) is satisfied provided $\tilde{s}_{b3} = t_{x,\omega} + t_{y,\omega}\sqrt{3}$. Now the last task is to check for the mapping equation for the connection vector for the incoming and outgoing leads coupled to the device, $\vec{w}$ and $\vec{u}$. To do this, use the same transformation matrix, $\mathbf{X}$ in Eq. (3.36) and then define the incoming connection vector, $\vec{w}$ by

$$\vec{w}^{\dagger} = \begin{pmatrix} -\frac{w}{2\sqrt{3}} & -\frac{w}{2} & -\frac{w}{\sqrt{3}} & -\frac{w}{2} & -\frac{w}{2\sqrt{3}} \end{pmatrix}. \tag{3.47}$$

This means that

$$\vec{w}^{\dagger}\mathbf{X} = \begin{pmatrix} -w & 0 & 0 & 0 & 0 \end{pmatrix}. \tag{3.48}$$

Thus in effect the mapping Eq. (3.11) is satisfied. Similarly define the outgoing connection vector, $\vec{u}$ as

$$\vec{u} = \begin{pmatrix} -\frac{u}{2\sqrt{3}} \\ -\frac{u}{2} \\ -\frac{u}{\sqrt{3}} \\ -\frac{u}{2} \\ -\frac{u}{2\sqrt{3}} \end{pmatrix}. \tag{3.49}$$

This means that

$$\mathbf{X}\vec{u} = \begin{pmatrix} -u \\ 0 \\ 0 \\ 0 \\ 0 \end{pmatrix}. \tag{3.50}$$

Thus in effect the mapping Eq. (3.12) is satisfied. Therefore to find quantum dragons tune the on-site energy of the atom at slice $j = \nu$ to $\epsilon_\nu = t_\nu\sqrt{3}$, as well as $\tilde{s}_{b3} = t_{x,\omega} + t_{y,\omega}\sqrt{3}$, and $\vec{w} = \vec{u} = \begin{pmatrix} -\frac{t_{eo}}{2\sqrt{3}} \\ -\frac{t_{eo}}{2} \\ -\frac{t_{eo}}{\sqrt{3}} \\ -\frac{t_{eo}}{2} \\ -\frac{t_{eo}}{2\sqrt{3}} \end{pmatrix}$.

Quantum dragons for $m = 5$, $l = 4$ can also be found when the device has only nn interactions. This means that for such a device, the inter-slice coupling matrices is proportional to the identity matrix. Thus $\mathbf{B}_{\omega,\omega+1} = -t_{x,\omega}\mathbf{I}$. This assumption has been used by Novotny in 2015 [24], to find quantum dragons. When the device consists of only nn interactions, to find quantum dragons, tune the on-site energy of the atom at slice $j = \nu$ to $\epsilon_\nu = t_\nu\sqrt{3}$, as well as $\tilde{s}_{b4} = t_{x,\omega}$ and $\vec{w} = \vec{u} = \begin{pmatrix} -\frac{t_{eo}}{2\sqrt{3}} \\ -\frac{t_{eo}}{2} \\ -\frac{t_{eo}}{\sqrt{3}} \\ -\frac{t_{eo}}{2} \\ -\frac{t_{eo}}{2\sqrt{3}} \end{pmatrix}$.

3.3 General mapping

To calculate the electron transmission probability, use the matrix method. For the sake of argument, the matrix method for $m = 3$ and $l = 2$ is presented here, although the same analysis can be extended to any number of atoms per slice in the device and any number of even slices in the device. The matrix equation to solve for the electron transmission probability for $m = 3$, $l = 2$ is expressed as [18]

$$\mathbf{M}_2\vec{\Psi} = \vec{\Xi} \tag{3.51}$$

where the 8×8 matrix

$$\mathbf{M}_2 = \begin{pmatrix} \xi(E) & -w_{11} & -w_{12} & -w_{13} & 0 & 0 & 0 & 0 \\ -w_{11} & \epsilon_a - E & -t_a & 0 & -t_x & -t_y & 0 & 0 \\ -w_{12} & -t_a & \epsilon_a - E & -t_a & -t_y & -t_x & -t_y & 0 \\ -w_{13} & 0 & -t_a & \epsilon_a - E & 0 & -t_y & -t_x & 0 \\ 0 & -t_x & -t_y & 0 & \epsilon_b - E & -t_b & 0 & -u_{11} \\ 0 & -t_y & -t_x & -t_y & -t_b & \epsilon_b - E & -t_b & -u_{12} \\ 0 & 0 & -t_y & -t_x & 0 & -t_b & \epsilon_b - E & -u_{13} \\ 0 & 0 & 0 & 0 & -u_{11} & -u_{12} & -u_{13} & \xi(E) \end{pmatrix}, \tag{3.52}$$

as well as

$$\vec{\Psi} = \begin{pmatrix} \chi + r\chi^* \\ \psi_{a,1} \\ \psi_{a,2} \\ \psi_{a,3} \\ \psi_{b,1} \\ \psi_{b,2} \\ \psi_{b,3} \\ t_T \end{pmatrix} \tag{3.53}$$

and

$$\Xi = \begin{pmatrix} \Lambda \\ 0 \\ 0 \\ 0 \\ 0 \\ 0 \\ 0 \\ 0 \end{pmatrix} . \tag{3.54}$$

3.3.1 General case mapping

The dimensions of the matrix to invert to calculate $\mathcal{T}(E)$ in Eq. (3.51) is 8×8 since $m = 3$ and $l = 2$ and hence $(2 + lm) \times (2 + lm) = 8 \times 8$. In general, 2D systems can sometimes be mapped onto 1D linear chains by the mapping equations. In most cases,

if one seeks to calculate the electron transmission probability for a nanodevice with a large number of atoms, the dimensions of the matrix on the LHS of Eq. (3.51) becomes large. This simply suggests that the solution could involve taking the inverse of a matrix of large dimensions. Although this can in priniciple be done numerically, getting an exact solution is not always possible. As in [18], a mapping is searched for in order to reduce the dimension of the matrix in Eq. (3.51). The matrix equation to solve for $\mathcal{T}(E)$ comes from the expression of the transmission amplitude, $t_T(E)$ with $\mathcal{T} = |t_T|^2$. The solution of the matrix equation Eq. (3.51), involves a matrix of the form

$$\mathbf{N}_\ell = \begin{pmatrix} \xi & \vec{w}^\dagger & \vec{0}^\dagger & \vec{0}^\dagger & \cdots & \vec{0}^\dagger & \vec{0}^\dagger & 0 \\ \vec{w} & \mathbf{F}_1 & \mathbf{B}_{12} & \mathbf{0} & \cdots & \mathbf{0} & \mathbf{0} & \vec{0} \\ \vec{0} & \mathbf{B}_{21} & \mathbf{F}_2 & \mathbf{B}_{23} & & \mathbf{0} & \mathbf{0} & \vec{0} \\ \vec{0} & \mathbf{0} & \mathbf{B}_{32} & \mathbf{F}_3 & & \mathbf{0} & \mathbf{0} & \vec{0} \\ \vdots & \vdots & & & \ddots & & & \vdots \\ \vec{0} & \mathbf{0} & \mathbf{0} & \mathbf{0} & & \mathbf{F}_{\ell-1} & \mathbf{B}_{\ell-1,\ell} & \vec{0} \\ \vec{0} & \mathbf{0} & \mathbf{0} & \mathbf{0} & & \mathbf{B}_{\ell,\ell-1} & \mathbf{F}_\ell & \vec{u} \\ 0 & \vec{0}^\dagger & \vec{0}^\dagger & \vec{0}^\dagger & \cdots & \vec{0}^\dagger & \vec{u}^\dagger & \xi \end{pmatrix} \tag{3.55}$$

with $\mathbf{F}_i = \mathbf{A}_i - E\mathbf{I}$ a $m_i \times m_i$ matrix. The $m_i \times m_i$ matrices $\mathbf{A}_i$, contain all the intra-slice coupling parameters and on-site energies, and is independent of the energy, E, of the incoming electron. The symbol $\mathbf{I}$ represents the identity matrix of the appropriate dimension, which in the equation for $\mathbf{F}_i$ is $m_i \times m_i$. The matrix equation which needs to

be solved for $\mathcal{T}(E) = |t_T|^2$ comes from the expression for $t_T(E)$ from the solution of the matrix equation

$$\mathbf{N}_\ell \begin{pmatrix} \chi + r\chi^* \\ \vec{\psi}_a \\ \vec{\psi}_b \\ \vdots \\ \vec{\psi}_\ell \\ t_T \end{pmatrix} = \begin{pmatrix} \Lambda \\ \vec{0} \\ \vec{0} \\ \vdots \\ \vec{0} \\ 0 \end{pmatrix} . \tag{3.56}$$

Use the eigenvectors of the intra-slice coupling matrices and form the appropiate matrix of transformation, $\mathbf{X}$. Next introduce the $m \times m$ block transformation matrices $\mathbf{X}_i$

$$\hat{\mathbf{X}} = \begin{pmatrix} 1 & & & & & & & \\ & \mathbf{X}_1 & & & & & & \\ & & \mathbf{X}_2 & & & & & \\ & & & \mathbf{X}_3 & & & & \\ & & & & \ddots & & & \\ & & & & & \mathbf{X}_{\ell-1} & & \\ & & & & & & \mathbf{X}_\ell & \\ & & & & & & & 1 \end{pmatrix} \tag{3.57}$$

where all $\mathbf{X}_i$ are non-singular. Also multiply both sides of Eq. (3.56) from the left by the matrix $\hat{\mathbf{X}}$, and insert the identity $\mathbf{I} = \hat{\mathbf{X}}^\dagger(\hat{\mathbf{X}}^\dagger)^{-1}$ between $\mathbf{N}_\ell$ and the vector of wavefunctions. The equation then reads

$$\hat{\mathbf{X}}\mathbf{N}_\ell\hat{\mathbf{X}}^\dagger \begin{pmatrix} \chi + r\chi^* \\ \left(\mathbf{X}_1^\dagger\right)^{-1}\vec{\psi}_a \\ \left(\mathbf{X}_2^\dagger\right)^{-1}\vec{\psi}_b \\ \vdots \\ \left(\mathbf{X}_\ell^\dagger\right)^{-1}\vec{\psi}_\ell \\ t_T \end{pmatrix} = \begin{pmatrix} \Lambda \\ \vec{0} \\ \vec{0} \\ \vdots \\ \vec{0} \\ 0 \end{pmatrix}. \tag{3.58}$$

Next define the $(2+lm)\times(2+lm)$ matrix $\mathbf{M}_\ell = \hat{\mathbf{X}}\mathbf{N}_\ell\hat{\mathbf{X}}^\dagger$ and perform the matrix multiplication. Hence, $\mathbf{M}_\ell$ has the form

$$\begin{pmatrix} \xi & \vec{w}^\dagger\mathbf{X}_1^\dagger & \vec{0}^\dagger & \vec{0}^\dagger & \cdots & \vec{0}^\dagger & \vec{0}^\dagger & 0 \\ \mathbf{X}_1\vec{w} & \mathbf{X}_1\mathbf{F}_1\mathbf{X}_1^\dagger & \mathbf{X}_1\mathbf{B}_{12}\mathbf{X}_2^\dagger & \mathbf{0} & \cdots & \mathbf{0} & \mathbf{0} & \vec{0} \\ \vec{0} & \mathbf{X}_2\mathbf{B}_{21}\mathbf{X}_1^\dagger & \mathbf{X}_2\mathbf{F}_2\mathbf{X}_2^\dagger & \mathbf{X}_2\mathbf{B}_{23}\mathbf{X}_3^\dagger & & \mathbf{0} & \mathbf{0} & \vec{0} \\ \vec{0} & \mathbf{0} & \mathbf{X}_3\mathbf{B}_{32}\mathbf{X}_2^\dagger & \mathbf{X}_3\mathbf{F}_3\mathbf{X}_3^\dagger & & \mathbf{0} & \mathbf{0} & \vec{0} \\ \vdots & \vdots & & & \ddots & & & \vdots \\ \vec{0} & \mathbf{0} & \mathbf{0} & \mathbf{0} & & \mathbf{X}_{\ell-1}\mathbf{F}_{\ell-1}\mathbf{X}_{\ell-1}^\dagger & \mathbf{X}_{\ell-1}\mathbf{B}_{\ell-1,\ell}\mathbf{X}_\ell^\dagger & \vec{0} \\ \vec{0} & \mathbf{0} & \mathbf{0} & \mathbf{0} & & \mathbf{X}_\ell\mathbf{B}_{\ell,\ell-1}\mathbf{X}_{\ell-1} & \mathbf{X}_\ell\mathbf{F}_\ell\mathbf{X}_\ell^\dagger & \mathbf{X}_\ell\vec{u} \\ 0 & \vec{0}^\dagger & \vec{0}^\dagger & \vec{0}^\dagger & \cdots & \vec{0}^\dagger & \vec{u}^\dagger\mathbf{X}_\ell^\dagger & \xi \end{pmatrix}. \tag{3.59}$$

The mapping onto a 1D linear chain of sites is accomplished by finding solutions to the sets of the mapping equations in Eq. (3.11) through Eq. (3.14). A successful mapping will

give that the transmission for this large matrix is exactly the same for all energies of the incident electron as that from a matrix of dimension $2+\ell$ that has the form

$$\widetilde{\mathbf{M}}_\ell = \begin{pmatrix} \xi & -\tilde{w} & 0 & 0 & \cdots & 0 & 0 & 0 \\ -\tilde{w} & \tilde{\kappa}_1 & -\tilde{t}_{12} & 0 & \cdots & 0 & 0 & 0 \\ 0 & -\tilde{t}_{21} & \tilde{\kappa}_2 & -\tilde{t}_{23} & & 0 & 0 & 0 \\ 0 & 0 & -\tilde{t}_{32} & \tilde{\kappa}_3 & & 0 & 0 & 0 \\ \vdots & \vdots & & & \ddots & & & \vdots \\ 0 & 0 & 0 & 0 & & \tilde{\kappa}_{\ell-1} & -\tilde{t}_{\ell-1,\ell} & 0 \\ 0 & 0 & 0 & 0 & & -\tilde{t}_{\ell,\ell-1} & \tilde{\kappa}_\ell & -\tilde{u} \\ 0 & 0 & 0 & 0 & \cdots & 0 & -\tilde{u} & \xi \end{pmatrix} \tag{3.60}$$

with $\tilde{\kappa}_j = \tilde{\epsilon}_j - E$. The transmission coefficient $t_T(E)$ can be found from either the $(l+2)\times(l+2)$ equation

$$\begin{pmatrix} \chi + r\chi^* \\ \tilde{\psi}_1 \\ \tilde{\psi}_2 \\ \vdots \\ \tilde{\psi}_\ell \\ t_T \end{pmatrix} = \widetilde{\mathbf{M}}_\ell^{-1} \begin{pmatrix} \Lambda \\ 0 \\ 0 \\ \vdots \\ 0 \\ 0 \end{pmatrix} \tag{3.61}$$

or the $(2+lm)\times(2+lm)$ equation

$$\left(\hat{\mathbf{X}}^{\dagger}\right)^{-1}\begin{pmatrix}\chi+r\chi^{*}\\ \vec{\psi}_1\\ \vec{\psi}_2\\ \vdots\\ \vec{\psi}_\ell\\ t_T\end{pmatrix}=\mathbf{M}_{\ell}^{-1}\begin{pmatrix}\Lambda\\ \vec{0}\\ \vec{0}\\ \vdots\\ \vec{0}\\ 0\end{pmatrix}, \tag{3.62}$$

and in either case the electron transmission probability is calculated from $\mathcal{T}(E)=|t_T|^2$.

3.3.2 General method for 2D system mapping

In this section, the general method to do the mapping for a general 2D system is presented. Let assume there are m atoms per slice in the nanodevice. The intra-slice coupling matrix associated with the device at site ν can be expressed as

$$\mathbf{A}_{\nu}=\epsilon_{\nu}\mathbf{I}-t_{\nu}\mathbf{Q}. \tag{3.63}$$

The eigenvalues of the matrix $\mathbf{A}_{\nu}$ can be expressed as [67, 68]

$$\lambda_{s,\nu}=\epsilon_{\nu}-2t_{\nu}\cos\left(\frac{\pi s}{m+1}\right) \tag{3.64}$$

where $s=1,....m$. Assume the inter-slice coupling matrices for the device (odd-even and even-odd) have the form

$$\mathbf{B}_{\omega,\omega+1}=-t_{x,\omega}\mathbf{I}-t_{y,\omega}\mathbf{Q}\,. \tag{3.65}$$

In Eq. (3.63), and Eq. (3.65) the matrix $\mathbf{Q}$ has been shown in Eq. (3.2) and the matrix $\mathbf{I}$ is an identity matrix of the same dimension as $\mathbf{Q}$. The eigenvalues of Eq. (3.65) can be expressed as [67, 68]

$$\lambda_{s,\nu} = -t_{x,\nu} - 2t_{y,\nu}\cos\left(\frac{\pi s}{m+1}\right) \tag{3.66}$$

where $s = 1, ...m$. Assume further that there is a single incoming lead atom which is coupled to the m atoms in the device at slice $\nu = 1$. This means that the incoming connection vector, $\vec{w}$, is of dimension m. This further suggests that the outgoing connection vector $\vec{u}$ is also of dimension m. After making these assumptions the sets of mapping equations are given in Eq. (3.11) through Eq. (3.14). The elements of the eigenvectors of the inter-slice and intra-slice coupling matrices, $\mathbf{B}_{\omega,\omega+1}$, and $\mathbf{A}_\nu$ are [67, 68]

$$x_j^{(s)} = \sqrt{\frac{2}{m+1}}\sin\left(\frac{\pi s j}{m+1}\right) \tag{3.67}$$

where $j = 1....., m$ and $s = 1, ...m$. With these eigenvectors, form the $m \times m$ matrix of transformation $\mathbf{X}$ such that

$$\mathbf{X} = \sqrt{\frac{2}{m+1}}\begin{pmatrix}
\sin\left(\frac{\pi}{m+1}\right) & \sin\left(\frac{2\pi}{m+1}\right) & \sin\left(\frac{3\pi}{m+1}\right) & \sin\left(\frac{4\pi}{m+1}\right) & \cdots & \cdots & \cdots & \cdots \\
\sin\left(\frac{2\pi}{m+1}\right) & \sin\left(\frac{4\pi}{m+1}\right) & \sin\left(\frac{6\pi}{m+1}\right) & \sin\left(\frac{8\pi}{m+1}\right) & \cdots & \cdots & \cdots & \cdots \\
\sin\left(\frac{3\pi}{m+1}\right) & \sin\left(\frac{6\pi}{m+1}\right) & \sin\left(\frac{9\pi}{m+1}\right) & \sin\left(\frac{12\pi}{m+1}\right) & \cdots & \cdots & \cdots & \cdots \\
\sin\left(\frac{4\pi}{m+1}\right) & \sin\left(\frac{8\pi}{m+1}\right) & \sin\left(\frac{12\pi}{m+1}\right) & \sin\left(\frac{16\pi}{m+1}\right) & \cdots & \cdots & \cdots & \cdots \\
\sin\left(\frac{5\pi}{m+1}\right) & \sin\left(\frac{10\pi}{m+1}\right) & \sin\left(\frac{15\pi}{m+1}\right) & \sin\left(\frac{20\pi}{m+1}\right) & \cdots & \cdots & \cdots & \cdots \\
\sin\left(\frac{6\pi}{m+1}\right) & \sin\left(\frac{12\pi}{m+1}\right) & \sin\left(\frac{18\pi}{m+1}\right) & \sin\left(\frac{24\pi}{m+1}\right) & \cdots & \cdots & \cdots & \cdots \\
\sin\left(\frac{7\pi}{m+1}\right) & \sin\left(\frac{14\pi}{m+1}\right) & \sin\left(\frac{21\pi}{m+1}\right) & \sin\left(\frac{28\pi}{m+1}\right) & \cdots & \cdots & \cdots & \cdots \\
\sin\left(\frac{8\pi}{m+1}\right) & \sin\left(\frac{16\pi}{m+1}\right) & \sin\left(\frac{24\pi}{m+1}\right) & \sin\left(\frac{32\pi}{m+1}\right) & \cdots & \cdots & \cdots & \cdots
\end{pmatrix} \tag{3.68}$$

where the matrix is written for $m = 8$, and only four columns are shown. Note that from Eq. (3.68)

$$\mathbf{X}\mathbf{X}^{\dagger} = \mathbf{I}\,. \tag{3.69}$$

Since $\mathbf{X}$ is unitary, $\mathbf{A}_{\nu}$ can be diagonalized as

$$\mathbf{X}\mathbf{A}_{\nu}\mathbf{X}^{\dagger} = \mathbf{A}_{diagonal} \tag{3.70}$$

here $\mathbf{A}_{diagonal}$ is

$$\mathbf{A}_{diagonal} = \begin{pmatrix} \lambda_1 & 0 & \cdots & 0 & 0 \\ 0 & \lambda_2 & \cdots & 0 & 0 \\ \vdots & \vdots & \ddots & \vdots & \vdots \\ 0 & 0 & \cdots & \lambda_{m-1} & 0 \\ 0 & 0 & \cdots & 0 & \lambda_m \end{pmatrix} \tag{3.71}$$

with the eigenvalue λ_i of Eq. (3.64). Similarly, for the inter-slice coupling matrices use the same transformation matrix $\mathbf{X}$ in Eq. (3.68). Upon multiplying through this gives

$$\mathbf{X}\mathbf{B}_{\omega,\omega+1}\mathbf{X}^{\dagger} = \mathbf{B}_{diagonal1} \tag{3.72}$$

here $\mathbf{B}_{diagonal1}$ is

$$\mathbf{B}_{diagonal1} = \begin{pmatrix} \lambda_{11} & 0 & \cdots & 0 & 0 \\ 0 & \lambda_{12} & \cdots & 0 & 0 \\ \vdots & \vdots & \ddots & \vdots & \vdots \\ 0 & 0 & \cdots & \lambda_{1,m-1} & 0 \\ 0 & 0 & \cdots & 0 & \lambda_{1m} \end{pmatrix}. \tag{3.73}$$

with the eigenvalue of Eq. (3.66). Now the last task is to check for the mapping equation for the connection vector for the incoming and the outgoing leads, $\vec{w}$ and $\vec{u}$. To do this, use the same transformation matrix, $\mathbf{X}$ in Eq. (3.68) and then define the connection vector, $\vec{w}$ by

$$\vec{w}^{\dagger} = \begin{pmatrix} -w_{11} & -w_{12} & -w_{13} & -w_{14} & \cdots & -w_{1m} \end{pmatrix} . \tag{3.74}$$

This means that from Eq. (3.67)

$$\vec{w}^{\dagger}\mathbf{X} = \begin{pmatrix} -w_{11} & 0 & 0 & 0 & 0 & \cdots & 0 \end{pmatrix} . \tag{3.75}$$

provided from Eq. (3.67) $\vec{w}^{\dagger} = -w_{11}\vec{v}^{(1)\dagger}$. Thus in effect the mapping Eq. (3.11) is satisfied. Similarly, define the outgoing connection vector $\vec{u}$ as

$$\vec{u} = \begin{pmatrix} -u_{11} \\ -u_{12} \\ -u_{13} \\ -u_{14} \\ -u_{15} \\ \vdots \\ -u_{1m} \end{pmatrix} \tag{3.76}$$

This means that

$$\mathbf{X}\vec{u} = \begin{pmatrix} -u_{11} \\ 0 \\ 0 \\ 0 \\ 0 \\ \vdots \\ 0 \end{pmatrix} \tag{3.77}$$

for $\vec{u}^{\dagger} = -u_{11}\vec{v}^{(1)}$, and hence the mapping equation mapping Eq. (3.12) is satisfied.

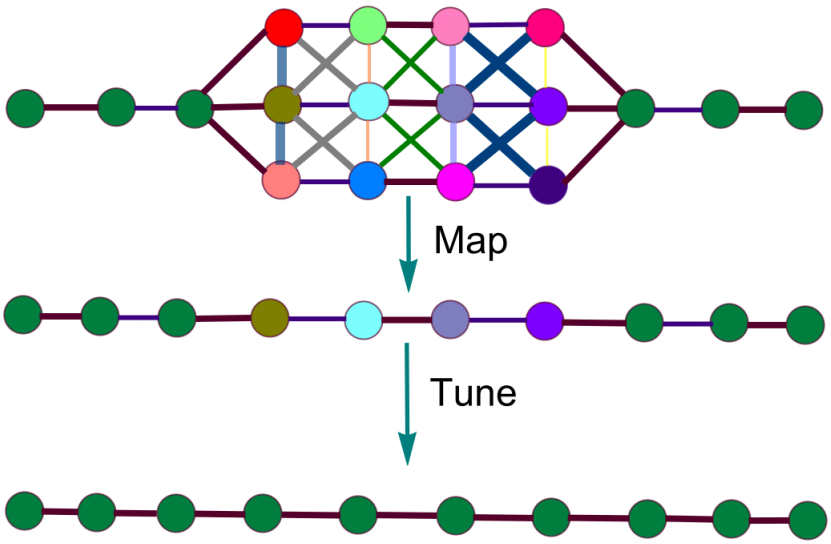

Figure 3.4

An example of mapping and tuning for a nanodevice with $m = 3, l = 4$.

Fig. 3.4, shows a 12 site device where mapping has been done as well tuning. The device is coupled to dimerized leads. Since, $m = 3$ and $l = 4$ this means that the device has $ml = 12$. Here, mapping onto a 1D linear chain has been performed, and tuning has also been done. Hence, the device is a quantum dragon.

3.3.3 Example of mapping for 2D system: Six site device

In this section, we will show how to do the mapping for a 6 site device. Here, $m = 3$, $l = 2$, and $m_L = 1$. Form the matrix of transformation, $\mathbf{X}$, from the eigenvectors and then introduce the block transformation matrix,

$$\hat{\mathbf{X}} = \begin{pmatrix} 1 & & & \\ & \mathbf{X} & & \\ & & \mathbf{X} & \\ & & & 1 \end{pmatrix}. \tag{3.78}$$

Here, the matrix of transformation, $\mathbf{X}$ is shown in Eq. (3.18).

It should be noted that since the dimension of the matrix to invert to calculate the electron transmission probability is an 8×8 matrix, the block transformation matrix is also

8×8 matrix. Clearly $\hat{\mathbf{X}}^\dagger = \hat{\mathbf{X}}$ and $\hat{\mathbf{X}}^\dagger \hat{\mathbf{X}} = \mathbf{I}_{8\times 8}$. Sandwiching $\mathbf{N}_3$ with the transformation matrices gives

$$\hat{\mathbf{X}}\mathbf{N}_3\hat{\mathbf{X}}^\dagger = \begin{pmatrix} \xi(E) & -w & 0 & 0 & 0 & 0 & 0 & 0 \\ -w & \kappa 1 & 0 & 0 & t1 & 0 & 0 & 0 \\ 0 & 0 & \epsilon_a - E & 0 & 0 & -t_x & 0 & 0 \\ 0 & 0 & 0 & \kappa 2 & 0 & 0 & t2 & 0 \\ 0 & t1 & 0 & 0 & \kappa 3 & 0 & 0 & -u \\ 0 & 0 & -t_x & 0 & 0 & \epsilon_b - E & 0 & 0 \\ 0 & 0 & 0 & t2 & 0 & 0 & \kappa 4 & 0 \\ 0 & 0 & 0 & 0 & -u & 0 & 0 & \xi(E) \end{pmatrix}. \tag{3.79}$$

Here,

$$\kappa 1 = \epsilon_a - t_a\sqrt{2} - E \tag{3.80}$$

$$t1 = -t_x - t_y\sqrt{2} \tag{3.81}$$

$$\kappa 2 = \epsilon_a + t_a\sqrt{2} - E \tag{3.82}$$

$$t2 = -t_x + t_y\sqrt{2} \tag{3.83}$$

$$\kappa 3 = \epsilon_b - t_b\sqrt{2} - E \tag{3.84}$$

$$\kappa 4 = \epsilon_b + t_b\sqrt{2} - E. \tag{3.85}$$

Collect the sites connected to the input and output leads, through $\xi(E)$, to give

$$\widetilde{\mathbf{M}}_3 = \begin{pmatrix} \xi(E) & -w & 0 & 0 \\ -w & \epsilon_a - t_a\sqrt{2} - E & -t_x - t_y\sqrt{2} & 0 \\ 0 & -t_x - t_y\sqrt{2} & \epsilon_b - t_b\sqrt{2} - E & -u \\ 0 & 0 & -u & \xi(E) \end{pmatrix}. \tag{3.86}$$

This is the $(l+2)\times(l+2)$ matrix to invert to calculate the electron transmission probability. The map-and-tune method of finding a quantum dragon is shown in Fig. 3.4.

3.4 General tuning: Quantum dragon

In the absence of a magnetic field, the maximum eigenvalue corresponds to $s = 1$, which means that from Eq. (3.71) and the mapping Eq. (3.13), tuning for the device and the lead requires that

$$\epsilon_L = \lambda_1 = 0. \tag{3.87}$$

Similarly, for the inter-slice coupling matrices for the device, Eq. (3.73), the mapping Eq. (3.14) is satisfied provided

$$\tilde{s}_{bx} = \lambda_{11}. \tag{3.88}$$

Thus in effect the mapping Eq. (3.12) is satisfied. Therefore to find quantum dragons tune $\epsilon_L = \lambda_1$, $\tilde{s}_{bx} = \lambda_{11}$ and $\vec{w} = \vec{u} = -t_{eo}\vec{v}^{(1)}$.

3.4.1 Specific tuning: Quantum dragon for $m = 3$, $l = 2$

The six site device in section 3.3.3, will be a quantum dragon with $\mathcal{T}(E) = 1$ as long as the four relations

$$\begin{aligned} -w &= -t_{eo} \\ \epsilon_j - t_j\sqrt{2} &= 0 \qquad j = \{1, 2\} \\ -t_x - t_y\sqrt{2} &= -t_{oe} \\ -u &= -t_{eo} \end{aligned} \tag{3.89}$$

are satisfied.

3.5 Data

In this section, the results obtained are presented. Here, we show quantum dragon solutions as well as Fano resonance in the electron transmission probability when there is uncorrelated complete randomness in the device. In Fig. 3.5 through Fig. 3.8, the plot of $\mathcal{T}$ vs E for both the dimerized leads and uniform leads coupled to the nanodevice are shown. As it can be seen from the graphs, when there is correlated random disorder between the single-band tight binding parameters, we obtain a quantum dragon solution as shown by the line $\mathcal{T} = 1$ (darker blue) as expected. As argued by Novotny, [18] quantum dragon solutions are obtained when there is an interplay between the nanodevice and the attached leads. When the tight-binding parameters are not correlated, Fano resonances are seen in the plots of $\mathcal{T}$ vs E. By using a simple Mathematica code for a particular strength of disorder, δ for we calculate numerically the mean electron transmission probability as well as the standard deviation of the electron transmisssion probability. As it can be seen

from Fig. 3.9 and Fig. 3.10, the mean electron transmission probability decreases with increasing strength of the disoder as expected. This makes complete sense because as the strength of the disorder increases, the uncorrelated randomness of the tight binding parameters in the device increases, and hence the electron transmission probability decreases and consequently a decrease in the mean electron transmission probability. It should be noted that there is no randomness of the tight-binding parameters of both the dimerized leads and uniform leads attached to the device. To generate random numbers we used RandomVariate[distribution] in Mathematica, which generates a pseudorandom variate or numbers from a particular distribution. In our study, the distribution we used is the normal distribution of mean zero and variance unity. In our choice of particular distribution we choose the normal distribution. Fig. 3.5 is a plot of transmission vs energy, E. The nanodevice

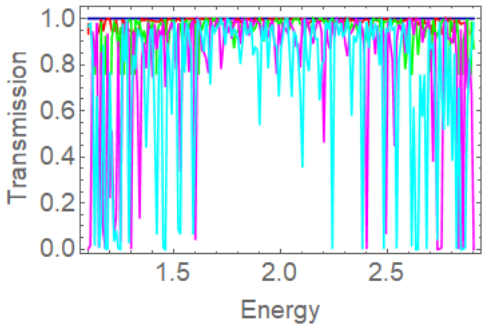

Figure 3.5

$\mathcal{T}$ vs E, boundary condition 00, dimerized leads.

has $m = 5$, $l = 14$ and therefore $ml = 70$ atoms. Here, $t_{oe} = 1$ and $t_{eo} = 2$. The line

$\mathcal{T} = 1$ (darker blue) has the on-site energy, $\epsilon_j = t_j\sqrt{3}$. The intra-slice hopping strengths used are non-uniform. The red, green, magenta and cyan color show Fano resonances in the electrical transmission probability of the nanodevice. The on-site energies are modeled by $\epsilon_j = t_j\sqrt{3} + \delta\Sigma$ and the intra-slice hopping terms are modeled by $t_j = t + \delta\Sigma$. The inter-slice hopping parameters are modeled by $t_x = t_{oe} + \delta\Sigma$ and $t_\alpha = t_{eo} + \delta\Sigma$ where $\delta = 0.0, 0.05, 0.1, 0.15, 0.2$ and Σ is a random number of mean 0 and unit standard deviation.

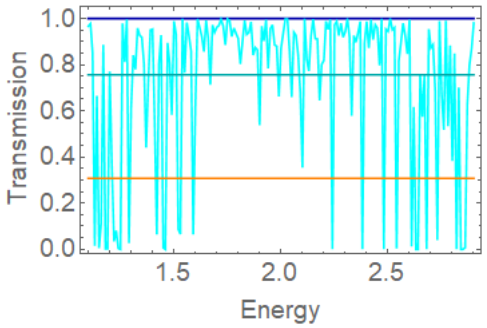

Figure 3.6

$\mathcal{T}$ vs E, boundary condition 00, dimerized leads, $\delta = 0.2$.

Fig. 3.6, is the same as Fig. 3.5, except only two values $\delta = 0$ (a quantum dragon) and $\delta = 0.2$ are shown. It should be noted that the mapping equation only hold when $\delta = 0$. The line $\mathcal{T} = 1$ (darker blue) has the on-site energy, $\epsilon_j = t_j\sqrt{3}$. The intra-slice hopping strengths used are non-uniform. The cyan color shows Fano resonances

in the nanodevice, the darker cyan color and the orange color shows the mean electron transmission probability and the standard deviation of the $\mathcal{T}$ vs E for $\delta = 0.2$.

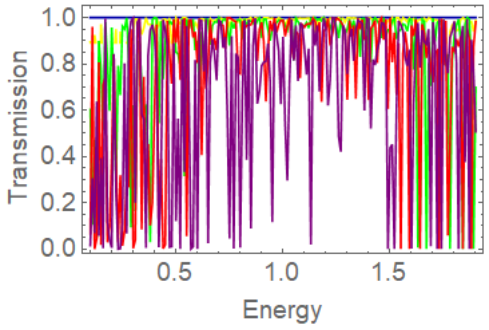

Figure 3.7

$\mathcal{T}$ vs E, boundary condition 00, uniform leads.

Fig. 3.7, shows a plot of transmission vs E. The nanodevice has $m = 5$, $l = 14$ and therefore $ml = 70$ atoms. Here, $t_{eo} = 1$ and $t_{eo} = 1$. The line $\mathcal{T} = 1$ (darker blue) has the on-site energy, $\epsilon_j = t_j\sqrt{3}$. The intra-slice hopping strengths used are non-uniform. The yellow, green, red and the purple color show Fano resonances in the nanodevice. The on-site energies are modeled by $\epsilon_j = t_j\sqrt{3}+\delta\Sigma$ and the intra-slice hopping terms are modeled by $t_j = t + \delta\Sigma$. The inter-slice hopping parameters are modeled by $t_x = t_{oe} + \delta\Sigma$ and $t_\alpha = t_{eo} + \delta\Sigma$ where $\delta = 0.0, 0.05, 0.1, 0.15, 0.2$ and Σ is a normally distributed random number.

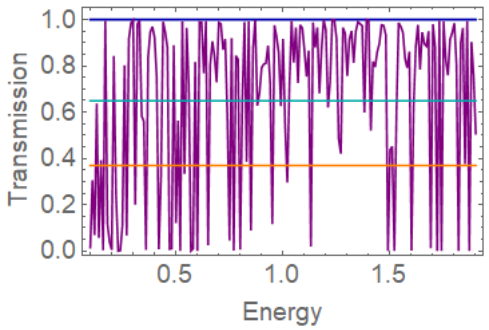

Figure 3.8

$\mathcal{T}$ vs E, boundary condition 00, uniform leads, $\delta = 0.2$.

Fig. 3.8, is the same as Fig. 3.7, except only for two values $\delta = 0$ (a quantum dragon) and $\delta = 0.2$ are shown. Here, $t_{eo} = 1$ and $t_{eo} = 1$. The cyan and the orange color shows the mean and the standard deviation of $\mathcal{T}$ vs E for $\delta = 0.2$ for the device.

3.6 Summary

In this chapter, it has been shown how to find quantum dragons for $m = 3$, $l = 4$ as well as $m = 5$ and $l = 4$ for single-layer planar rectangular crystals with boundary conditions 00. Here, the connection hopping strengths $\vec{w}$ and $\vec{u}$ to the nanodevice are a modified form of the busbar connection. In the presence of uncorrelated random disorder in the nanodevice, Fano resonances in the electron transmission probability are seen in Fig. 3.5 through Fig. 3.8 for both the dimerized and uniform leads with inhomogeneous slices in the device. Quantum dragons have no Fano resonances just $\mathcal{T}(E) = 1$. The quantum dragon solutions obtained are nanodevices with non-uniform intra-slice hopping

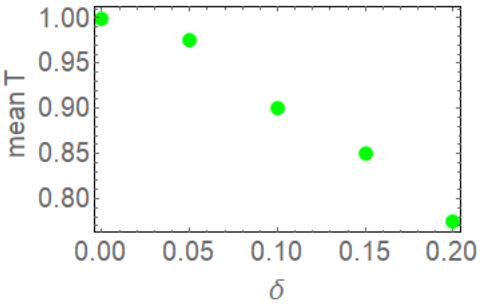

Figure 3.9

$\langle \mathcal{T} \rangle$ vs δ, boundary condition 00, non-uniform leads

terms. However, quantum dragons solution can also be obtained with uniform intra-slices in the nanodevice. Fano resonances are also expected to be observed when the dimerized and non-dimerized leads are connected to homogeneous slices when there is uncorrelated disorder of the tight-binding parameters in the nanodevice. For the six site device, we have shown how to use the mapping technique to obtain quantum dragon solutions. For m atoms per slice in the device with l number of slices in the nanodevice, where here l is an even number, the general approach to find quantum dragons has also been shown. As the amount of uncorrelated disorder increases (δ increases) the mean transmission falls and the standard deviation of the transmission increases. This is shown in Fig. 3.9 through Fig. 3.12 for both dimerized and uniform leads.

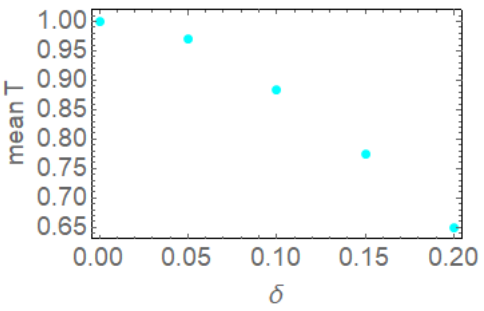

Figure 3.10

$\langle \mathcal{T} \rangle$ vs δ, boundary condition 00, uniform leads.

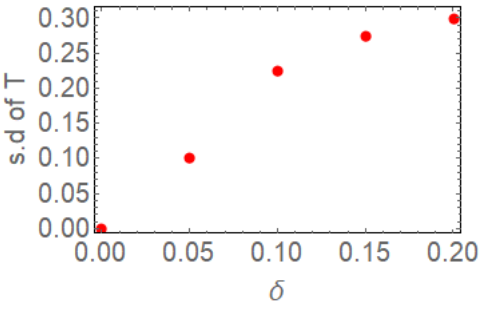

Figure 3.11

std $\mathcal{T}$ vs δ, boundary condition 00, dimerized leads.

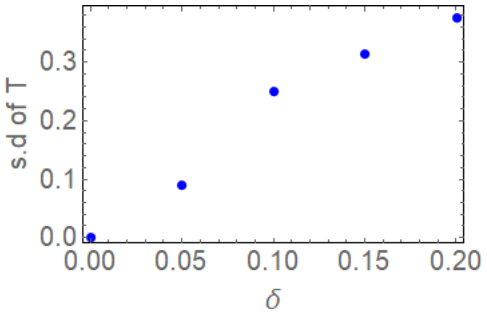

Figure 3.12

std $\mathcal{T}$ vs δ, boundary condition 00, uniform leads.

CHAPTER 4

QUANTUM DRAGON SOLUTIONS FOR RECTANGULAR CRYSTALS : CASE 2 : BOUNDARY CONDITION $--$

It is shown in this section how to find quantum dragons for single-layer planar rectangular crystals using boundary conditions which we label as $--$. We call the boundary conditions $--$ because in Eq. (1.25), we set ($\beta = \gamma = -b$). The connections used in this chapter are the busbar. There are two ways to find quantum dragons: (1) we assume the inter-slice coupling matrices for the nanodevice has nn and nnn interactions and (2) we assume the inter-slice coupling matrices are proportional to the identity matrix. In other words, the device has only nn interactions. In the absence of nnn interactions this gives results in [24]. From Eq. (1.25), by setting ($\beta = \gamma = -b$), the symmetric tridiagonal matrix of dimension $m \times m$ has the form

$$\mathbf{A} = \begin{pmatrix} a-b & -b & 0 & \cdots & 0 & 0 \\ -b & a & -b & \cdots & 0 & 0 \\ 0 & -b & a & \cdots & 0 & 0 \\ \vdots & \vdots & \vdots & \ddots & \vdots & \vdots \\ 0 & 0 & 0 & \cdots & a & -b \\ 0 & 0 & 0 & \cdots & -b & a-b \end{pmatrix} = a\mathbf{I} - b\mathbf{Q} - b\mathbf{\Omega} \tag{4.1}$$

where a and b are real numbers. In Eq. (4.1), the matrix $\mathbf{Q}$ is shown in Eq. (3.2) and the matrix $\mathbf{\Omega}$ is defined as

$$\mathbf{\Omega} = \begin{pmatrix} 1 & 0 & 0 & \cdots & 0 & 0 \\ 0 & 0 & 0 & \cdots & 0 & 0 \\ 0 & 0 & 0 & \cdots & 0 & 0 \\ \vdots & \vdots & \vdots & \ddots & \vdots & \vdots \\ 0 & 0 & 0 & \cdots & 0 & 0 \\ 0 & 0 & 0 & \cdots & 0 & 1 \end{pmatrix}. \tag{4.2}$$

Our nanodevice has an intra-slice matrix of the form (written for $m = 8$)

$$\mathbf{A} = \begin{pmatrix} \epsilon - t & -t & 0 & 0 & 0 & 0 & 0 & 0 \\ -t & \epsilon & -t & 0 & 0 & 0 & 0 & 0 \\ 0 & -t & \epsilon & -t & 0 & 0 & 0 & 0 \\ 0 & 0 & -t & \epsilon & -t & 0 & 0 & 0 \\ 0 & 0 & 0 & -t & \epsilon & -t & 0 & 0 \\ 0 & 0 & 0 & 0 & -t & \epsilon & -t & 0 \\ 0 & 0 & 0 & 0 & 0 & -t & \epsilon & -t \\ 0 & 0 & 0 & 0 & 0 & 0 & -t & \epsilon - t \end{pmatrix} = \epsilon\mathbf{I} - t\mathbf{Q} - t\mathbf{\Omega} \tag{4.3}$$

and an inter-slice matrix of the form (written for $m = 8$)

$$\mathbf{B} = \begin{pmatrix} -t_x - t_y & -t_y & 0 & 0 & 0 & 0 & 0 & 0 \\ -t_y & -t_x & -t_y & 0 & 0 & 0 & 0 & 0 \\ 0 & -t_y & -t_x & -t_y & 0 & 0 & 0 & 0 \\ 0 & 0 & -t_y & -t_x & -t_y & 0 & 0 & 0 \\ 0 & 0 & 0 & -t_y & -t_x & -t_y & 0 & 0 \\ 0 & 0 & 0 & 0 & -t_y & -t_x & -t_y & 0 \\ 0 & 0 & 0 & 0 & 0 & -t_y & -t_x & -t_y \\ 0 & 0 & 0 & 0 & 0 & 0 & -t_y & -t_x - t_y \end{pmatrix} = -t_x\mathbf{I} - t_y\mathbf{Q} - t_y\mathbf{\Omega} \tag{4.4}$$

where t's are the hopping strengths which are non-negative real numbers and ϵ is the on-site energy of the atom which is a real number. Eq. (4.1) is a matrix with eigenvalues expressed as [67, 68]

$$\lambda_s = a - 2b\cos\left(\frac{(s-1)\pi}{m}\right) \tag{4.5}$$

for $s = 1, 2, ...m$ and eigenvectors

$$x_j^{(1)} = \frac{1}{\sqrt{m}} \tag{4.6}$$

and

$$x_j^{(s)} = \sqrt{\frac{2}{m}}\cos\left(\frac{(2j-1)(s-1)\pi}{2m}\right) \tag{4.7}$$

where $j = 1....., m$ and $s = 2, ...m$. The outline of this chapter is as follows. In section 4.1, we show how to find quantum dragons for $m = 5$, $l = 4$. The main objective of this section is to show how to find quantum dragons for a small number of atoms per slice and

a small number of slices in the device. However, this same analysis can be extended to any number of atoms per slice and any number of even slices, l, in the device. This section will be followed by the general method for 2D system mapping. In section 4.2, we will show the general tuning to obtain quantum dragon. Section 4.3 puts all the results into perspective. Here all plots obtained will be shown and discussed. The summary of results for our $--$ boundary condition are given in section 4.4.

4.1 Quantum dragons for $m = 5$, $l = 4$ with nn and nnn interactions

Assume the nanodevice has five atoms per slice at slice $j = \mu$. See Fig. 4.1.

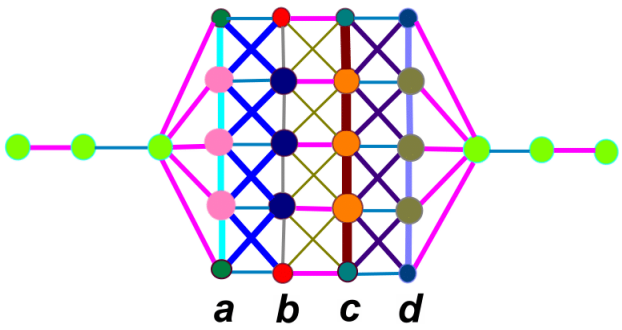

Figure 4.1

An example of the case of dimerized leads, and rectangular nanodevice for $--$ boundary conditions.

In Fig. 4.1, the vertical lines show the intra-slice hopping. Here, $m = 5$, $l = 4$ and therefore $ml = 20$. The device has non-uniform intra-slices. The device is coupled to

the single channel incoming and outgoing leads. Here, only three atoms in the lead are shown. The inter-slice coupling matrices are for nn shown by the horizontal line (magenta and light blue color) and the nnn shown by (deep blue, dark yellow and black color) line segments which form an X-shape. Appropriate choices of the tight-binding parameters makes this disordered nanodevice into a quantum dragon.

The intra-slice coupling matrices have the form

$$\mathbf{A}_\mu = \begin{pmatrix} \epsilon_\mu - t_\mu & -t_\mu & 0 & 0 & 0 \\ -t_\mu & \epsilon_\mu & -t_\mu & 0 & 0 \\ 0 & -t_\mu & \epsilon_\mu & -t_\mu & 0 \\ 0 & 0 & -t_\mu & \epsilon_\mu & -t_\mu \\ 0 & 0 & 0 & -t_\mu & \epsilon_\mu - t_\mu \end{pmatrix} = \epsilon_\mu \mathbf{I} - t_\mu \mathbf{\Omega} - t_\mu \mathbf{Q} \tag{4.8}$$

where $\mu = a, b, c, d$ for the $l = 4$ slices and ϵ_μ are the on-site energies for the atoms at slice $j = \mu$ and t_μ are the intra-slice hopping parameters between atoms. The eigenvalues of Eq. (4.8) gives $\lambda_{\mu,1} = \epsilon_\mu - 2t_\mu$, $\lambda_{\mu,2} = \frac{1}{2}(-t_\mu - t_\mu\sqrt{5} + 2\epsilon_\mu)$, $\lambda_{\mu,3} = \frac{1}{2}(t_\mu - t_\mu\sqrt{5} + 2\epsilon_\mu)$, $\lambda_{\mu,4} = \frac{1}{2}(-t_\mu + t_\mu\sqrt{5} + 2\epsilon_\mu)$, and $\lambda_{\mu,5} = \frac{1}{2}(t_\mu + t_\mu\sqrt{5} + 2\epsilon_\mu)$.

Now assume the device inter-slice coupling matrices have the form

$$\mathbf{B}_{\varphi,\varphi+1} = \begin{pmatrix} -t_{p,\varphi} - t_{q,\varphi} & -t_{q,\varphi} & 0 & 0 & 0 \\ -t_{q,\varphi} & -t_{p,\varphi} & -t_{q,\varphi} & 0 & 0 \\ 0 & -t_{q,\varphi} & -t_{p,\varphi} & -t_{q,\varphi} & 0 \\ 0 & 0 & -t_{q,\varphi} & -t_{p,\varphi} & -t_{q,\varphi} \\ 0 & 0 & 0 & -t_{q,\varphi} & -t_{p,\varphi} - t_{q,\varphi} \end{pmatrix} = -t_{p,\varphi}\mathbf{I} - t_{q,\varphi}\mathbf{\Omega} - t_{q,\varphi}\mathbf{Q} \tag{4.9}$$

where we will let φ even be $\mathbf{B}_{eo}$ and φ odd be $\mathbf{B}_{oe}$. In the matrix equations above, the matrix $\mathbf{\Omega}$ is explicitly for $m = 5$

$$\mathbf{\Omega} = \begin{pmatrix} 1 & 0 & 0 & 0 & 0 \\ 0 & 0 & 0 & 0 & 0 \\ 0 & 0 & 0 & 0 & 0 \\ 0 & 0 & 0 & 0 & 0 \\ 0 & 0 & 0 & 0 & 1 \end{pmatrix} \tag{4.10}$$

and the matrix $\mathbf{Q}$ is defined as Eq. (3.30). The identity matrix, $\mathbf{I}$ has same dimension as $\mathbf{Q}$. The eigenvectors of Eq. (4.8) and Eq. (4.9) are

$$\vec{v}_5^{5\dagger} = \begin{pmatrix} 1 & 1 & 1 & 1 & 1 \end{pmatrix} \tag{4.11}$$

$$\vec{v}_4^{5\dagger} = \begin{pmatrix} -1 & \frac{1}{2}(1-\sqrt{5}) & 0 & \frac{1}{2}(-1+\sqrt{5}) & 1 \end{pmatrix} \tag{4.12}$$

$$\vec{v}_3^{5\dagger} = \begin{pmatrix} 1 & \frac{1}{2}(-3+\sqrt{5}) & 1-\sqrt{5} & \frac{1}{2}(-3+\sqrt{5}) & 1 \end{pmatrix} \tag{4.13}$$

$$\vec{v}_2^{5\dagger} = \begin{pmatrix} -1 & \frac{1}{2}(1+\sqrt{5}) & 0 & \frac{1}{2}(-1-\sqrt{5}) & 1 \end{pmatrix} \tag{4.14}$$

and

$$\vec{v}_1^{5\dagger} = \begin{pmatrix} 1 & \frac{1}{2}(-3-\sqrt{5}) & 1+\sqrt{5} & \frac{1}{2}(-3-\sqrt{5}) & 1 \end{pmatrix} . \tag{4.15}$$

Now let the matrix of transformation, $\mathbf{X}$ be defined as

$$\mathbf{X} = \begin{pmatrix} \vec{c}_5^{5\dagger} \\ \vec{c}_4^{5\dagger} \\ \vec{c}_3^{5\dagger} \\ \vec{c}_2^{5\dagger} \\ \vec{c}_1^{5\dagger} \end{pmatrix} \tag{4.16}$$

where $\vec{c}_i^{5\dagger}$ and $i = 1$ to $i = 5$ are the normalized vectors of Eq. (4.11) through Eq. (4.15).

Note that from Eq. (4.16)

$$\mathbf{X}\mathbf{X}^{\dagger} = \mathbf{I}\,. \tag{4.17}$$

This means that the device intra-slice matrix at slice $j = \mu$ has been transformed to

$$\mathbf{X}\mathbf{A}_{\mu}\mathbf{X}^{\dagger} = \begin{pmatrix} \lambda_1 & 0 & 0 & 0 & 0 \\ 0 & \lambda_2 & 0 & 0 & 0 \\ 0 & 0 & \lambda_3 & 0 & 0 \\ 0 & 0 & 0 & \lambda_4 & 0 \\ 0 & 0 & 0 & 0 & \lambda_5 \end{pmatrix}. \tag{4.18}$$

Here

$$\lambda_{\mu,1} = \epsilon_{\mu} - 2t_{\mu} \tag{4.19}$$

$$\lambda_{\mu,2} = \frac{1}{2}(-t_{\mu} - t_{\mu}\sqrt{5} + 2\epsilon_{\mu}) \tag{4.20}$$

$$\lambda_{\mu,3} = \frac{1}{2}(t_{\mu} - t_{\mu}\sqrt{5} + 2\epsilon_{\mu}) \tag{4.21}$$

$$\lambda_{\mu,4} = \frac{1}{2}(-t_{\mu} + t_{\mu}\sqrt{5} + 2\epsilon_{\mu} \tag{4.22}$$

and

$$\lambda_{\mu,5} = \frac{1}{2}(t_{\mu} + t_{\mu}\sqrt{5} + 2\epsilon_{\mu}). \tag{4.23}$$

From Eq. (4.19) tuning for the device and the lead hence requires

$$\epsilon_L = \epsilon_{\mu} - 2t_{\mu} \tag{4.24}$$

where ϵ_L is the on-site energy of the atom in the lead. Since the on-site energy of the atom in the lead is set to zero, $\epsilon_L = 0$, this means Eq. (4.24) can be re-expressed as

$$\epsilon_\mu = 2t_\mu. \tag{4.25}$$

Note that ϵ_μ can be any value, and tuning only requires t_μ and ϵ_μ satisfy Eq. (4.25). Furthermore, note Eq. (4.25), allows a different ϵ_μ for every device slice μ. Similarly, for the inter-slice coupling matrices, use the same transformation matrix, $\mathbf{X}$ in Eq. (4.16). Upon multiplying through, this gives

$$\mathbf{X}\mathbf{B}_{\varphi,\varphi+1}\mathbf{X}^\dagger = \mathbf{B}_{diagonal9} \tag{4.26}$$

where

$$\mathbf{B}_{diagonal9} = \begin{pmatrix} \lambda_1 & 0 & 0 & 0 & 0 \\ 0 & \lambda_2 & 0 & 0 & 0 \\ 0 & 0 & \lambda_3 & 0 & 0 \\ 0 & 0 & 0 & \lambda_4 & 0 \\ 0 & 0 & 0 & 0 & \lambda_5 \end{pmatrix} \tag{4.27}$$

Here

$$\lambda_{\varphi,1} = -t_{p,\varphi} - 2t_{q,\varphi} \tag{4.28}$$

$$\lambda_{\varphi,2} = \frac{1}{2}(-t_{p,\varphi} - t_{q,\varphi}\sqrt{5} - 2t_{q,\varphi}) \tag{4.29}$$

$$\lambda_{\varphi,3} = \frac{1}{2}(t_{p,\varphi} - t_{q,\varphi}\sqrt{5} - 2t_{q,\varphi}) \tag{4.30}$$

$$\lambda_{\varphi,4} = \frac{1}{2}(-t_{p,\varphi} + t_{q,\varphi}\sqrt{5} - 2t_{q,\varphi}) \tag{4.31}$$

and

$$\lambda_{\varphi,5} = \frac{1}{2}(t_{p,\varphi} + t_{q,\varphi}\sqrt{5} - 2t_{q,\varphi}). \tag{4.32}$$

From Eq. (4.28), the mapping equation, Eq. (3.14) is satisfied provided $\tilde{s}_{b5} = t_{p,\varphi} + 2t_{q,\varphi}$. Now the last task is to check for the mapping equation for the connection vector for both the incoming and outgoing leads, $\vec{w}$ and $\vec{u}$. To do this, use the same transformation matrix, $\mathbf{X}$ in Eq. (4.16) and define the incoming connection vector, $\vec{w}$ by

$$\vec{w}^{\dagger} = \begin{pmatrix} -\frac{w}{\sqrt{5}} & -\frac{w}{\sqrt{5}} & -\frac{w}{\sqrt{5}} & -\frac{w}{\sqrt{5}} & -\frac{w}{\sqrt{5}} \end{pmatrix} . \tag{4.33}$$

This means that

$$\vec{w}^{\dagger}\mathbf{X} = \begin{pmatrix} -w & 0 & 0 & 0 & 0 \end{pmatrix} . \tag{4.34}$$

Hence the mapping Eq. (3.11) is satisfied. Similarly define, the outgoing connection vector, $\vec{u}$ as

$$\vec{u} = \begin{pmatrix} -\frac{u}{\sqrt{5}} \\ -\frac{u}{\sqrt{5}} \\ -\frac{u}{\sqrt{5}} \\ -\frac{u}{\sqrt{5}} \\ -\frac{u}{\sqrt{5}} \end{pmatrix} . \tag{4.35}$$

This means that

$$\mathbf{X}\vec{u} = \begin{pmatrix} -u \\ 0 \\ 0 \\ 0 \\ 0 \end{pmatrix} . \tag{4.36}$$

Thus the mapping Eq. (3.12) is satisfied. Therefore to find quantum dragons tune the on-site energy of the atoms at slice μ to $\epsilon_\mu = 2t_\mu$, as well as $\tilde{s}_{b5} = t_{p,\varphi} + 2t_{q,\varphi}$, and $\vec{w} = \vec{u} = \begin{pmatrix} -\frac{t_{eo}}{\sqrt{5}} \\ -\frac{t_{eo}}{\sqrt{5}} \\ -\frac{t_{eo}}{\sqrt{5}} \\ -\frac{t_{eo}}{\sqrt{5}} \\ -\frac{t_{eo}}{\sqrt{5}} \end{pmatrix}$.

Quantum dragons can also be found when the device has only nn interactions. This means that for such a device, the inter-slice coupling matrices are proportional to the identity matrix. Thus $\mathbf{B}_{\varphi,\varphi+1} = -t_{p,\varphi}\mathbf{I}$. This assumption has been used by Novotny in 2015 [24] to find quantum dragons. When the device has only nn interactions, to find quantum dragons, tune the on-site energies of the atoms at slice $j = \mu$ to $\epsilon_\mu = 2t_\mu$, as well as $\tilde{s}_{b6} = t_{p,\varphi}$, and $\vec{w} = \vec{u} = \begin{pmatrix} -\frac{t_{eo}}{\sqrt{5}} \\ -\frac{t_{eo}}{\sqrt{5}} \\ -\frac{t_{eo}}{\sqrt{5}} \\ -\frac{t_{eo}}{\sqrt{5}} \\ -\frac{t_{eo}}{\sqrt{5}} \end{pmatrix}$.

4.1.1 General method for 2D system mapping

In this section, the general method to do the mapping for a general 2D system is presented for the single-layer planar rectangular crystals with boundary condition $--$. As-

sume there are m atoms per slice in the nanodevice. The intra-slice coupling matrix associated with the device at slice $j = \mu$ can be expressed as

$$\mathbf{A}_{\mu} = \epsilon_{\mu}\mathbf{I} - t_{\mu}\mathbf{Q} - t_{\mu}\mathbf{\Omega}\,. \tag{4.37}$$

The eigenvalues of the matrix $\mathbf{A}_{\mu}$ can be expressed as [67, 68]

$$\lambda_{s,\mu} = \epsilon_{\mu} - 2t_{\mu}\cos\left(\frac{(s-1)\pi}{m}\right) \tag{4.38}$$

where $s = 1, ...m$. Assume the inter-slice coupling matrices for the device (odd-even and even-odd) have the form

$$\mathbf{B}_{\varphi,\varphi+1} = -t_{p,\varphi}\mathbf{I} - t_{q,\varphi}\mathbf{Q} - t_{q,\varphi}\mathbf{\Omega}\,. \tag{4.39}$$

In Eq. (4.37) and Eq. (4.39), the matrix $\mathbf{Q}$ has been shown in Eq. (3.2) and the matrix $\mathbf{I}$ is an identity matrix with same dimension as matrix $\mathbf{Q}$. The eigenvalues of Eq. (4.39) can be expressed as [67, 68]

$$\lambda_{s,\varphi} = -t_{p,\varphi} - 2t_{q,\varphi}\cos\left(\frac{(s-1)\pi}{m}\right) \tag{4.40}$$

where $s = 1, ...m$. Assume further that there is a single incoming lead atom which is coupled to the m atoms in the device at slice $\mu = 1$. This means that the incoming connection vector $\vec{w}$ is of dimension m. This further suggests that the outgoing connection vector $\vec{u}$ is of dimension m. After making these assumptions the sets of mapping equations are given in Eq. (3.11) through Eq. (3.14). The elements of the eigenvectors of the inter-slice and intra-slice coupling matrices are [67, 68]

$$x_j^{(1)} = \frac{1}{\sqrt{m}} \tag{4.41}$$

and

$$x_j^{(s)} = \sqrt{\frac{2}{m}} \cos\left(\frac{(2j-1)(s-1)\pi}{2m}\right) \tag{4.42}$$

where $j = 1.....,m$ and $s = 2, ...m$. With these eigenvectors, form the matrix of transformation $\mathbf{X}$ such that

$$\mathbf{X} = \sqrt{\frac{2}{m}} \begin{pmatrix} \frac{1}{\sqrt{2}} & \frac{1}{\sqrt{2}} & \frac{1}{\sqrt{2}} & \frac{1}{\sqrt{2}} & \cdots & \cdots & \cdots & \cdots \\ \cos(\frac{\pi}{2m}) & \cos(\frac{\pi}{m}) & \cos(\frac{3\pi}{2m}) & \cos(\frac{2\pi}{m}) & \cdots & \cdots & \cdots & \\ \cos(\frac{3\pi}{2m}) & \cos(\frac{3\pi}{m}) & \cos(\frac{9\pi}{2m}) & \cos(\frac{6\pi}{m}) & \cdots & \cdots & \cdots & \cdots \\ \cos(\frac{5\pi}{2m}) & \cos(\frac{5\pi}{m}) & \cos(\frac{15\pi}{2m}) & \cos(\frac{10\pi}{m}) & \cdots & \cdots & \cdots & \cdots \\ \cos(\frac{7\pi}{2m}) & \cos(\frac{7\pi}{m}) & \cos(\frac{21\pi}{2m}) & \cos(\frac{14\pi}{m}) & \cdots & \cdots & \cdots & \cdots \\ \cos(\frac{9\pi}{2m}) & \cos(\frac{9\pi}{m}) & \cos(\frac{27\pi}{2m}) & \cos(\frac{18\pi}{m}) & \cdots & \cdots & \cdots & \cdots \\ \cos(\frac{11\pi}{2m}) & \cos(\frac{11\pi}{m}) & \cos(\frac{33\pi}{2m}) & \cos(\frac{22\pi}{m}) & \cdots & \cdots & \cdots & \cdots \\ \cos(\frac{13\pi}{2m}) & \cos(\frac{13\pi}{m}) & \cos(\frac{39\pi}{2m}) & \cos(\frac{26\pi}{m}) & \cdots & \cdots & \cdots & \cdots \end{pmatrix} \tag{4.43}$$

where the matrix is written for $m = 8$, and only four columns are shown. Note that from Eq. (4.43)

$$\mathbf{X}\mathbf{X}^\dagger = \mathbf{I}\,. \tag{4.44}$$

Since $\mathbf{X}$ is unitary, $\mathbf{A}_\mu$ can be diagonalized as

$$\mathbf{X}\mathbf{A}_\mu\mathbf{X}^\dagger = \mathbf{A}_{diagonal} \tag{4.45}$$

here $\mathbf{A}_{diagonal}$ is

$$\mathbf{A}_{diagonal} = \begin{pmatrix} \lambda_{31} & 0 & \cdots & 0 & 0 \\ 0 & \lambda_{32} & \cdots & 0 & 0 \\ \vdots & \vdots & \ddots & \vdots & \vdots \\ 0 & 0 & \cdots & \lambda_{3,m-1} & 0 \\ 0 & 0 & \cdots & 0 & \lambda_{3m} \end{pmatrix} \tag{4.46}$$

with the eigenvalues of Eq. (4.40). Similarly, for the inter-slice coupling matrices use the same transformation $\mathbf{X}$. Upon multiplying through this gives

$$\mathbf{X}\mathbf{B}_{\varphi,\varphi+1}\mathbf{X}^{\dagger} = \mathbf{B}_{diagonal} \tag{4.47}$$

here $\mathbf{B}_{diagonal}$ is

$$\mathbf{B}_{diagonal} = \begin{pmatrix} \lambda_{41} & 0 & \cdots & 0 & 0 \\ 0 & \lambda_{42} & \cdots & 0 & 0 \\ \vdots & \vdots & \ddots & \vdots & \vdots \\ 0 & 0 & \cdots & \lambda_{4,m-1} & 0 \\ 0 & 0 & \cdots & 0 & \lambda_{4m} \end{pmatrix} \tag{4.48}$$

with the eigenvalues of Eq. (4.40). Now the last task is to check for the mapping equation for the connection vector for both the incoming and outgoing leads, $\vec{w}$ and $\vec{u}$. To do this, use the same transformation matrix, $\mathbf{X}$ in Eq. (4.43) and define the incoming connection vector, $\vec{w}$ by

$$\vec{w}^{\dagger} = \begin{pmatrix} -w_{11} & -w_{12} & -w_{13} & -w_{14} & \cdots & -w_{1m} \end{pmatrix} . \tag{4.49}$$

This means that

$$\vec{w}^{\dagger}\mathbf{X} = \begin{pmatrix} -w_{11} & 0 & 0 & 0 & 0 & \cdots & \cdots & 0 \end{pmatrix} \tag{4.50}$$

provided from Eq. (4.41) $\vec{w}^{\dagger} = -w_{11}\vec{v}^{(1)\dagger}$. Thus in effect the mapping Eq. (3.11) is satisfied. Similarly define the outgoing connection vector, $\vec{u}$ as

$$\vec{u} = \begin{pmatrix} -u_{11} \\ -u_{12} \\ -u_{13} \\ -u_{14} \\ -u_{15} \\ \vdots \\ -u_{1n} \end{pmatrix} . \tag{4.51}$$

This means that

$$\mathbf{X}\vec{u} = \begin{pmatrix} -u_{11} \\ 0 \\ 0 \\ 0 \\ 0 \\ \vdots \\ \vdots \\ 0 \end{pmatrix} \tag{4.52}$$

for $\vec{u}^{\dagger} = -u_{11}\vec{v}^{(1)}$ and hence mapping Eq. (3.12) is satisfied.

4.2 General tuning: Quantum dragon

In the absence of a magnetic field, the maximum eigenvalue corresponds to $s = 1$, which means that from Eq. (4.46) and the mapping Eq. (3.13), tuning for the device and the lead requires that

$$\epsilon_L = \lambda_{31} = 0. \tag{4.53}$$

Here also, the assumption that the atoms in the incoming and outgoing leads are the same has been made. It is traditional to chose ϵ_L as the zero of energy. Similarly, for the device inter-slice coupling matrices, Eq. (4.48), the mapping Eq. (3.14) is satisfied provided

$$\tilde{s}_{bxx} = \lambda_{41}. \tag{4.54}$$

Here, $\vec{w} = \vec{u} = -t_{eo}\vec{v}^{(1)}$.

4.3 Results

In this section of the thesis, the results for the boundary condition $--$ are presented and then discussed. Here, we show quantum dragon solutions, Fano resonance of the electron transmission probability, as well as the mean and the standard deviation of the electron transmission probability vs δ. As seen in Fig. 4.2 through Fig. 4.5, quantum dragons exist for the nanodevice when there is correlated disorder and when we tune correctly some tight binding parameters in the device. The quantum dragon solutions are shown by $\mathcal{T}(E) = 1$ (darker blue) in all cases. Because quantum dragons have unity electron transmission probability, this means that quantum dragons have no Fano resonance, F, since $F = 1-\mathcal{T}(E)$. When the tight-binding parameters are uncorrelated, Fano resonances are seen in all cases. As can be seen in Fig. 4.2 through Fig. 4.5, as the strength of the

disorder increases, we move away from the quantum dragon solutions. As seen in Fig. 4.6 and Fig. 4.7, the mean electron transmission probability decreases with increasing disorder, δ. This makes perfect sense because as the strength of disorder increases, the uncorrelated randomness in the device increases and hence the mean electron transmission probability decreases. This result is true for both dimerized leads and uniform leads attached to the nanodevice. It should be pointed out that in all cases the leads attached to the device do not have disorder.

In quantum dragon solutions, there is correlated disorder between the leads and the nanodevice and the parameters in the device must be tuned correctly to obtain $\mathcal{T} = 1$ for all energies. In the case of Fano resonance the random numbers are generated using a normal distribution.

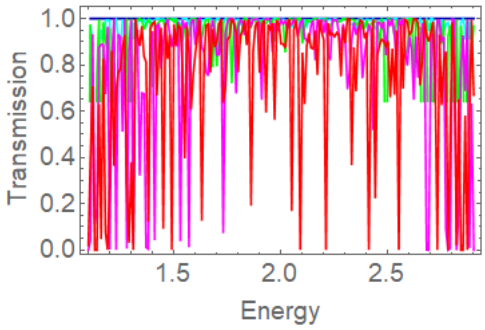

Figure 4.2

$\mathcal{T}$ vs E, boundary condition $--$, dimerized leads.

Fig. 4.2, is a plot of transmission vs E. The device has $m = 5$, $l = 14$ and therefore $ml = 70$ atoms. This plot is for the non-uniform leads ($t_{oe} = 1$ and $t_{eo} = 2$). The line $\mathcal{T} = 1$ (darker blue) has the on-site energy, $\epsilon_j = 2t_j$. The on-site energies are modeled by $\epsilon_j = 2t_j + \delta\Sigma$ and the intra-slice hopping terms are modeled by $t_j = t + \delta\Sigma$. The inter-slice hopping parameters are modeled by $t_p = t_{oe} + \delta\Sigma$ and $t_\lambda = t_{eo} + \delta\Sigma$ where $\delta = 0.0, 0.05, 0.1, 0.15, 0.2$ and Σ is a Gaussian random number of zero mean and unit standard deviation. The intra-slice hopping strengths used are non-uniform. The cyan, green, magenta and the red color shows Fano resonances in the nanodevice.

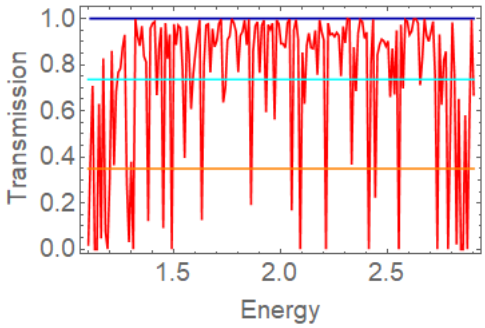

Figure 4.3

$\mathcal{T}$ vs E, boundary condition $--$, dimerized leads, $\delta = 0.2$

Fig. 4.3, is the same as Fig. 4.2, except only for the two values $\delta = 0$ (a quantum dragon) and $\delta = 0.2$. The red color shows Fano resonances in the nanodevice. The cyan and the orange color shows the mean and the standard deviation of the electron transmission probability as a function of E in the nanodevice for $\delta = 0.2$.

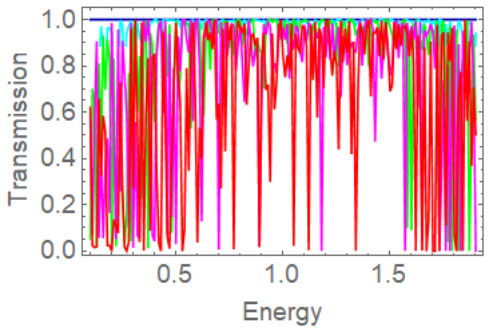

Figure 4.4

$\mathcal{T}$ vs E, boundary condition $--$, uniform leads.

Fig. 4.4, is a plot of transmision vs E. The nanodevice has $m = 5$, $l = 14$ and therefore $ml = 70$ atoms. This plot is for the uniform leads ($t_{oe} = 1$ and $t_{eo} = 1$). The line $\mathcal{T} = 1$ (darker blue) has the on-site energy, $\epsilon_j = 2t_j$. The on-site energies are modeled by $\epsilon_j = 2t_j + \delta\Sigma$ and the intra-slice hopping terms are modeled by $t_j = t + \delta\Sigma$. The inter-slice hopping parameters are modeled by $t_p = t_{oe} + \delta\Sigma$ and $t_\lambda = t_{eo} + \delta\Sigma$ where $\delta = 0.0, 0.05, 0.1, 0.15, 0.2$ and Σ is a normally distibuted random number. The intra-slice hopping strengths used are non-uniform. The cyan, green, magenta and red color shows Fano resonances in the nanodevice.

Fig. 4.5, is the same as Fig. 4.4, except only for two values $\delta = 0$ (a quantum dragon) and $\delta = 0.2$. The cyan and the orange color shows the mean and the standard deviation of the electron transmission probability as a function of E for $\delta = 0.2$.

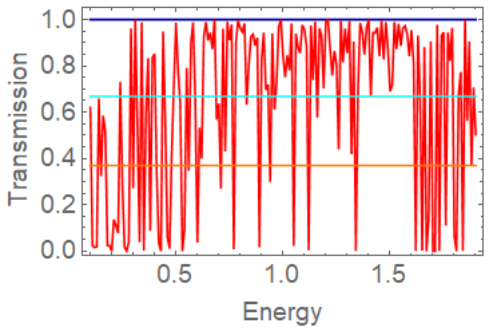

Figure 4.5

$\mathcal{T}$ vs E, boundary condition $--$, uniform leads, $\delta = 0.2$.

4.4 Summary

In this chapter, it has been shown how to find quantum dragons for $m = 5$, $l = 4$ for single-layer planar rectangular crystals with boundary condition $--$. Here, the connection vector used is busbar. That is the connection between the leads and every atom in the first and last slice of the device are of the same strength. When there is uncorrelated random disorder in the nanodevice, Fano resonances are seen as in Fig. 4.2 through Fig. 4.5. Quantum dragons have no Fano resonances since the electron tranmission probability is unity for all energies. Fano resonances are also expected to be observed when the dimerized and non-dimerized leads are connected to homogeneous slices when there is complete uncorrelated randomness in the nanodevice. For m atoms per slice in the device with l number of slices in the nanodevice, where here l is even number, the general approach to find quantum dragons has also been shown.

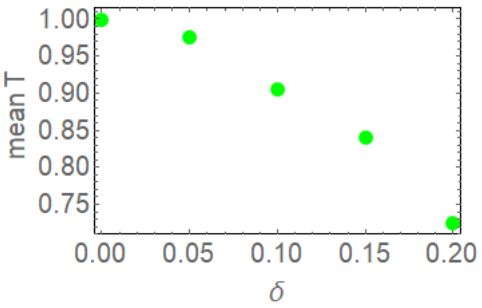

Figure 4.6

$\langle \mathcal{T} \rangle$ vs δ, boundary condition $--$, non-uniform leads.

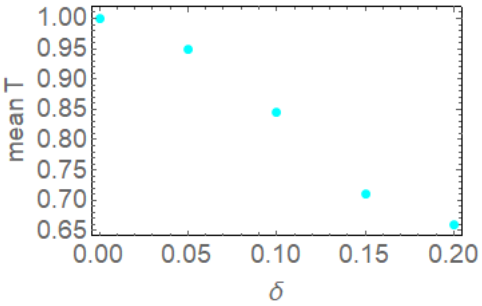

Figure 4.7

$\langle \mathcal{T} \rangle$ vs δ, boundary condition $--$, uniform leads

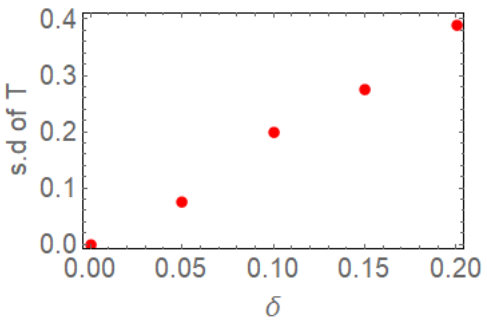

Figure 4.8

std $\mathcal{T}$ vs δ, boundary condition $--$, dimerized leads

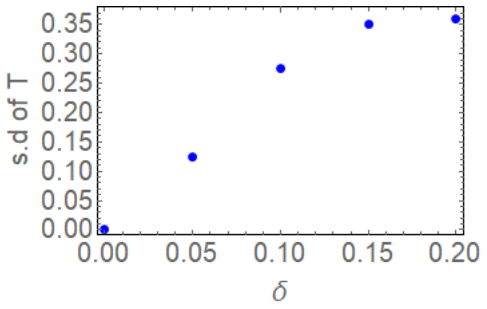

Figure 4.9

std $\mathcal{T}$ vs δ, boundary condition $--$, uniform leads

CHAPTER 5

QUANTUM DRAGON SOLUTIONS FOR RECTANGULAR CRYSTALS : CASE 3: BOUNDARY CONDITION $++$

It is shown in this section how to find quantum dragons for single-layer planar rectangular crystals using boundary conditions which we label as $++$. We call the boundary conditions $++$ because in Eq. (1.25), we set ($\beta = \gamma = b$). The connections used in this chapter are modified busbar. There are two ways to find quantum dragons: (1) we assume the inter-slice coupling matrices for the nanodevice has nn and nnn interactions and (2) we assume the inter-slice coupling matrices is proportional to the identity matrix. In other words, the device has only nn interactions. In the absence of nnn interactions this gives results in [24]. From Eq. (1.25), by setting ($\beta = \gamma = b$), the tridiagonal matrix of dimension $m \times m$ has the form

$$\mathbf{A} = \begin{pmatrix} a+b & -b & 0 & \cdots & 0 & 0 \\ -b & a & -b & \cdots & 0 & 0 \\ 0 & -b & a & \cdots & 0 & 0 \\ \vdots & \vdots & \vdots & \ddots & \vdots & \vdots \\ 0 & 0 & 0 & \cdots & a & -b \\ 0 & 0 & 0 & \cdots & -b & a+b \end{pmatrix} = a\mathbf{I} + b\mathbf{\Omega} - b\mathbf{Q} \tag{5.1}$$

where a and b are real numbers. In Eq. (5.1), the matrix $\mathbf{Q}$ has been shown in Eq. (3.2) and the matrix $\mathbf{\Omega}$ is defined as Eq. (4.2). Our nanodevice has an intra-slice coupling matrix of the form (written for $m = 8$)

$$\mathbf{A} = \begin{pmatrix} \epsilon + t & -t & 0 & 0 & 0 & 0 & 0 & 0 \\ -t & \epsilon & -t & 0 & 0 & 0 & 0 & 0 \\ 0 & -t & \epsilon & -t & 0 & 0 & 0 & 0 \\ 0 & 0 & -t & \epsilon & -t & 0 & 0 & 0 \\ 0 & 0 & 0 & -t & \epsilon & -t & 0 & 0 \\ 0 & 0 & 0 & 0 & -t & \epsilon & -t & 0 \\ 0 & 0 & 0 & 0 & 0 & -t & \epsilon & -t \\ 0 & 0 & 0 & 0 & 0 & 0 & -t & \epsilon + t \end{pmatrix} = \epsilon\mathbf{I} - t\mathbf{Q} + t\mathbf{\Omega} \tag{5.2}$$

and an inter-slice coupling matrix of the form (written for $m = 8$)

$$\mathbf{B} = \begin{pmatrix} -t_x + t_y & -t_y & 0 & 0 & 0 & 0 & 0 & 0 \\ -t_y & -t_x & -t_y & 0 & 0 & 0 & 0 & 0 \\ 0 & -t_y & -t_x & -t_y & 0 & 0 & 0 & 0 \\ 0 & 0 & -t_y & -t_x & -t_y & 0 & 0 & 0 \\ 0 & 0 & 0 & -t_y & -t_x & -t_y & 0 & 0 \\ 0 & 0 & 0 & 0 & -t_y & -t_x & -t_y & 0 \\ 0 & 0 & 0 & 0 & 0 & -t_y & -t_x & -t_y \\ 0 & 0 & 0 & 0 & 0 & 0 & -t_y & -t_x + t_y \end{pmatrix} = -t_x\mathbf{I} - t_y\mathbf{Q} + t_y\mathbf{\Omega} \tag{5.3}$$

where t's are the hopping strengths which are non-negative real numbers and ϵ is the on-site energy of the atom which is a real number. Eq. (5.1) is a matrix with eigenvalues expressed as [67, 68]

$$\lambda_s = a + 2b\cos\left(\frac{s\pi}{m}\right) \tag{5.4}$$

where $s = 1, ...m$ and with eigenvectors expressed as

$$x_j^{(s)} = \frac{\sqrt{2}}{\sqrt{m}}\sin\left(\frac{(2j-1)s\pi}{2m}\right) \tag{5.5}$$

where $j = 1....., m$ and $s = 1, ...m$. The outline for this chapter is as follows. In section 5.1 and section 5.2, we show how to find quantum dragons for $m = 3$, $l = 4$ and $m = 5$, $l = 4$ respectively. The main objective of these sections are to show how to find quantum dragons for a small number of atoms per slice and a small number of slices in the device. However, this same analysis can be extended to any number of atoms per slice and any number of even slices, l in the device. In section 5.3, we will introduce the general method for 2D system mapping. In section 5.4, we will show the general tuning to obtain quantum dragons. Section 5.5, puts all the results into perspective. Here all plots obtained will be shown and then discussed. The summary of results for our $++$ boundary condition are given in section 5.6.

5.1 Quantum dragons for $m = 3$, $l = 4$ with nnn and nn interactions

Assume the nanodevice has three atoms per slice at slice $j = \upsilon$. See Fig. 5.1. Fig. 5.1 is an example of rectangular device with boundary condition $++$. The vertical lines show intra-slice hopping. Here, $m = 3$, $l = 4$ and therefore $ml = 12$. The nanodevice has non-uniform intra-slice parameters. The nanodevice is coupled to the single incoming and

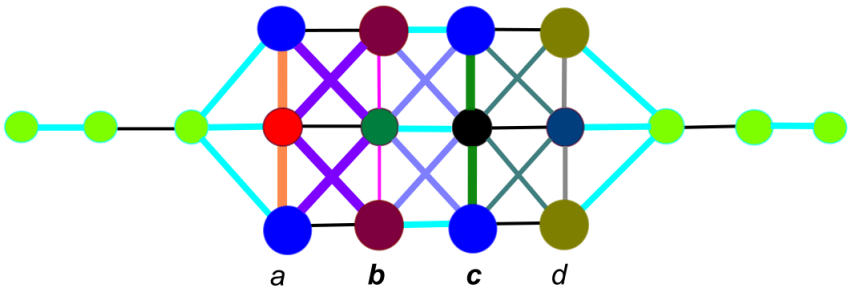

Figure 5.1

An example of the case of dimerized leads, and a rectangular device, for $++$ boundary conditions

outgoing dimerized lead. The inter-slice coupling matrices are for nn shown by the horizontal line (black and cyan colors) and the nnn shown by (violet, light blue and deep green color) line segments which form an X-shape. Appropriate choices of the tight-binding parameters makes this disordered nanodevice into a quantum dragon.

Let assume the intra-slice coupling matrices have the form

$$A_\upsilon = \begin{pmatrix} \epsilon_\upsilon + t_\upsilon & -t_\upsilon & 0 \\ -t_\upsilon & \epsilon_\upsilon & -t_\upsilon \\ 0 & -t_\upsilon & \epsilon_\upsilon + t_\upsilon \end{pmatrix} = \epsilon_\upsilon \mathbf{I} + t_\upsilon \mathbf{\Omega} - t_\upsilon \mathbf{Q} \tag{5.6}$$

where $\upsilon = a, b, c, d$ for the $l = 4$ slices and ϵ_υ are the on-site energies of the atoms at slice $j = \upsilon$ and t_υ are the intra-slice hopping parameters between atoms. The eigenvalues of

Eq. (5.6), are $\lambda_{\upsilon,1} = \epsilon_\upsilon - t_\upsilon$, $\lambda_{\upsilon,2} = \epsilon_\upsilon + t_\upsilon$, $\lambda_{\upsilon,3} = \epsilon_\upsilon + 2t_\upsilon$. Now assume the device inter-slice coupling matrices have the form

$$\mathbf{B}_{\tau,\tau+1} = \begin{pmatrix} -t_{\sigma,\tau} + t_{\rho,\tau} & -t_{\rho,\tau} & 0 \\ -t_{\rho,\tau} & -t_{\sigma,\tau} & -t_{\rho,\tau} \\ 0 & -t_{\rho,\tau} & -t_{\sigma,\tau} + t_{\rho,\tau} \end{pmatrix} = -t_{\sigma,\tau}\mathbf{I} + t_{\rho,\tau}\mathbf{\Omega} - t_\rho\mathbf{Q} \tag{5.7}$$

where we will let $\mathbf{B}_{\tau,\tau+1}$ with τ even be $\mathbf{B}_{eo}$ and τ odd be $\mathbf{B}_{oe}$. The normalized eigenvectors of Eq. (5.6) and Eq. (5.7) are

$$\vec{v}_3^{3\dagger} = \begin{pmatrix} \frac{1}{\sqrt{6}} & \frac{2}{\sqrt{6}} & \frac{1}{\sqrt{6}} \end{pmatrix} \tag{5.8}$$

$$\vec{v}_2^{3\dagger} = \begin{pmatrix} \frac{-1}{\sqrt{2}} & 0 & \frac{1}{\sqrt{2}} \end{pmatrix} \tag{5.9}$$

and

$$\vec{v}_1^{3\dagger} = \begin{pmatrix} \frac{1}{\sqrt{3}} & \frac{-1}{\sqrt{3}} & \frac{1}{\sqrt{3}} \end{pmatrix} . \tag{5.10}$$

Now let the matrix of transformation, $\mathbf{X}$ be defined as

$$\mathbf{X} = \begin{pmatrix} \vec{v}_3^{3\dagger} \\ \vec{v}_2^{3\dagger} \\ \vec{v}_1^{3\dagger} \end{pmatrix} . \tag{5.11}$$

Note that from Eq. (5.11),

$$\mathbf{X}\mathbf{X}^\dagger = \mathbf{I} . \tag{5.12}$$

This means that the device intra-slice matrix at slice $j = \upsilon$ has been transformed to

$$\mathbf{X}\mathbf{A}_\upsilon\mathbf{X}^\dagger = \begin{pmatrix} \epsilon_\upsilon - t_\upsilon & 0 & 0 \\ 0 & \epsilon_\upsilon + t_\upsilon & 0 \\ 0 & 0 & \epsilon_\upsilon + 2t_\upsilon \end{pmatrix} . \tag{5.13}$$

From Eq. (5.13) and the mapping Eq. (3.13), tuning for the device and the lead hence requires

$$\epsilon_L = \epsilon_\upsilon - t_\upsilon \tag{5.14}$$

where ϵ_L is the on-site energy of the atom in the lead. Since the on-site energy of the atom in the lead is set to zero, $\epsilon_L = 0$, this means Eq. (5.14) and can be re-expressed as

$$\epsilon_\upsilon = t_\upsilon. \tag{5.15}$$

Note that ϵ_υ can be any value, and the tuning t_υ and ϵ_υ must satisy Eq. (5.15). Furthermore, note Eq. (5.15) allows a different ϵ_υ for every device slice υ. Similarly, for the inter-slice coupling matrices, use the same transformation matrix, $\mathbf{X}$ in Eq. (5.11). Upon multiplying through, this gives

$$\mathbf{X}\mathbf{B}_{\tau,\tau+1}\mathbf{X}^\dagger = \mathbf{B}_{diagonal11} \tag{5.16}$$

where

$$\mathbf{B}_{diagonal11} = \begin{pmatrix} -t_{\sigma,\tau} - t_\rho & 0 & 0 \\ 0 & -t_\sigma + t_\rho & 0 \\ 0 & 0 & -t_\sigma + 2t_\rho \end{pmatrix}. \tag{5.17}$$

Therefore the mapping equation, Eq. (3.14) is satisfied provided $\tilde{s}_{b7} = t_{\sigma,\tau} + t_\rho$. Now the last task is to check for the mapping equation for the connection vector for the incoming and outgoing leads, $\vec{w}$ and $\vec{u}$. To do this, use the same transformation matrix, $\mathbf{X}$ in Eq. (5.11) and then define the connection vector for the incoming lead, $\vec{w}$ by

$$\vec{w}^\dagger = \begin{pmatrix} -\frac{w}{\sqrt{6}} & -\frac{2w}{\sqrt{6}} & -\frac{w}{\sqrt{6}} \end{pmatrix}. \tag{5.18}$$

This means that

$$\vec{w}^{\dagger}\mathbf{X} = \begin{pmatrix} -w & 0 & 0 \end{pmatrix} . \tag{5.19}$$

Similarly define the connection vector for the outgoing leads, $\vec{u}$, by

$$\vec{u} = \begin{pmatrix} -\frac{u}{\sqrt{6}} \\ -\frac{2u}{\sqrt{6}} \\ -\frac{u}{\sqrt{6}} \end{pmatrix} . \tag{5.20}$$

This means that

$$\mathbf{X}\vec{u} = \begin{pmatrix} -u \\ 0 \\ 0 \end{pmatrix} . \tag{5.21}$$

Thus in effect the mapping equations, Eq. (3.11) and Eq. (3.12) are satisfied. Therefore to find quantum dragons tune the on-site energy of the atoms at slice $j = \upsilon$ to $\epsilon_{\upsilon} = t_{\upsilon}$, as well as $\tilde{s}_{b7} = t_{\sigma,\tau} + t_{\rho}$ and $\vec{w} = \vec{u} = \begin{pmatrix} -\frac{t_{eo}}{\sqrt{6}} \\ -\frac{2t_{eo}}{\sqrt{6}} \\ -\frac{t_{eo}}{\sqrt{6}} \end{pmatrix}$.

5.1.1 Quantum dragons for $m = 3$, $l = 4$ with nn interactions

In Eq. (5.7), the inter-slice coupling matrices odd-even and even-odd are defined in terms of nearest neighbor and next neighbor interaction. This assumption has already been used to find quantum dragons for the three atom device. Quantum dragons can also be found by relaxing this earlier assumption. Here assume that the inter-slice coupling matrices, $\mathbf{B}_{\tau,\tau+1}$ are proportional to the identity matrix. Hence the device has $\mathbf{B}_{\tau,\tau+1} =$

$-t_{\sigma,\tau}\mathbf{I}$. Therefore to find quantum dragons tune the on-site energy of the atoms at slice $j = \upsilon$ to $\epsilon_\upsilon = t_\upsilon$, as well as $\tilde{s}_{b8} = t_{\sigma,\tau}$ and $\vec{w} = \vec{u} = \begin{pmatrix} -\frac{t_{eo}}{\sqrt{6}} \\ -\frac{2t_{eo}}{\sqrt{6}} \\ -\frac{t_{eo}}{\sqrt{6}} \end{pmatrix}$.

5.2 Quantum dragons for $m = 5, l = 4$ with nn and nnn interactions

Assume that the nanodevice has five atoms per slice at slice $j = \upsilon$. See Fig. 5.2.

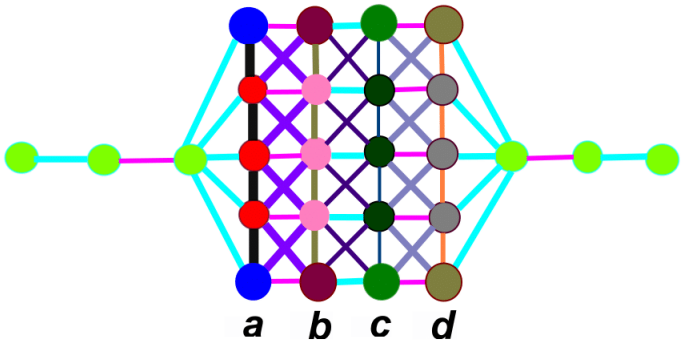

Figure 5.2

An example of the case of dimerized leads, and a rectangular device for boundary conditions $++$.

Fig. 5.2 is an example of rectangular device with boundary condition $++$. The vertical lines show intra-slice hopping. Here, $m = 5$ and $l = 4$ and therefore $ml = 20$. The device

has non-uniform intra-slice terms. The nanodevice is coupled to the single incoming and outgoing lead. The inter-slice coupling matrices are for nn shown by the horizontal line segments (blush and cyan color) and the nnn interactions shown by (violet, cyan and light violet color) line segments which form an X-shape. Appropriate choices of the tight-binding parameters makes this disordered nanodevice into a quantum dragon.

Assume the intra-slice coupling matrices have the form

$$\mathbf{A}_{\upsilon} = \begin{pmatrix} \epsilon_{\upsilon}+t_{\upsilon} & -t_{\upsilon} & 0 & 0 & 0 \\ -t_{\upsilon} & \epsilon_{\upsilon} & -t_{\upsilon} & 0 & 0 \\ 0 & -t_{\upsilon} & \epsilon_{\upsilon} & -t_{\upsilon} & 0 \\ 0 & 0 & -t_{\upsilon} & \epsilon_{\upsilon} & -t_{\upsilon} \\ 0 & 0 & 0 & -t_{\upsilon} & \epsilon_{\upsilon}+t_{\upsilon} \end{pmatrix} = \epsilon_{\upsilon}\mathbf{I} + t_{\upsilon}\mathbf{\Omega} - t_{\upsilon}\mathbf{Q} \tag{5.22}$$

where $\upsilon = a, b, c, d$ for the $l = 4$ slices and ϵ_{υ} are the on-site energies for the atoms at slice $j = \upsilon$ and t_{υ} are the intra-slice hopping parameters between atoms. Finding the eigenvalues of Eq. (5.22) gives $\lambda_{\upsilon,1} = \epsilon_{\upsilon} + 2t_{\upsilon}$, $\lambda_{\upsilon,2} = \frac{1}{2}(-t_{\upsilon} - t_{\upsilon}\sqrt{5} + 2\epsilon_{\upsilon})$, $\lambda_{\upsilon,3} = \frac{1}{2}(t_{\upsilon} - t_{\upsilon}\sqrt{5} + 2\epsilon_{\upsilon})$, $\lambda_{\upsilon,4} = \frac{1}{2}(-t_{\upsilon} + t_{\upsilon}\sqrt{5} + 2\epsilon_{\upsilon})$, and $\lambda_{\upsilon,5} = \frac{1}{2}(t_{\upsilon} + t_{\upsilon}\sqrt{5} + 2\epsilon_{\upsilon})$. Now assume the device inter-slice coupling matrices have the form

$$\mathbf{B}_{\tau,\tau+1} = \begin{pmatrix} -t_{\sigma,\tau}+t_{\rho,\tau} & -t_{\rho,\tau} & 0 & 0 & 0 \\ -t_{\rho,\tau} & -t_{\sigma,\tau} & -t_{\rho,\tau} & 0 & 0 \\ 0 & -t_{\rho,\tau} & -t_{\sigma,\tau} & -t_{\rho,\tau} & 0 \\ 0 & 0 & -t_{\rho,\tau} & -t_{\sigma,\tau} & -t_{\rho,\tau} \\ 0 & 0 & 0 & -t_{\rho,\tau} & -t_{\sigma,\tau}+t_{\rho,\tau} \end{pmatrix} = -t_{\sigma,\tau}\mathbf{I}+t_{\rho,\tau}\mathbf{\Omega}-t_{\rho,\tau}\mathbf{Q}. \tag{5.23}$$

The eigenvectors are of Eq. (5.22) and Eq. (5.23) are

$$\vec{v}_5^{5\dagger} = \begin{pmatrix} 1 & -1 & 1 & -1 & 1 \end{pmatrix} \tag{5.24}$$

$$\vec{v}_4^{5\dagger} = \begin{pmatrix} 1 & \frac{1}{2}(3+\sqrt{5}) & 1+\sqrt{5} & \frac{1}{2}(3+\sqrt{5}) & 1 \end{pmatrix} \tag{5.25}$$

$$\vec{v}_3^{5\dagger} = \begin{pmatrix} -1 & \frac{1}{2}(-1-\sqrt{5}) & 0 & \frac{1}{2}(1+\sqrt{5}) & 1 \end{pmatrix} \tag{5.26}$$

$$\vec{v}_2^{5\dagger} = \begin{pmatrix} 1 & \frac{1}{2}(3-\sqrt{5}) & 1-\sqrt{5} & \frac{1}{2}(3-\sqrt{5}) & 1 \end{pmatrix} \tag{5.27}$$

and

$$\vec{v}_1^{5\dagger} = \begin{pmatrix} -1 & \frac{1}{2}(-1+\sqrt{5}) & 0 & \frac{1}{2}(1-\sqrt{5}) & 1 \end{pmatrix} . \tag{5.28}$$

Let the matrix of transformation, $\mathbf{X}$ be defined as

$$\mathbf{X} = \begin{pmatrix} \vec{x}_5^{5\dagger} \\ \vec{x}_4^{5\dagger} \\ \vec{x}_3^{5\dagger} \\ \vec{x}_2^{5\dagger} \\ \vec{x}_1^{5\dagger} \end{pmatrix} \tag{5.29}$$

where $\vec{x}_i^{5\dagger}$ and $i = 1$ to $i = 5$ are the normalized vectors of Eq. (5.24) through Eq. (5.28).

Note that from Eq. (5.29)

$$\mathbf{X}\mathbf{X}^{+} = \mathbf{I} . \tag{5.30}$$

This means that the device intra-slice matrix at slice $j = \upsilon$ has been transformed to

$$\mathbf{X}\mathbf{A}_\upsilon\mathbf{X}^\dagger = \begin{pmatrix} \lambda_1 & 0 & 0 & 0 & 0 \\ 0 & \lambda_2 & 0 & 0 & 0 \\ 0 & 0 & \lambda_3 & 0 & 0 \\ 0 & 0 & 0 & \lambda_4 & 0 \\ 0 & 0 & 0 & 0 & \lambda_5 \end{pmatrix}. \tag{5.31}$$

Here

$$\begin{aligned} \lambda_{\upsilon,1} &= \epsilon_\upsilon + 2t_\upsilon \\ \lambda_{\upsilon,2} &= \frac{1}{2}(-t_\upsilon - t_\upsilon\sqrt{5} + 2\epsilon_\upsilon) \\ \lambda_{\upsilon,3} &= \frac{1}{2}(t_\upsilon - t_\upsilon\sqrt{5} + 2\epsilon_\upsilon) \quad . \\ \lambda_{\upsilon,4} &= \frac{1}{2}(-t_\upsilon + t_\upsilon\sqrt{5} + 2\epsilon_\upsilon) \\ \lambda_{\upsilon,5} &= \frac{1}{2}(t_\upsilon + t_\upsilon\sqrt{5} + 2\epsilon_\upsilon) \end{aligned} \tag{5.32}$$

From Eq. (5.32), tuning for the device and the lead hence requires

$$\epsilon_L = \frac{1}{2}(-t_\upsilon - t_\upsilon\sqrt{5} + 2\epsilon_\upsilon) \tag{5.33}$$

where ϵ_L is the on-site energy of the atom in the lead. Since we assume the atoms in the incoming as well as the outgoing leads are the same, hence it is acceptable to set $\epsilon_L = 0$. This means Eq. (5.33) can be re-expressed as

$$\epsilon_\upsilon = \frac{t_\upsilon}{2}(1 + \sqrt{5}). \tag{5.34}$$

Note ϵ_υ can be any value, and the tuning requires t_υ and ϵ_υ to satisfy Eq. (5.34). Furthermore, note Eq. (5.34) allows a different ϵ_υ for every slice υ. Similarly, for the inter-slice

coupling matrices, use the same transformation matrix, $\mathbf{X}$ in Eq. (5.29). Upon multiplying through, this gives

$$\mathbf{X}\mathbf{B}_{\tau,\tau+1}\mathbf{X}^{\dagger} = \mathbf{B}_{diagonal13} \tag{5.35}$$

where

$$\mathbf{B}_{diagonal13} = \begin{pmatrix} \lambda_1 & 0 & 0 & 0 & 0 \\ 0 & \lambda_2 & 0 & 0 & 0 \\ 0 & 0 & \lambda_3 & 0 & 0 \\ 0 & 0 & 0 & \lambda_4 & 0 \\ 0 & 0 & 0 & 0 & \lambda_5 \end{pmatrix} . \tag{5.36}$$

Here

$$\begin{aligned} \lambda_{\tau,1} &= -t_{\sigma,\tau} + 2t_\rho \\ \lambda_{\tau,2} &= \frac{1}{2}(-t_{\sigma,\tau} - t_\rho\sqrt{5} + 2t_\rho) \\ \lambda_{\tau,3} &= \frac{1}{2}(t_{\sigma,\tau} - t_\rho\sqrt{5} + 2t_\rho) \quad . \\ \lambda_{\tau,4} &= \frac{1}{2}(-t_{\sigma,\tau} + t_\rho\sqrt{5} + 2t_\rho) \\ \lambda_{\tau,5} &= \frac{1}{2}(t_{\sigma,\tau} + t_\rho\sqrt{5} + 2t_\rho) \end{aligned} \tag{5.37}$$

Therefore from Eq. (5.37) the mapping equation, Eq. (3.15) is satisfied provided $\tilde{s}_{b9} = \frac{1}{2}(t_{\sigma,\tau} + t_\rho\sqrt{5} - 2t_\mu)$. Now the last task we do is to check for the mapping equation for the connection vector, $\vec{w}$ and $\vec{u}$. To do this, use the same transformation matrix, $\mathbf{X}$ in Eq. (5.29) and then define the connection vector, $\vec{w}$ as

$$\vec{w}^{\dagger} = \begin{pmatrix} -w\eta_1 & -w\eta_2 & -w\eta_3 & -w\eta_4 & -w\eta_5 \end{pmatrix} . \tag{5.38}$$

This means that

$$\vec{w}^{\dagger}\mathbf{X} = \begin{pmatrix} -w & 0 & 0 & 0 & 0 \end{pmatrix} . \tag{5.39}$$

Note here that for convenience we have let η_i's to be elements of the eigenvector which has all elements of the same sign. Similarly define, the outgoing connection vector, $\vec{u}$ as

$$\vec{u} = \begin{pmatrix} -u\eta_1 \\ -u\eta_2 \\ -u\eta_3 \\ -u\eta_4 \\ -u\eta_5 \end{pmatrix} . \tag{5.40}$$

This means that

$$\mathbf{X}\vec{u} = \begin{pmatrix} -u \\ 0 \\ 0 \\ 0 \\ 0 \end{pmatrix} . \tag{5.41}$$

Thus the mapping Eq. (3.12) has been satisfied. Therefore to find quantum dragons tune the on-site energy of the atom at slice $j = \upsilon$ to $\epsilon_\upsilon = \frac{t_\upsilon}{2}(1 + \sqrt{5})$, as well as $\tilde{s}_{b9} = \frac{1}{2}(t_{\sigma,\tau} + t_\rho\sqrt{5} - 2t_\mu)$ and $\vec{w} = \vec{u} = \begin{pmatrix} -t_{eo}\eta_1 \\ -t_{eo}\eta_2 \\ -t_{eo}\eta_3 \\ -t_{eo}\eta_4 \\ -t_{eo}\eta_5 \end{pmatrix}$ Note here that, η_i's are the elements of the normalized eigenvectors of the inter-slice and intra-slice matrices for the device which corresponds to the maximum eigenvalue when you invoke the Perron Frobenius theorem.

Quantum dragon solutions can also be obtained for $m = 5$ and $l = 4$ when the device has only nn interactions. Assume the inter-slice coupling matrices for the device have the following simple forms. Thus $\mathbf{B}_{\tau,\tau+1} = -t_{\sigma,\tau}\mathbf{I}$. Here, to find quantum dragons, tune the atoms at slice $j = \upsilon$ to $\epsilon_\upsilon = \frac{t_\upsilon}{2}(1+\sqrt{5})$, as well as $\tilde{s}_{b10} = t_{\sigma,\tau}$ and $\vec{w} = \vec{u} = \begin{pmatrix} -t_{eo}\eta_1 \\ -t_{eo}\eta_2 \\ -t_{eo}\eta_3 \\ -t_{eo}\eta_4 \\ -t_{eo}\eta_5 \end{pmatrix}$.

5.3 General method for 2D system mapping

In this section, the general method to do the mapping for a general 2D system is presented for $++$. Assume there are m atoms per slice in the nanodevice. The intra-slice coupling matrix associated with the device at site υ can be expressed as

$$A_\upsilon = \epsilon_\upsilon \mathbf{I} + t_\upsilon \mathbf{\Omega} - t_\upsilon \mathbf{Q}. \tag{5.42}$$

The eigenvalues of the matrix $\mathbf{A}_\upsilon$ can be expressed as [67, 68]

$$\lambda_{s,\upsilon} = \epsilon_\upsilon - 2t_\upsilon \cos\left(\frac{s\pi}{m}\right) \tag{5.43}$$

where $s = 1, ...m$. Assume the inter-slice coupling matrices for the device odd-even and even-odd interactions have the form

$$\mathbf{B}_{\tau,\tau+1} = -t_{\sigma,\tau}\mathbf{I} + t_{\rho,\tau}\mathbf{\Omega} - t_{\rho,\tau}\mathbf{Q}. \tag{5.44}$$

In Eq. (5.42), and Eq. (5.44) the matrix $\mathbf{Q}$ has been shown in Eq. (3.2) and the matrix $\mathbf{I}$ is an identity matrix of same dimension as the matrix $\mathbf{Q}$. The eigenvalues of Eq. (5.44) can be expressed as [67, 68]

$$\lambda_{s,\upsilon} = -t_{\sigma,\tau} - 2t_{\rho,\tau}\cos\left(\frac{s\pi}{m}\right) \tag{5.45}$$

where $s = 1, ...m$. The elements of the eigenvectors of the inter-slice and intra-slice coupling matrices are [67, 68]

$$x_j^{(s)} = \sqrt{\frac{2}{m}}\sin\left(\frac{(2j-1)s\pi}{2m}\right) \tag{5.46}$$

where $j = 1.....m$ and $s = 1, ...m$. With these eigenvectors, form the $m \times m$ matrix of transformation $\mathbf{X}$ such that

$$\mathbf{X} = \sqrt{\frac{2}{m}}\begin{pmatrix} \sin(\frac{\pi}{2m}) & \sin(\frac{\pi}{m}) & \sin(\frac{3\pi}{2m}) & \sin(\frac{2\pi}{m}) & \cdots & \cdots & \cdots & \cdots \\ \sin(\frac{3\pi}{2m}) & \sin(\frac{3\pi}{m}) & \sin(\frac{9\pi}{2m}) & \sin(\frac{6\pi}{m}) & \cdots & \cdots & \cdots & \cdots \\ \sin(\frac{5\pi}{2m}) & \sin(\frac{5\pi}{m}) & \sin(\frac{15\pi}{2m}) & \sin(\frac{10\pi}{m}) & \cdots & \cdots & \cdots & \cdots \\ \sin(\frac{7\pi}{2m}) & \sin(\frac{7\pi}{m}) & \sin(\frac{21\pi}{2m}) & \sin(\frac{14\pi}{m}) & \cdots & \cdots & \cdots & \cdots \\ \sin(\frac{9\pi}{2m}) & \sin(\frac{9\pi}{m}) & \sin(\frac{27\pi}{2m}) & \sin(\frac{18\pi}{m}) & \cdots & \cdots & \cdots & \cdots \\ \sin(\frac{11\pi}{2m}) & \sin(\frac{11\pi}{m}) & \sin(\frac{33\pi}{2m}) & \sin(\frac{22\pi}{m}) & \cdots & \cdots & \cdots & \cdots \\ \sin(\frac{13\pi}{2m}) & \sin(\frac{13\pi}{m}) & \sin(\frac{33\pi}{2m}) & \sin(\frac{26\pi}{m}) & \cdots & \cdots & \cdots & \cdots \\ \sin(\frac{15\pi}{2m}) & \sin(\frac{15\pi}{m}) & \sin(\frac{45\pi}{2m}) & \sin(\frac{30\pi}{m}) & \cdots & \cdots & \cdots & \cdots \end{pmatrix}, \tag{5.47}$$

where the matrix is written for $m = 8$ and only four columns are shown. Note that from Eq. (5.47)

$$\mathbf{X}\mathbf{X}^{\dagger} = \mathbf{I}\,. \tag{5.48}$$

Since $\mathbf{X}$ is unitary, $\mathbf{A}_v$ can be diagonalized as

$$\mathbf{X}\mathbf{A}_v\mathbf{X}^\dagger = \mathbf{A}_{diagonal} \tag{5.49}$$

here $\mathbf{A}_{diagonal}$ is

$$\mathbf{A}_{diagonal} = \begin{pmatrix} \lambda_{61} & 0 & \cdots & 0 & 0 \\ 0 & \lambda_{62} & \cdots & 0 & 0 \\ \vdots & \vdots & \ddots & \vdots & \vdots \\ 0 & 0 & \cdots & \lambda_{6,m-1} & 0 \\ 0 & 0 & \cdots & 0 & \lambda_{6m} \end{pmatrix} \tag{5.50}$$

with the eigenvalue of Eq. (5.43). Similarly, for the inter-slice coupling matrices use the same transformation $\mathbf{X}$ in Eq. (5.47). Upon multiplying through this gives

$$\mathbf{X}\mathbf{B}_{\tau,\tau+1}\mathbf{X}^\dagger = \mathbf{B}_{diagonal} \tag{5.51}$$

here $\mathbf{B}_{diagonal}$ is

$$\mathbf{B}_{diagonaloe} = \begin{pmatrix} \lambda_{71} & 0 & \cdots & 0 & 0 \\ 0 & \lambda_{72} & \cdots & 0 & 0 \\ \vdots & \vdots & \ddots & \vdots & \vdots \\ 0 & 0 & \cdots & \lambda_{7,m-1} & 0 \\ 0 & 0 & \cdots & 0 & \lambda_{7m} \end{pmatrix} \tag{5.52}$$

with the eigenvalues of Eq. (5.45). Now the last task is to check for the mapping equation for the incoming and outgoing connection vector, $\vec{w}$ and $\vec{u}$. To do this, use the same transformation matrix, $\mathbf{X}$ in Eq. (5.47) and then define the incoming connection vector, $\vec{w}$ by

$$\vec{w}^\dagger = \begin{pmatrix} -w_{11} & -w_{12} & -w_{13} & -w_{14} & \cdots & -w_{1m} \end{pmatrix} . \tag{5.53}$$

This means that

$$\vec{w}^{\dagger}\mathbf{X} = \begin{pmatrix} -w_{11} & 0 & 0 & 0 & 0 & \cdots & 0 \end{pmatrix} \tag{5.54}$$

provided from Eq. (5.46) $\vec{w}^{\dagger} = -w_{11}\vec{v}^{(1)\dagger}$. Thus in effect we have satisfied the mapping Eq. (3.11). Similarly define the outgoing connection vector, $\vec{u}$ as

$$\vec{u} = \begin{pmatrix} -u_{11} \\ -u_{12} \\ -u_{13} \\ -u_{14} \\ -u_{15} \\ \vdots \\ -u_{1m} \end{pmatrix}. \tag{5.55}$$

This means that

$$\mathbf{X}\vec{u} = \begin{pmatrix} -u_{11} \\ 0 \\ 0 \\ 0 \\ 0 \\ \vdots \\ 0 \end{pmatrix} \tag{5.56}$$

for $\vec{u}^{\dagger} = -u_{11}\vec{v}^{(1)}$. Thus in effect the mapping Eq. (3.12) is satisfied.

5.4 General tuning: quantum dragon

Therefore to find quantum dragons tune the on-site energy of the atoms to $\epsilon_L = \lambda_{31} = 0$, as well as $\tilde{s}_{bzz} = \lambda_{71}$ and $\vec{w} = \vec{u} = -t_{eo}\vec{v}^{(1)}$.

5.5 Data

In this section, the results obtained for our boundary condition $++$ are presented. Here, we show quantum dragon solutions as well as Fano resonance plots in $\mathcal{T}$ when there is complete randomness in the device. Here also, we show the plot of the mean electron transmission probability vs δ as well as the standard deviation of the electron transmission probability vs δ. In Fig. 5.3 through Fig. 5.6, quantum dragon solutions are obtained when there is correlated disorder and the tight binding parameters in the device are tuned correctly to particular values. The quantum dragon solutions are shown by line $\mathcal{T}(E) = 1$ (darker blue) in all cases. Since the electron transmission probability is unity, quantum dragons do not have Fano resonance. The stronger the strength of the disorder, the more we move away from quantum dragon solutions. This can be seen in Fig. 5.3 through Fig. 5.6. The random numbers used in our study are the normal distribution [Gausssian] with zero mean and the unity standard deviation. Fig. 5.3 is a plot of $\mathcal{T}$ vs energy, E for the rectangular crystal with boundary condition $++$. The nanodevice has $m = 3$, $l = 14$ and therefore $ml = 42$. This plot is for the dimerized leads ($t_{oe} = 1$ and $t_{eo} = 2$). The line $\mathcal{T} = 1$ (darker blue) has the on-site energy, $\epsilon_j = t_j$. The intra-slice hopping strengths used are non-uniform. The red, green, magenta and purple color shows Fano resonances in the nanodevice. The on-site energy is modeled by $\epsilon_j = t_j + \delta\Sigma$, and the intra-slice hopping

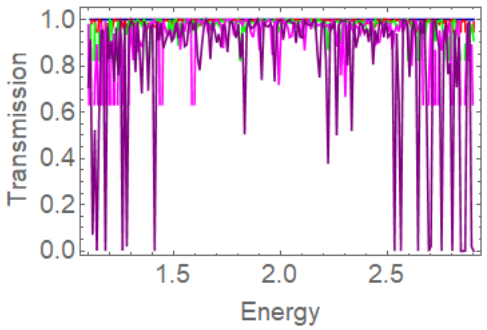

Figure 5.3

$\mathcal{T}$ vs E, boundary condition $++$, dimerized leads.

parameter is modeled by $t_j = t + \delta\Sigma$. The inter-slice hopping parameter is modeled by $t_\sigma = t_{oe} + \delta\Sigma$ and $t_\tau = t_{eo} + \delta\Sigma$ where $\delta = 0.0, 0.05, 0.1, 0.15, 0.2$ where Σ is a Gaussian random number of zero mean and unity standard deviation. Fig. 5.4 is same as Fig. 5.3, except only for the two values $\delta = 0$ (a quantum dragon) and $\delta = 0.2$. The line $\mathcal{T} = 1$ (darker blue) has the on-site energy, $\epsilon_j = t_j$. The intra-slice hopping strengths used are non-uniform. The purple color shows Fano resonances in the nanodevice, the cyan and the orange color shows the mean and the standard deviation of $\mathcal{T}$ as a function of E for $\delta = 0.2$. Fig. 5.5 is a plot of $\mathcal{T}$ vs E for the rectangular crystal with boundary condition $++$. The device has $m = 3$, $l = 14$ and therefore $ml = 42$. This plot is for the non-dimerized leads $t_{oe} = 1$, $t_{eo} = 1$. The line $\mathcal{T} = 1$ (darker blue) has the on-site energy, $\epsilon_j = t_j$. The intra-slice hopping strengths used are non-uniform. The red, green, magenta and purple color shows Fano resonances in the nanodevice. The on-site energy is modeled by $\epsilon_j = t_j + \delta\Sigma$, and the intra-slice hopping parameter is modeled by $t_j = t + \delta\Sigma$. The

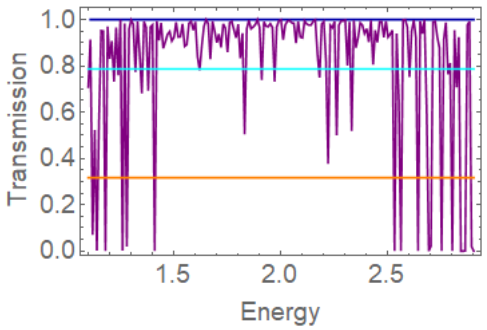

Figure 5.4

$\mathcal{T}$ vs E, boundary condition $++$, dimerized leads, $\delta = 0.0, 0.2$

inter-slice hopping parameter is modeled by $t_\sigma = t_{oe} + \delta\Sigma$ and $t_\tau = t_{eo} + \delta\Sigma$ where $\delta = 0.0, 0.05, 0.1, 0.15, 0.2$ where Σ is a Gaussian random number of zero mean and unit standard deviation.

Fig. 5.6 is the same as Fig. 5.5, except only for the two values $\delta = 0$ (a quantum dragon) and $\delta = 0.2$. The line $\mathcal{T} = 1$ (darker blue) has the on-site energy, $\epsilon_j = t_j$. The intra-slice hopping strengths used are non-uniform. The purple color shows Fano resonances in the nanodevice, the cyan and orange color shows the mean and standard deviation of $\mathcal{T}$ vs E of the incoming electron for $\delta = 0.2$.

5.6 Summary

In this chapter, the technique to find quantum dragons from boundary condition $++$ for $m = 3$, $l = 4$ as well as $m = 5$, $l = 4$ has been shown. Two different ways were used to find quantum dragons. Here, the connection vector is a modified busbar connection but this

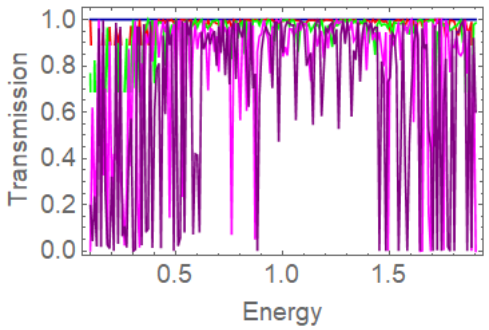

Figure 5.5

$\mathcal{T}$ vs E, boundary condition $++$, uniform leads.

connection vector is different from Chapter 3. When the nanodevice has random disorder as a result of uncorrelated random variations of the tight binding parameters in the device, Fano resonances are observed as seen in Fig. 5.3 through Fig. 5.6. Fano resonances are also expected to be observed when the dimerized and non-dimerized leads are connected to nanodevices with both homogeneous and non-homogeneous slices when there is complete randomness in the nanodevice. It has also been shown how to find quantum dragons with boundary condition $++$ for m atoms per slice and l slices in the device where here the number of slices l is even. Here also, as the amount of uncorrelated disorder increases (δ increases) the mean electron transmission probability falls and the standard deviation of the electron transmission probability increases. This is shown in Fig. 5.7 through Fig. 5.10 for both dimerized and uniform leads.

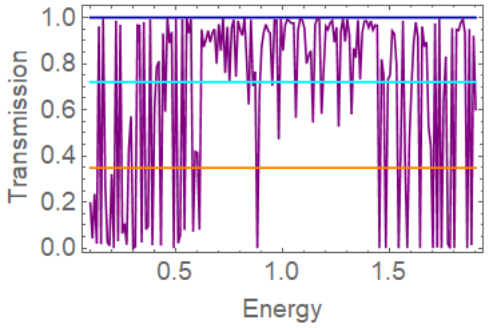

Figure 5.6

$\mathcal{T}$ vs E, boundary condition $++$, uniform leads, $\delta = 0.2$.

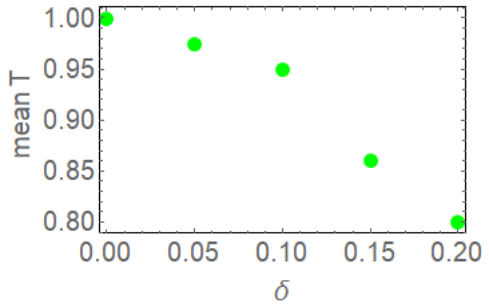

Figure 5.7

$\langle \mathcal{T} \rangle$ vs δ, boundary condition $++$, non-uniform leads.

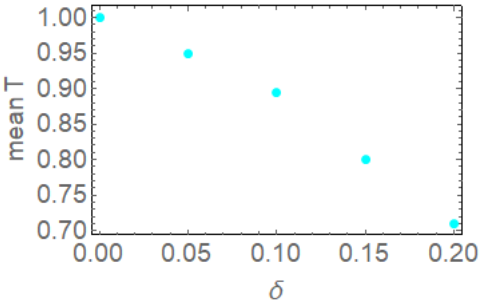

Figure 5.8

$\langle \mathcal{T} \rangle$ vs δ, boundary condition $++$, uniform leads.

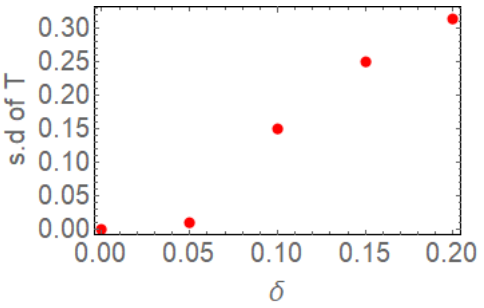

Figure 5.9

std $\mathcal{T}$ vs δ, boundary condition $++$, dimerized leads.

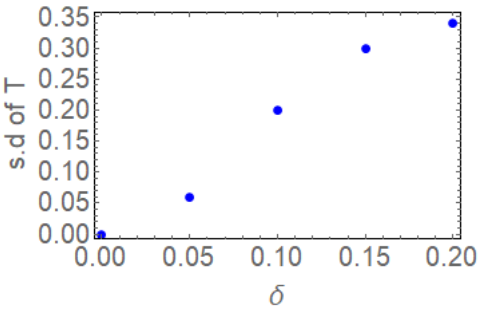

Figure 5.10

std $\mathcal{T}$ vs δ, boundary condition $++$, uniform leads.

CHAPTER 6

QUANTUM DRAGON SOLUTIONS FOR RECTANGULAR CRYSTALS : CASE 4: BOUNDARY CONDITION $-+ = +-$

It is shown in this chapter, how to find quantum dragons for single-layer planar rectangular crystals using boundary conditions which we label as $-+$. We call the boundary conditions $-+$ because in Eq. (1.25), we set $\beta = -b$ and $\gamma = b$. The $-+$ boundary conditions are equivalent to $+-$ for planar systems. The connection vector used is a modified busbar. There are two ways to find quantum dragons: (1) we assume the inter-slice coupling matrices for the nanodevice has nn and nnn interactions and (2) we assume the inter-slice coupling matrices are proportional to the identity matrix. In other words, the device has only nn interactions. In the absence of nnn interactions this gives results in

[24]. From Eq. (1.25), by setting $\beta = -b$ and $\gamma = b$, the symmetric tridiagonal matrix of dimension $m \times m$ has the form

$$\mathbf{A} = \begin{pmatrix} a-b & -b & 0 & \cdots & 0 & 0 \\ -b & a & -b & \cdots & 0 & 0 \\ 0 & -b & a & \cdots & 0 & 0 \\ \vdots & \vdots & \vdots & \ddots & \vdots & \vdots \\ 0 & 0 & 0 & \cdots & a & -b \\ 0 & 0 & 0 & \cdots & -b & a+b \end{pmatrix} = a\mathbf{I} - b\mathbf{Q} + b\mathbf{P} \tag{6.1}$$

where a and b are real numbers. In Eq. (6.1), the matrix $\mathbf{Q}$ is defined as Eq. (3.2) and the matrix $\mathbf{P}$ is defined as

$$\mathbf{P} = \begin{pmatrix} -1 & 0 & 0 & \cdots & 0 & 0 \\ 0 & 0 & 0 & \cdots & 0 & 0 \\ 0 & 0 & 0 & \cdots & 0 & 0 \\ \vdots & \vdots & \vdots & \ddots & \vdots & \vdots \\ 0 & 0 & 0 & \cdots & 0 & 0 \\ 0 & 0 & 0 & \cdots & 0 & 1 \end{pmatrix}. \tag{6.2}$$

Here note that from Eq. (6.1),

$$a\mathbf{I} - b\mathbf{Q} + b\mathbf{P} = a\mathbf{I} - b\mathbf{Q} - b\mathbf{P} \tag{6.3}$$

based on the symmetry of the single-layer planar rectangular crystals, and also how you count the atoms in the single slice in the nanodevice. Our nanodevice has an intra-slice matrix of the form (written for $m = 8$)

$$\mathbf{A} = \begin{pmatrix} \epsilon - t & -t & 0 & 0 & 0 & 0 & 0 & 0 \\ -t & \epsilon & -t & 0 & 0 & 0 & 0 & 0 \\ 0 & -t & \epsilon & -t & 0 & 0 & 0 & 0 \\ 0 & 0 & -t & \epsilon & -t & 0 & 0 & 0 \\ 0 & 0 & 0 & -t & \epsilon & -t & 0 & 0 \\ 0 & 0 & 0 & 0 & -t & \epsilon & -t & 0 \\ 0 & 0 & 0 & 0 & 0 & -t & \epsilon & -t \\ 0 & 0 & 0 & 0 & 0 & 0 & -t & \epsilon + t \end{pmatrix} = \epsilon\mathbf{I} - t\mathbf{Q} + t\mathbf{P} \tag{6.4}$$

and an inter-slice matrix of the form (written for $m = 8$)

$$\mathbf{B} = \begin{pmatrix} -t_x - t_y & -t_y & 0 & 0 & 0 & 0 & 0 & 0 \\ -t_y & -t_x & -t_y & 0 & 0 & 0 & 0 & 0 \\ 0 & -t_y & -t_x & -t_y & 0 & 0 & 0 & 0 \\ 0 & 0 & -t_y & -t_x & -t_y & 0 & 0 & 0 \\ 0 & 0 & 0 & -t_y & -t_x & -t_y & 0 & 0 \\ 0 & 0 & 0 & 0 & -t_y & -t_x & -t_y & 0 \\ 0 & 0 & 0 & 0 & 0 & -t_y & -t_x & -t_y \\ 0 & 0 & 0 & 0 & 0 & 0 & -t_y & -t_x + t_y \end{pmatrix} = -t_x\mathbf{I} - t_y\mathbf{Q} + t_y\mathbf{P} \tag{6.5}$$

where t's are the hopping strengths which are non-negative real numbers and ϵ is the on-site energy of the atom which is a real number. The tridiagonal matrix in Eq. (6.1) has eigenvalues expressed as [67, 68]

$$\lambda_s = a + 2b\cos\left(\frac{(2s-1)\pi}{2m}\right) \tag{6.6}$$

where $s = 1, ...m$ and eigenvectors expressed as

$$x_j^{(s)} = \frac{\sqrt{2}}{\sqrt{m}}\sin\left(\frac{(2j-1)(2s-1)\pi}{4m}\right) \tag{6.7}$$

where $j = 1....., m$ and $s = 1, ...m$. The outline for the chapter is as follows. In section 6.1, quantum dragon solutions for $m = 3$ and $l = 4$ are presented. Section 6.2, shows the general method for 2D system mapping. Section 6.3, presents the general tuning on how to obtain quantum dragon solutions. The data and the summary of this chapter are given in section 6.4 and section 6.5, respectively.

6.1 Quantum dragons for $m = 3$, $l = 4$ with nnn and nn interactions

Assume the nanodevice has three atoms per slice at sites $j = \iota$. See Fig. 6.1.

Fig. 6.1, is an example of rectangular device with boundary condition $-+$ coupled to dimerized leads. The vertical lines show the intra-slice hopping. The device has $m = 3$, $l = 4$ and therefore $ml = 12$ atoms. The device has non-uniform intra-slice hopping parameters. Only three atoms in the incoming lead are shown. The lead atoms are shown by the green color. The connections between leads and the device are shown by line segments (pink). The inter-slice coupling matrices are for nn shown by the horizontal line (brown and pink color) and the nnn interactions shown by (blue, light brown and dark yellow

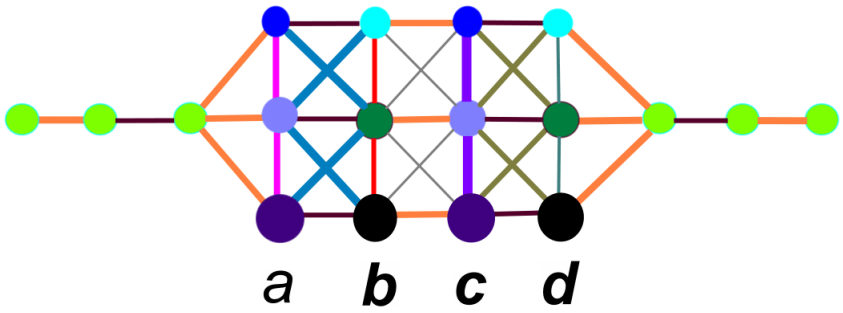

Figure 6.1

An example of the case of dimerized leads, and a rectangular nanodevice with bounadry condition $-+$.

color) line segments which form an X-shape. Appropriate choices of the tight-binding parameters makes this disordered nanodevice into a quantum dragon.

Let assume the intra-slice coupling matrices have the form

$$\mathbf{A}_\iota = \begin{pmatrix} \epsilon_\iota - t_\iota & -t_\iota & 0 \\ -t_\iota & \epsilon_\iota & -t_\iota \\ 0 & -t_\iota & \epsilon_\iota + t_\iota \end{pmatrix} = \epsilon_\iota \mathbf{I} + t_\iota \mathbf{P} - t_\iota \mathbf{Q} \tag{6.8}$$

where $\iota = a, b, c, d$ for the $l = 4$ slices and ϵ_ι are the on-site energies for the atoms at slice $j = \iota$ and t_ι are the intra-slice hopping parameters between the atoms. The eigenvalues

of Eq. (6.8) are $\lambda_{\iota,1} = \epsilon_\iota - t_\iota\sqrt{3}$, $\lambda_{\iota,2} = \epsilon_\iota + t_\iota\sqrt{3}$, $\lambda_{\iota,3} = \epsilon_\iota$. Now assume the device inter-slice coupling matrices have the form

$$\mathbf{B}_{\varpi,\varpi+1} = \begin{pmatrix} -t_{f,\varpi} - t_{z,\varpi} & -t_{z,\varpi} & 0 \\ -t_{z,\varpi} & -t_{f,\iota} & -t_{z,\varpi} \\ 0 & -t_{z,\varpi} & -t_{f,\varpi} + t_{z,\varpi} \end{pmatrix} = -t_{f,\varpi}\mathbf{I} + t_{z,\varpi}\mathbf{P} - t_{z,\varpi}\mathbf{Q}. \quad (6.9)$$

In Eq. (6.8) and Eq. (6.9), the matrix $\mathbf{P}$ is explicitly, for $m = 3$

$$\mathbf{P} = \begin{pmatrix} -1 & 0 & 0 \\ 0 & 0 & 0 \\ 0 & 0 & 1 \end{pmatrix}. \quad (6.10)$$

The normalized eigenvectors of Eq. (6.8) and Eq. (6.9) are

$$\vec{v}_3^{3\dagger} = \begin{pmatrix} \sqrt{\frac{1}{6}(2+\sqrt{3})} & \frac{1+\sqrt{3}}{\sqrt{6(2+\sqrt{3})}} & \frac{1}{\sqrt{6(2+\sqrt{3})}} \end{pmatrix} \quad (6.11)$$

$$\vec{v}_2^{3\dagger} = \begin{pmatrix} \sqrt{\frac{1}{6}(2-\sqrt{3})} & \frac{1-\sqrt{3}}{\sqrt{6(2-\sqrt{3})}} & \frac{1}{\sqrt{6(2-\sqrt{3})}} \end{pmatrix} \quad (6.12)$$

and

$$\vec{v}_1^{3\dagger} = \begin{pmatrix} \frac{-1}{\sqrt{3}} & \frac{1}{\sqrt{3}} & \frac{1}{\sqrt{3}} \end{pmatrix}. \quad (6.13)$$

Now let the matrix of transformation, $\mathbf{X}$ be defined as

$$\mathbf{X} = \begin{pmatrix} \vec{v}_3^{3\dagger} \\ \vec{v}_2^{3\dagger} \\ \vec{v}_3^{3\dagger} \end{pmatrix}. \quad (6.14)$$

Note that from Eq. (6.14) that

$$\mathbf{X}\mathbf{X}^\dagger = \mathbf{I}. \quad (6.15)$$

This means that the device intra-slice matrix at slice $j = \iota$ has been transformed to

$$\mathbf{X}\mathbf{A}_\iota\mathbf{X}^\dagger = \begin{pmatrix} \epsilon_\iota - t_\iota\sqrt{3} & 0 & 0 \\ 0 & \epsilon_\iota + t_\iota\sqrt{3} & 0 \\ 0 & 0 & \epsilon_\iota \end{pmatrix}. \tag{6.16}$$

From Eq. (6.16), tuning for the device and the lead hence requires

$$\epsilon_L = \epsilon_\iota - t_\iota\sqrt{3} \tag{6.17}$$

where ϵ_L is the onsite energy of the atom in the lead. Since the on-site energy of the atom in the lead to zero, $\epsilon_L = 0$, this means Eq. (6.17) can be re-expressed as

$$\epsilon_\iota = t_\iota\sqrt{3} \tag{6.18}$$

where ϵ_ι can be any value, and the tuning only requires t_ι and ϵ_ι satisfy Eq. (6.18). Similarly, for the inter-slice coupling matrices, use the same transformation matrix, $\mathbf{X}$ in Eq. (6.14). Upon multiplying through, this gives

$$\mathbf{X}\mathbf{B}_{\varpi,\varpi+1}\mathbf{X}^\dagger = \mathbf{B}_{\mathbf{diagonal14}} \tag{6.19}$$

where

$$\mathbf{B}_{\mathbf{diagonal14}} = \begin{pmatrix} -t_{f,\varpi} - t_{z,\varpi}\sqrt{3} & 0 & 0 \\ 0 & -t_{f,\varpi} + t_{z,\varpi}\sqrt{3} & 0 \\ 0 & 0 & -t_{f,\varpi} \end{pmatrix}. \tag{6.20}$$

Therefore the mapping equation, Eq. (3.14), is satisfied provided $\tilde{s}_{b11} = t_{f,\varpi} + t_{z,\varpi}\sqrt{3}$. Now the last task is to check for the mapping equation for the connection vector, $\vec{w}$ and $\vec{u}$.

To do this, use the same transformation matrix, $\mathbf{X}$ and then define the incoming connection vector, $\vec{w}$ by

$$\vec{w}^{\dagger} = \begin{pmatrix} -w\sqrt{\frac{1}{6}(2+\sqrt{3})} & \frac{-w(1+\sqrt{3})}{\sqrt{6(2+\sqrt{3})}} & \frac{-w}{\sqrt{6(2+\sqrt{3})}} \end{pmatrix} . \tag{6.21}$$

This means that

$$\vec{w}^{\dagger}\mathbf{X} = \begin{pmatrix} -w & 0 & 0 \end{pmatrix} . \tag{6.22}$$

Similarly define the outgoing connection vector, $\vec{u}$,

$$\vec{u} = \begin{pmatrix} -u\sqrt{\frac{1}{6}(2+\sqrt{3})} \\ \frac{-u(1+\sqrt{3})}{\sqrt{6(2+\sqrt{3})}} \\ \frac{-u}{\sqrt{6(2+\sqrt{3})}} \end{pmatrix} . \tag{6.23}$$

This means that

$$\mathbf{X}\vec{u} = \begin{pmatrix} -u \\ 0 \\ 0 \end{pmatrix} . \tag{6.24}$$

Therefore to find quantum dragons tune the on-site energy of the atom at slice $j = \iota$ to $\epsilon_{\iota} = t_{\iota}\sqrt{3}$, as well as $\tilde{s}_{b11} = t_{f,\varpi} + t_{z,\varpi}\sqrt{3}$ and $\vec{w} = \vec{u} = \begin{pmatrix} -t_{eo}\sqrt{\frac{1}{6}(2+\sqrt{3})} \\ -\frac{t_{eo}(1+\sqrt{3})}{\sqrt{6(2+\sqrt{3})}} \\ -\frac{t_{eo}}{\sqrt{6(2+\sqrt{3})}} \end{pmatrix}$.

Quantum dragons can also be found when the inter-slice coupling matrices contain only nn interactions. This assumption has been used by Novotny in 2015 [24] to find quantum

dragons. Here, to find quantum dragons tune the on-site energy of the atom at slice $j = \iota$ to $\epsilon_\iota = t_\iota\sqrt{3}$, as well as $\tilde{s}_{b12} = t_{f,\varpi}$ and $\vec{w} = \vec{u} = \begin{pmatrix} -t_{eo}\sqrt{\frac{1}{6}(2+\sqrt{3})} \\ -\frac{t_{eo}(1+\sqrt{3})}{\sqrt{6(2+\sqrt{3})}} \\ -\frac{t_{eo}}{\sqrt{6(2+\sqrt{3})}} \end{pmatrix}$.

6.2 General method for 2D system mapping

In this section, the general method to do the mapping for the 2D system is presented. Let assume there are m atoms per slice in the nanodevice. The intra-slice coupling matrix associated with the device at site ι can be expressed as

$$\mathbf{A}_\iota = \epsilon_\iota \mathbf{I} + t_\iota \mathbf{P} - t_\iota \mathbf{Q}. \tag{6.25}$$

The eigenvalues of the matrix $\mathbf{A}_\iota$ can be expressed as [67, 68]

$$\lambda_{s,\iota} = \epsilon_\iota - 2t_\iota \cos\left(\frac{(2s-1)\pi}{2m}\right) \tag{6.26}$$

where $s = 1, ...m$. Assume the inter-slice coupling matrices for the device odd-even and even-odd interactions have the form

$$\mathbf{B}_{\varpi,\varpi+1} = -t_{f,\varpi}\mathbf{I} + t_{z,\varpi}\mathbf{P} - t_{z,\varpi}\mathbf{Q}. \tag{6.27}$$

In Eq. (6.25) and Eq. (6.27) the matrix $\mathbf{Q}$ has been shown in Eq. (3.2), the matrix $\mathbf{P}$ has been shown as Eq. (6.2) and the matrix $\mathbf{I}$ is an identity matrix. The eigenvalues of Eq. (6.27) can be expressed as [67, 68]

$$\lambda_{s,\varpi} = -t_{f,\varpi} - 2t_{z,\varpi} \cos\left(\frac{(2s-1)\pi}{2m}\right) \tag{6.28}$$

where $s = 1, ...m$. The elements of the eigenvectors of the inter-slice and intra-slice coupling matrices $\mathbf{B}_{\varpi,\varpi+1}$ and $\mathbf{A}_\iota$ are [67, 68]

$$x_j^{(s)} = \sqrt{\frac{2}{m}} \sin\left(\frac{(2j-1)(2s-1)\pi}{4m}\right) \tag{6.29}$$

where $j = 1....., m$ and $s = 2, ...m$. With these eigenvectors, form the $m \times m$ matrix of transformation $\mathbf{X}$ such that

$$\mathbf{X} = \sqrt{\frac{2}{m}} \begin{pmatrix} \sin(\frac{\pi}{4m}) & \sin(\frac{3\pi}{4m}) & \sin(\frac{5\pi}{4m}) & \sin(\frac{7\pi}{4m}) & \cdots & \cdots & \cdots & \cdots \\ \sin(\frac{3\pi}{4m}) & \sin(\frac{9\pi}{4m}) & \sin(\frac{15\pi}{2m}) & \sin(\frac{21\pi}{4m}) & \cdots & \cdots & \cdots & \cdots \\ \sin(\frac{5\pi}{4m}) & \sin(\frac{15\pi}{4m}) & \sin(\frac{25\pi}{4m}) & \sin(\frac{35\pi}{4m}) & \cdots & \cdots & \cdots & \cdots \\ \sin(\frac{7\pi}{4m}) & \sin(\frac{21\pi}{4m}) & \sin(\frac{35\pi}{4m}) & \sin(\frac{49\pi}{2m}) & \cdots & \cdots & \cdots & \cdots \\ \sin(\frac{9\pi}{4m}) & \sin(\frac{27\pi}{4m}) & \sin(\frac{45\pi}{4m}) & \sin(\frac{63\pi}{4m}) & \cdots & \cdots & \cdots & \cdots \\ \sin(\frac{11\pi}{4m}) & \sin(\frac{33\pi}{4m}) & \sin(\frac{55\pi}{4m}) & \sin(\frac{77\pi}{4m}) & \cdots & \cdots & \cdots & \cdots \\ \sin(\frac{13\pi}{4m}) & \sin(\frac{39\pi}{4m}) & \sin(\frac{65\pi}{4m}) & \sin(\frac{91\pi}{4m}) & \cdots & \cdots & \cdots & \cdots \\ \sin(\frac{15\pi}{4m}) & \sin(\frac{45\pi}{4m}) & \sin(\frac{75\pi}{4m}) & \sin(\frac{105\pi}{4m}) & \cdots & \cdots & \cdots & \cdots \end{pmatrix}. \tag{6.30}$$

where the matrix is written for $m = 8$ and only four colums are shown. Note that from Eq. (6.30)

$$\mathbf{X}\mathbf{X}^\dagger = \mathbf{I}. \tag{6.31}$$

Since $\mathbf{X}$ is unitary, $\mathbf{A}_\iota$ can be diagonalized as

$$\mathbf{X}\mathbf{A}_\iota\mathbf{X}^\dagger = \mathbf{A}_{diagonal} \tag{6.32}$$

here $\mathbf{A}_{diagonal}$ is

$$\mathbf{A}_{diagonal} = \begin{pmatrix} \lambda_{31}^{*} & 0 & \cdots & 0 & 0 \\ 0 & \lambda_{32}^{*} & \cdots & 0 & 0 \\ \vdots & \vdots & \ddots & \vdots & \vdots \\ 0 & 0 & \cdots & \lambda_{3m_l-1}^{*} & 0 \\ 0 & 0 & \cdots & 0 & \lambda_{3m_l}^{*} \end{pmatrix} \tag{6.33}$$

with the eigenvalue of Eq. (6.26). Similarly, for the inter-slice coupling matrices use the same transformation matrix $\mathbf{X}$ in Eq. (6.30). Upon multiplying through this gives

$$\mathbf{X}\mathbf{B}_{\varpi,\varpi+1}\mathbf{X}^{\dagger} = \mathbf{B}_{diagonal} \tag{6.34}$$

here $\mathbf{B}_{diagonal}$ is

$$\mathbf{B}_{diagonaloe} = \begin{pmatrix} \lambda_{41}^{*} & 0 & \cdots & 0 & 0 \\ 0 & \lambda_{42}^{*} & \cdots & 0 & 0 \\ \vdots & \vdots & \ddots & \vdots & \vdots \\ 0 & 0 & \cdots & \lambda_{4m_l-1}^{*} & 0 \\ 0 & 0 & \cdots & 0 & \lambda_{4m_l}^{*} \end{pmatrix}. \tag{6.35}$$

Now the last task is to check for the mapping equation for the connection vector, $\vec{w}$ and $\vec{u}$. To do this, use the same transformation matrix, $\mathbf{X}$ in Eq. (6.30) and then define the connection vector, $\vec{w}$ by

$$\vec{w}^{\dagger} = \begin{pmatrix} -w_{11} & -w_{12} & -w_{13} & -w_{14} & \cdots & -w_{1n} \end{pmatrix}. \tag{6.36}$$

This means that

$$\vec{w}^{\dagger}\mathbf{X} = \begin{pmatrix} -w_{11} & 0 & 0 & 0 & 0 & \cdots & 0 \end{pmatrix} \tag{6.37}$$

provided from Eq. (6.29) $\vec{w}^{\dagger} = -w_{11}\vec{v}^{(3)\dagger}$. Thus in effect the mapping Eq. (3.11) is satisfied. Similarly define, the outgoing connection, $\vec{u}$ as

$$\vec{u} = \begin{pmatrix} -u_{11} \\ -u_{12} \\ -u_{13} \\ -u_{14} \\ -u_{15} \\ \cdots \\ -u_{1n} \end{pmatrix} . \tag{6.38}$$

This means that

$$\mathbf{X}\vec{u} = \begin{pmatrix} -u_{11} \\ 0 \\ 0 \\ 0 \\ 0 \\ \cdots \\ 0 \end{pmatrix} . \tag{6.39}$$

for $\vec{u} = -u_{11}\vec{v}^{(3)}$, and hence the mapping Eq. (3.12) is satisfied.

6.3 General tuning

Therefore to find quantum dragons tune the on-site energies $\epsilon_l = \lambda_{31}$, as well as $\tilde{s}_{bhh} = \lambda_{41}^*$ and $\vec{w} = \vec{u} = -t_{eo}\vec{v}^{(1)}$.

6.4 Data

In this section, the results obtained for boundary condition $-+$ are presented and then discussed. Here, quantum dragon solutions, Fano resonances as well the mean electron transmission probability vs δ and the standard deviation of the electron transmission probability vs δ are shown. As seen in Fig. 6.2 through Fig. 6.5, quantum dragon solutions are obtained when there is interplay between the leads and the device. The quantum dragon solutions are shown by the line $\mathcal{T}(E) = 1$ (darker blue) in all cases. Because quantum dragons have unity electron transmission probability, this means quantum dragons have no Fano resonance. Fano resonances are seen in Fig. 6.2 through Fig. 6.5 when there is uncorrelated disorder in the tight binding parameters within the device. From Fig. 6.6 and Fig. 6.7, for both the dimerized leads and the uniform leads, the mean electron transmission probability decreases with increasing disorder strength. This is simply due to the fact that when the strength of the disorder increases the more uncorrelated disorder we have in the device, and hence a decrease in the mean electron transmission probability. The random number used here is also the normal distribution with zero mean and unit standard deviation. Fig. 6.2 through Fig. 6.5 suggest that if an experimentalist intends to find quantum dragons using the planar rectangular crystal with boundary condition $-+$, the appropriate leads must match the device to obtain $\mathcal{T} = 1$ for all energies in the case of correlated disorder. When the disorder in the device is uncorrlated, Fano resonances are seen in the device in all cases.

In Fig. 6.2, the nanodevice has $m = 3$, $l = 14$ and therefore $ml = 42$. Here, the rectangular planar crystal has boundary condition $-+$. This plot is for the dimerized leads

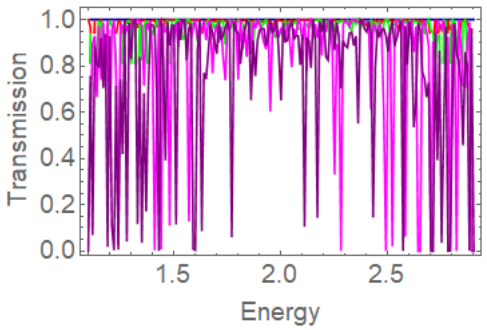

Figure 6.2

$\mathcal{T}$ vs E, boundary condition $-+$, dimerized leads.

$t_{oe} = 1$ and $t_{eo} = 2$. The line $\mathcal{T} = 1$ (darker blue) has the on-site energy, $\epsilon_j = t_j\sqrt{3}$. The intra-slice hopping strengths used are non-uniform. The red, green, magenta and purple colors show Fano resonances in the nanodevice. The on-site energy is modeled by $\epsilon_j = t_j\sqrt{3} + \delta\Sigma$, and the intra-slice hopping parameter is modeled by $t_j = t + \delta\Sigma$. The inter-slice hopping parameter is modeled by $t_1 = t_{oe} + \delta\Sigma$ and $t_3 = t_{eo} + \delta\Sigma$ where $\delta = 0.0, 0.05, 0.1, 0.15, 0.2$ where Σ is a normally distributed random number.

Fig. 6.3, is same as Fig. 6.2, except only for the two values $\delta = 0$ (a quantum dragon) and $\delta = 0.2$. The purple color show Fano resonances in the nanodevice, the cyan and the orange colors show the mean and the standard deviation of $\mathcal{T}$ as a function of E for $\delta = 0.2$.

In Fig. 6.4, the nanodevice has $m = 3$, $l = 14$ and therefore $ml = 42$. This plot is for the non-dimerized leads $t_{oe} = 1$, $t_{eo} = 1$. The line $\mathcal{T} = 1$ (darker blue) has the on-site energy, $\epsilon_j = t_j\sqrt{3}$. The intra-slice hopping strengths are non-uniform. The red,

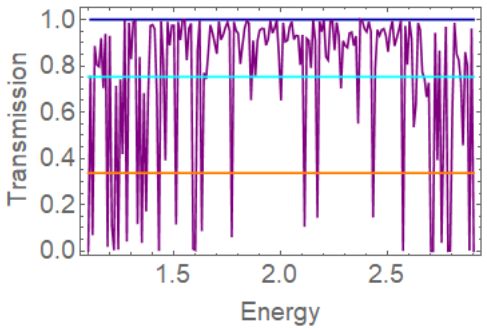

Figure 6.3

$\mathcal{T}$ vs E, boundary condition $-+$, dimerized leads, $\delta = 0.2$.

green, magenta and purple color shows Fano resonances in the nanodevice. The on-site energy is modeled by $\epsilon_j = t_j\sqrt{3} + \delta\Sigma$, and the intra-slice hopping parameter is modeled by $t_j = t + \delta\Sigma$. The inter-slice hopping parameter is modeled by $t_1 = t_{oe} + \delta\Sigma$ and $t_3 = t_{eo} + \delta\Sigma$ where $\delta = 0.0, 0.05, 0.1, 0.15, 0.2$ where Σ is a random number of zero mean and unit standard deviation.

Fig. 6.5, is the same as Fig. 6.4, except only for the two values $\delta = 0$ (a quantum dragon) and $\delta = 0.2$. The line $\mathcal{T} = 1$ (darker blue) has the on-site energy, $\epsilon_j = t_j\sqrt{3}$. The intra-slice hopping strengths used are non-uniform. The purple color shows Fano resonances in the nanodevice, the cyan and orange color shows the mean and standard deviation of $\mathcal{T}$ vs E of the incoming electron for $\delta = 0.2$.

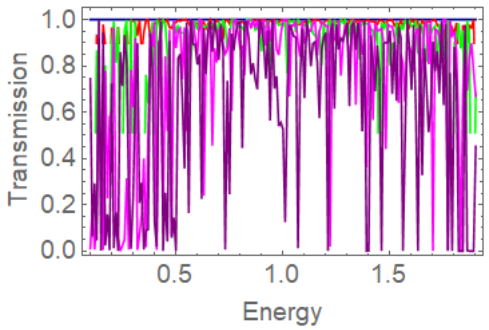

Figure 6.4

$\mathcal{T}$ vs E, boundary condition $-+$, uniform leads.

6.5 Summary

In chapter 6, it has been shown that for $m = 3$, $l = 4$ for both nnn and nn interactions and only nn interactions, quantum dragon solutions exist for both ways for boundary condition $-+$. Here, the connection vector used is a modified busbar but this connection vector is different from Chapter 3 and Chapter 5. When there is uncorrelated random disorder of the tight-binding parameters in the nanodevice, Fano resonances are seen in all cases as shown in Fig. 6.2 through Fig. 6.5. Fano resonances are also expected to be observed when the dimerized and non-dimerized leads are connected to homogeneous slices when there is complete randomness in the nanodevice. It has also been shown how to find quantum dragons for m atoms per slice in the device and l slices where the number of slices is even. As the amount of uncorrelated disorder increases (δ increases) the mean transmission falls and the standard deviation of the transmission increases. This is shown in Fig. 6.6 through Fig. 6.9 for both dimerized and uniform leads.

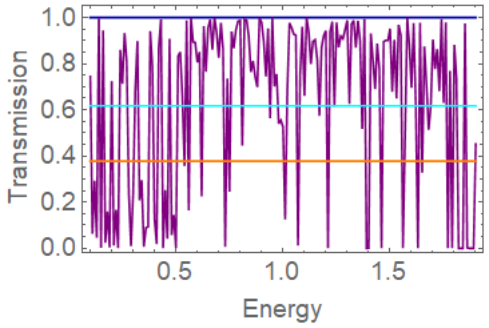

Figure 6.5

$\mathcal{T}$ vs E, boundary condition $-+$, uniform leads, $\delta = 0.2$.

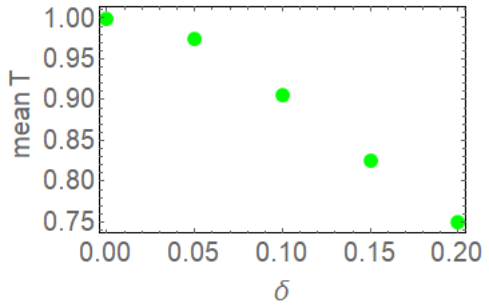

Figure 6.6

$\langle \mathcal{T} \rangle$ vs δ, boundary condition $-+$, non-uniform leads.

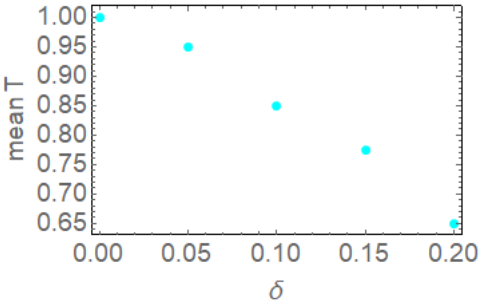

Figure 6.7

$\langle \mathcal{T} \rangle$ vs δ, boundary condition $-+$, uniform leads.

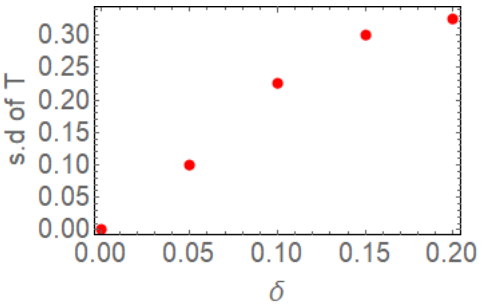

Figure 6.8

std $\mathcal{T}$ vs δ, boundary condition $-+$, non-uniform leads.

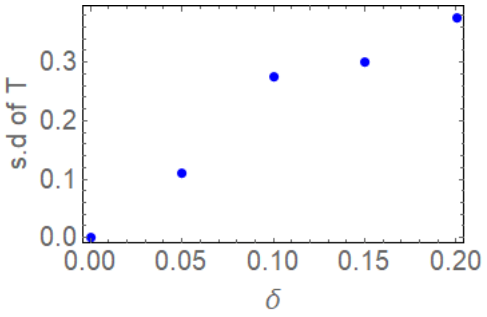

Figure 6.9

std $\mathcal{T}$ vs δ, boundary condition $-+$, uniform leads.

CHAPTER 7

DISCUSSION AND CONCLUSIONS

In this dissertation, the technique to find quantum dragons within the single-band tight binding model has been shown for single-layer thickness nanodevices based on rectangular lattices. This has been accomplished for four different types of boundary conditions.

In chapter 2, the electron transmission probability for dimerized leads coupled to a two site device is calculated using the matrix method, the RG method, and the standard Green's function method. These methods give the same result for the electron transmission probability, since they all solve the time-independent Schrödinger equation for semi-infinite leads coupled to the device. Here also, it was seen that there are certain tight binding parameters where $\mathcal{T}(E) = 1$ for all energies, E.

In chapters 3,4,5, and 6, the methodology to find quantum dragons for single-layer planar rectangular crystals using the map-and-tune approach has been shown. The quantum dragons found could have strong disorder, but still the electron transmission probability is unity for all energies. This means that in a two-probe technique, the electrical conductance is quantized, and in a four-probe technique the electrical resistance is zero ($R = 0$). This further suggests that in the four-probe technique, quantum dragons are perfect conductors. For a two-terminal coherent device, quantum dragons have zero shot power noise ($P = 0$)

and consequently, an electric current would not cause any heating of the nanodevice. Since not all conductors have shot power noise [72], quantum dragons could be one example. This is the first time the matrix method has been used to take into account dimerized leads as well as dimerized on-site energies in the leads, as derived in Appendix A.1.

To allow the nanodevice to become a quantum dragon requires tuning of specific parameters in the tight-binding model. With careful tuning, all electrons which impinge on the nanodevice are fully transmitted, and hence the electron transmission probability is $\mathcal{T}(E) = 1$.

In chapters 3,4,5, and 6 two different ways are presented in each chapter which allows quantum dragons to be found for both the non-dimerized leads as well as the dimerized leads. That is, when the nanodevice inter-slice consists of nn and nnn interactions, as well when the inter-slice coupling matrices for the device consist of only nn interactions. In all cases, the quantum dragons found can be for nanodevices with non-uniform leads, but this also holds true for uniform leads. These quantum dragons found have experimental relevance since single-atom layer planar systems with rectangular cross section have been fabricated [47]. The analysis in Chapter 3, 4, 5 and 6 may also hold true for single-layer planar square lattices with both nearest neighbor and next nearest neighbor interactions. In looking for quantum dragons within the single-band tight-binding model, the energy E of the incident electron is primarily at the position of the Fermi-level. This is quite significant because in nanosystems such as nanowires and nanoribbons and even in field effect transistors, the position of the Fermi-level with respect to the energy subbands can be varied by applying an external electric field which is created by a gate electrode [6].

This technique could help in tuning the nanodevices (within the single-band tight-binding model) to become a quantum dragon.

The predictions of the existence of quantum dragons for single-layer planar crystals need to be verified experimentally. Recently, free standing single-atom thick rectangular lattices of Fe with rectangular crystal structure and single-atom-thick copper oxide with square lattices have been published [47, 48]. Therefore such tight-binding studies could be very important to experimental studies. Furthermore, quite recently [73], PbTe nanocrystals of rectangular cross section have been synthesized and therefore our tight-binding studies could also be very relevant to these experimental studies. When there is tuned correlated disorder, $\mathcal{T}(E) = 1$ for all energies. In finding quantum dragons, the nanodevice is connected to a 1D single channel of single-atom width leads, which is either uniform or dimerized. Uniform wires such as gold, nickel and platinum [74, 75, 76] of single-atom width have already been fabricated, and therefore these wires could help in experimental studies.

Furthermore, by varying the tight-binding parameters in the nanodevice randomly, novel coherent effects such as Fano resonances of the electrical transmission probability are expected to be observed in all cases. It can also be seen that the strength of the disorder determines how pronounced the Fano resonances are as you move away from the quantum dragon solutions. In all the boundary conditions studied, as seen in Fig. 7.1 and Fig. 7.2, the mean electron transmission probability decreases with increasing strength of disorder, δ. It should be pointed out that in all our calculations, our averaging of the electron

transmission probability is done over a single random variate distribution, the averaging is performed over all transmitted energy values.

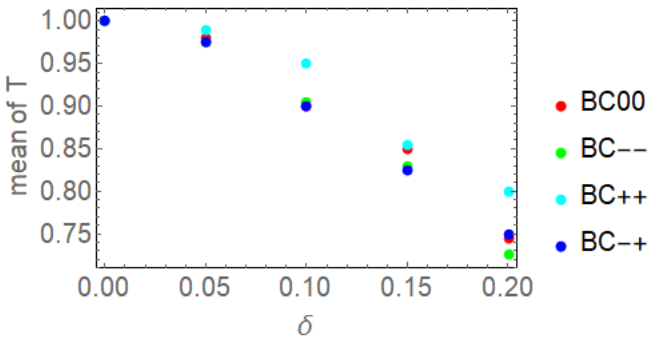

Figure 7.1

$\langle \mathcal{T} \rangle$ vs δ, all boundary conditions for dimerized leads

As the amount of uncorrelated disorder increases (δ increases) the mean transmission falls and the standard deviation of the transmission increases. This is shown in Fig. 7.1 through Fig. 7.4 for both dimerized and uniform leads for all the four different types of boundary conditions studied. Experimentally, since measuring the electrical resistance yields information on the mean electron transmission probability, the mean electron transmission probability is calculated and plotted against E.

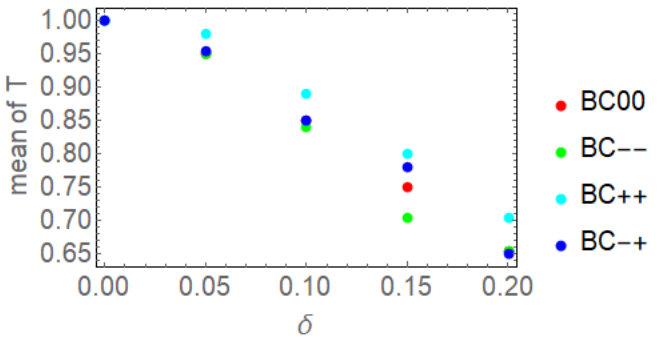

Figure 7.2

$\langle \mathcal{T} \rangle$ vs δ, all boundary conditions for uniform leads.

From all the above considerations, the proof of the existence of quantum dragons for $m = 1$, and $l = 2$ as well as for single-layer planar rectangular crystals with different boundary conditions for a single conducting channel has been shown. The proof provided in this study is within the single-band tight-binding model. If a nanodevice is connected to appropriate leads, the electron transmission probability is unity and hence all the electrons which are incident on the nanodevice are fully transmitted. Quantum dragons have energy independent total electron transmission probability of electrons. In the presence of uncorrelated randomness of the tight-binding parameters, Fano resonances are seen in the nanodevice.

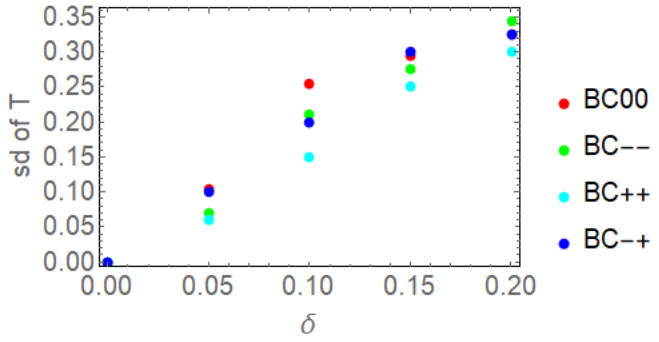

Figure 7.3

std $\mathcal{T}$ vs δ for all boundary conditions for dimerized leads.

It may be possible to extend this study to a multi-channel leads with even-odd structure connected to a nanodevice with even-odd symmetry. It is hoped that quantum dragons will have similar applications as ballistic electron transport devices [5, 9, 77, 78, 79, 80, 81] and other optoelectronic devices which are based on full electron transmission.

It is found in this thesis that quantum dragon solutions are not only limited to nanostructures with cylindrical symmetry as previously discovered in [18], but the concepts of quantum dragons are applicable to single-layer planar crystals, such as rectangular lattices and square lattices. In other words, there are nanodevices with planar symmetry such as rectangular crystals and possibly square lattices which when connected to appropiate leads could have unity electron transmission probability, even if the device has strong disorder.

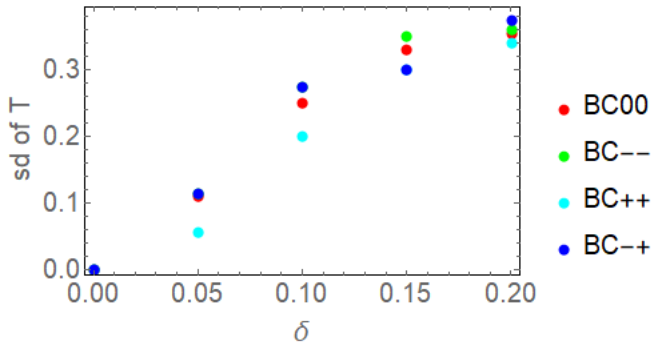

Figure 7.4

std $\mathcal{T}$ vs δ for all boundary conditions for uniform leads.

Although the underlying nanodevice graphs are planar, randomness may cause buckling of the actual device, as illustrated in Fig. 7.5 and Fig. 7.6

This dissertation has already resulted in one publication in [1] M.A.Novotny, L. Solomon and G. Inkoom. "Quantum transport through fully connected network with disorder". Physics Procedia (53) 2014, 71-74.

There are two papers in preparation: (1) 00 boundary condition as seen in Fig. 7.5 and Fig. 7.6 and (2) the other boundary conditions, ($--$, $++$ and $-+$).

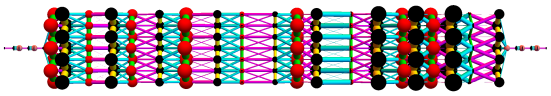

Figure 7.5

An example of rectangular nanodevice coupled to dimerized leads. Here, $m = 7$ and $l = 20$.

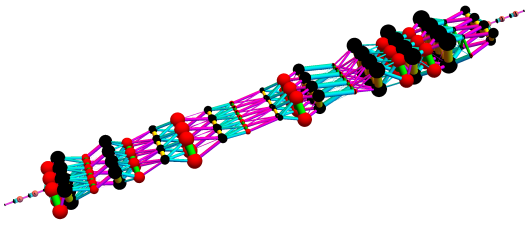

Figure 7.6

The same device as in Fig. 7.5, showing a different view point.

REFERENCES

[1] Tchavdar N Todorov. Tight-binding simulation of current-carrying nanostructures. *Journal of Physics: Condensed Matter*, 14(11):3049, 2002.

[2] Rolf Landauer. Spatial variation of currents and fields due to localized scatterers in metallic conduction. *IBM Journal of Research and Development*, 1(3):223–231, 1957.

[3] Supriyo Datta. *Electronic transport in mesoscopic systems*. Cambridge University Press, 1997.

[4] Supriyo Datta. *Quantum transport: atom to transistor*. Cambridge University Press, 2005.

[5] David Ferry and Stephen Marshall Goodnick. *Transport in nanostructures*. Number 6. Cambridge University Press, 1997.

[6] Philippe Dollfus et al. *Simulation of Transport in Nanodevices*. John Wiley & Sons, 2016.

[7] Rolf Landauer. Electrical resistance of disordered one-dimensional lattices. *Philosophical Magazine*, 21(172):863–867, 1970.

[8] M. Büttiker, Y. Imry, R. Landauer, and S. Pinhas. Generalized many-channel conductance formula with application to small rings. *Physical Review B*, 31(10):6207, 1985.

[9] Thierry Ouisse. *Electron transport in nanostructures and mesoscopic devices: An introduction*. John Wiley & Sons, 2013.

[10] Stefan Frank, Philippe Poncharal, Z.L. Wang, and Walt A. De Heer. Carbon nanotube quantum resistors. *Science*, 280(5370):1744–1746, 1998.

[11] Carter T. White and Tchavdar N. Todorov. Carbon nanotubes as long ballistic conductors. *Nature*, 393(6682):240–242, 1998.

[12] R de Picciotto, HL Stormer, LN Pfeiffer, KW Baldwin, and KW West. Four-terminal resistance of a ballistic quantum wire. *Nature*, 411(6833):51–54, 2001.

[13] Jens Baringhaus, Ming Ruan, Frederik Edler, Antonio Tejeda, Muriel Sicot, Amina Taleb-Ibrahimi, An-Ping Li, Zhigang Jiang, Edward H Conrad, Claire Berger, et al. Exceptional ballistic transport in epitaxial graphene nanoribbons. *Nature*, 506(7488):349–354, 2014.

[14] Adrian Bachtold, Peter Hadley, Takeshi Nakanishi, and Cees Dekker. Logic circuits with carbon nanotube transistors. *Science*, 294(5545):1317–1320, 2001.

[15] Philip W. Anderson. Absence of diffusion in certain random lattices. *Physical Review*, 109(5):1492, 1958.

[16] Bernhard Kramer and Angus MacKinnon. Localization: theory and experiment. *Reports on Progress in Physics*, 56(12):1469, 1993.

[17] Patrick A. Lee and Daniel S. Fisher. Anderson localization in two dimensions. *Physical Review Letters*, 47(12):882, 1981.

[18] M.A. Novotny. Energy-independent total quantum transmission of electrons through nanodevices with correlated disorder. *Physical Review B*, 90(16):165103, 2014.

[19] D. Daboul, I. Chang, and A. Aharony. Series expansion study of quantum percolation on the square lattice. *The European Physical Journal B-Condensed Matter and Complex Systems*, 16(2):303–316, 2000.

[20] M. Fhokrul Islam and Hisao Nakanishi. Localization-delocalization transition in a two-dimensional quantum percolation model. *Physical Review E*, 77(6):061109, 2008.

[21] Eduardo Cuansing and J-S Wang. Quantum transport in honeycomb lattice ribbons with armchair and zigzag edges coupled to semi-infinite linear chain leads. *The European Physical Journal B-Condensed Matter and Complex Systems*, 69(4):505–513, 2009.

[22] S. Boettcher, C. Varghese, and M.A. Novotny. Quantum transport through hierarchical structures. *Physical Review E*, 83(4):041106, 2011.

[23] M.A. Novotny, L. Solomon, and G. Inkoom. Quantum transport through a fully connected network with disorder. *Physics Procedia*, 53:71–74, 2014.

[24] M.A. Novotny. How ubiquitous are dragon segments in quantum transmission? *arXiv preprint arXiv:1502.07814*, 2015.

[25] Zhiping Lin and Youyan Liu. Electronic transport properties of the Bethe lattices. *Physics Letters A*, 320(1):70–80, 2003.

[26] Chris Varghese and M.A. Novotny. Quantum transport through fully connected Bethe lattices. *International Journal of Modern Physics C*, 23(08):1240010, 2012.

[27] Guiseppe Grosso and Pastori Guiseppel Parravicini. *Solid State Physics*. Number 2. Elsevier Ltd, 2014.

[28] Philip F. Bagwell and Terry P. Orlando. Landauer's conductance formula and its generalization to finite voltages. *Physical Review B*, 40(3):1456, 1989.

[29] Deji Akinwande, Nicholas Petrone, and James Hone. Two-dimensional flexible nanoelectronics. *Nature Communications*, 5:5678, 2014.

[30] Sheneve Z Butler, Shawna M Hollen, Linyou Cao, Yi Cui, Jay A Gupta, Humberto R Gutiérrez, Tony F Heinz, Seung Sae Hong, Jiaxing Huang, Ariel F Ismach, et al. Progress, challenges, and opportunities in two-dimensional materials beyond graphene. *ACS Nano*, 7(4):2898–2926, 2013.

[31] Ji-Hui Yang, Yueyu Zhang, Wan-Jian Yin, XG Gong, Boris I Yakobson, and Su-Huai Wei. Two-dimensional sis layers with promising electronic and optoelectronic properties: theoretical prediction. *Nano Letters*, 16(2):1110–1117, 2016.

[32] QH Wang, K Kalantar Zadeh, JN Coleman Kis, A, and MS Strano. Electronics and optoelectronics of two-dimenional transition metal dichalcogenides. *Nature Nanotechnologyl*, 7:699, 2012.

[33] Gianluca Fiori, Francesco Bonaccorso, Giuseppe Iannaccone, Tomás Palacios, Daniel Neumaier, Alan Seabaugh, Sanjay K Banerjee, and Luigi Colombo. Electronics based on two-dimensional materials. *Nature Nanotechnology*, 9(10):768–779, 2014.

[34] KS Novoselov and AH Castro Neto. Two-dimensional crystals-based heterostructures: materials with tailored properties. *Physica Scripta*, 2012(T146):014006, 2012.

[35] Kostya S Novoselov, Andre K Geim, Sergei V Morozov, D Jiang, Y_Zhang, Sergey V Dubonos, Irina V Grigorieva, and Alexandr A Firsov. Electric field effect in atomically thin carbon films. *Science*, 306(5696):666–669, 2004.

[36] Sumio Iijima. Helical microtubules of graphitic carbon. *Nature*, 354(6348):56, 1991.

[37] Ray H Baughman, Anvar A Zakhidov, and Walt A De Heer. Carbon nanotubes–the route toward applications. *Science*, 297(5582):787–792, 2002.

[38] R Tenne. Inorganic nanotubes and fullerene-like nanoparticles. *Journal of Materials Research*, 21(11):2726–2743, 2006.

[39] Jun Song Chen and Xiong Wen David Lou. Sno2 -based nanomaterials: Synthesis and application in lithium-ion batteries. *Small*, 9(11):1877–1893, 2013.

[40] Luhua Li, Ying Chen, and Zbigniew H Stachurski. Boron nitride nanotube reinforced polyurethane composites. *Progress in Natural Science: Materials International*, 23(2):170–173, 2013.

[41] Jaeil Bai, Xiao Cheng Zeng, Hideki Tanaka, and JY Zeng. Metallic single-walled silicon nanotubes. *Proceedings of the National Academy of Sciences of the United States of America*, 101(9):2664–2668, 2004.

[42] MJ Lagos, Fernando Sato, Jeferson Bettini, Varlei Rodrigues, Douglas S Galvao, and Daniel Ugarte. Observation of the smallest metal nanotube with a square cross-section. *Nature Nanotechnology*, 4(3):149–152, 2009.

[43] Junqing Hu, Zhigang Chen, Hao Jiang, Yangang Sun, Yoshio Bando, and Dmitri Golberg. Rectangular or square, tapered, and single-crystal pbte nanotubes. *Journal of Materials Chemistry*, 19(19):3063–3068, 2009.

[44] KS Novoselov, A Mishchenko, A Carvalho, and AH Castro Neto. 2d materials and van der waals heterostructures. *Science*, 353(6298):aac9439, 2016.

[45] KS Novoselov, D Jiang, F Schedin, TJ Booth, VV Khotkevich, SV Morozov, and AK Geim. Two-dimensional atomic crystals. *Proceedings of the National Academy of Sciences of the United States of America*, 102(30):10451–10453, 2005.

[46] Daowei He, Yuhan Zhang, Qisheng Wu, Rui Xu, Haiyan Nan, Junfang Liu, Jianjun Yao, Zilu Wang, Shijun Yuan, Yun Li, et al. Two-dimensional quasi-freestanding molecular crystals for high-performance organic field-effect transistors. *Nature Communications*, 5, 2014.

[47] Jiong Zhao, Qingming Deng, Alicja Bachmatiuk, Gorantla Sandeep, Alexey Popov, Jürgen Eckert, and Mark H Rümmeli. Free-standing single-atom-thick iron membranes suspended in graphene pores. *Science*, 343(6176):1228–1232, 2014.

[48] Kuibo Yin, Yu-Yang Zhang, Yilong Zhou, Litao Sun, Matthew F Chisholm, Sokrates T Pantelides, and Wu Zhou. Unsupported single-atom-thick copper oxide monolayers. *2D Materials*, 4(1):011001, 2016.

[49] Lei Liu, Jieshu Qian, Bo Li, Yuming Cui, Xingfu Zhou, Xuefeng Guo, and Weiping Ding. Fabrication of rutile tio2 tapered nanotubes with rectangular cross-sections via anisotropic corrosion route. *Chemical Communications*, 46(14):2402–2404, 2010.

[50] PAS Autreto, SB Legoas, MZS Flores, and DS Galvao. Carbon nanotube with square cross-section: An ab initio investigation. *The Journal of Chemical Physics*, 133(12):124513, 2010.

[51] B Babić and C Schönenberger. Observation of fano resonances in single-wall carbon nanotubes. *Physical Review B*, 70(19):195408, 2004.

[52] TA Papadopoulos, IM Grace, and CJ Lambert. Control of electron transport through fano resonances in molecular wires. *Physical Review B*, 74(19):193306, 2006.

[53] VA Margulis and MA Pyataev. Fano resonances in a three-terminal nanodevice. *Journal of Physics: Condensed Matter*, 16(24):4315, 2004.

[54] J Göres, D Goldhaber-Gordon, S Heemeyer, MA Kastner, Hadas Shtrikman, D Mahalu, and U Meirav. Fano resonances in electronic transport through a single-electron transistor. *Physical Review B*, 62(3):2188, 2000.

[55] Erkan Tekman and Philip F Bagwell. Fano resonances in quasi-one-dimensional electron waveguides. *Physical Review B*, 48(4):2553, 1993.

[56] Jinhee Kim, Jae-Ryoung Kim, Jeong-O Lee, Jong Wan Park, Hye Mi So, Nam Kim, Kicheon Kang, Kyung-Hwa Yoo, and Ju-Jin Kim. Fano resonance in crossed carbon nanotubes. *Physical Review Letters*, 90(16):166403, 2003.

[57] Stefano Stassi, Alessandro Chiadò, Giuseppe Calafiore, Gianluca Palmara, Stefano Cabrini, and Carlo Ricciardi. Experimental evidence of fano resonances in nanomechanical resonators. *Scientific Reports*, 7(1):1065, 2017.

[58] Ho-Tong Lee and Andrew W Poon. Fano resonances in prism-coupled square micropillars. *Optics Letters*, 29(1):5–7, 2004.

[59] MV Rybin, AB Khanikaev, M Inoue, KB Samusev, MJ Steel, G Yushin, and MF Limonov. Fano resonance between mie and bragg scattering in photonic crystals. *Physical Review Letters*, 103(2):023901, 2009.

[60] Shanhui Fan. Sharp asymmetric line shapes in side-coupled waveguide-cavity systems. *Applied Physics Letters*, 80(6):908–910, 2002.

[61] Bei-Bei Li, Yun-Feng Xiao, Chang-Ling Zou, Yong-Chun Liu, Xue-Feng Jiang, You-Ling Chen, Yan Li, and Qihuang Gong. Experimental observation of fano resonance in a single whispering-gallery microresonator. *Applied Physics Letters*, 98(2):021116, 2011.

[62] S Satpathy, A Roy, and A Mohapatra. Fano interference in classical oscillators. *European Journal of Physics*, 33(4):863, 2012.

[63] Yong S Joe, Arkady M Satanin, and Chang Sub Kim. Classical analogy of fano resonances. *Physica Scripta*, 74(2):259, 2006.

[64] A Kumar, L Saminadayar, DC Glattli, Y Jin, and B Etienne. Experimental test of the quantum shot noise reduction theory. *Physical review letters*, 76(15):2778.

[65] Wen-Chyuan Yueh. Eigenvalues of several tridiagonal matrices. *Applied mathematics e-notes*, 5(66-74):210–230, 2005.

[66] E Cuansing and Hisao Nakanishi. Quantum interference effects in particle transport through square lattices. *Physical Review E*, 70(6):066142, 2004.

[67] G Lombardi and R Rebaudo. Eigenvalues and eigenvectors of a special class of band matrices. 1988.

[68] Anil K Jain. A sinusoidal family of unitary transforms. *IEEE Transactions on Pattern Analysis and Machine Intelligence*, (4):356–365, 1979.

[69] Charles R MacCluer. The many proofs and applications of perron's theorem. *Siam Review*, 42(3):487–498, 2000.

[70] Serre Denis. *Matrices Theory and Applications*. Springer-Verlag, 2002.

[71] Gilbert Strang. *Introduction to linear algebra*, volume 3. Cambridge University Press, 2009.

[72] MJM De Jong and CWJ Beenakker. Shot noise in mesoscopic systems. In *Mesoscopic Electron Transport*, pages 225–258. 1997.

[73] U Nithiyanantham, M Fevzi Ozaydin, Abdullah S Tazebay, and Subrata Kundu. Low temperature formation of rectangular pbte nanocrystals and their thermoelectric properties. *New Journal of Chemistry*, 40(1):265–277, 2016.

[74] C Sirvent, JG Rodrigo, S Vieira, L Jurczyszyn, N Mingo, and F Flores. Conductance step for a single-atom contact in the scanning tunneling microscope: Noble and transition metals. *Physical Review B*, 53(23):16086, 1996.

[75] Tokushi Kizuka and Kosuke Monna. Atomic configuration, conductance, and tensile force of platinum wires of single-atom width. *Physical review B*, 80(20):205406, 2009.

[76] SK Nielsen, Yves Noat, Mads Brandbyge, RHM Smit, K Hansen, LY Chen, AI Yanson, Flemming Besenbacher, and JM Van Ruitenbeek. Conductance of single-atom platinum contacts: Voltage dependence of the conductance histogram. *Physical Review B*, 67(24):245411, 2003.

[77] George W Hanson. *Fundamentals of nanoelectronics*. Pearson/Prentice Hall Upper Saddle River, 2008.

[78] Ali Javey, Jing Guo, Qian Wang, Mark Lundstrom, and Hongjie Dai. Ballistic carbon nanotube field-effect transistors. *Nature*, 424(6949):654–657, 2003.

[79] Justin Wu, Liming Xie, Guosong Hong, Hong En Lim, Boanerges Thendie, Yasumitsu Miyata, Hisanori Shinohara, and Hongjie Dai. Short channel field-effect transistors from highly enriched semiconducting carbon nanotubes. *Nano Research*, pages 1–7, 2012.

[80] Sung-Jin Choi, Patrick Bennett, Kuniharu Takei, Chuan Wang, Cheuk Chi Lo, Ali Javey, and Jeffrey Bokor. Short-channel transistors constructed with solution-processed carbon nanotubes. *ACS Nano*, 7(1):798–803, 2012.

[81] Sung Ho Kim, Wooseok Song, Min Wook Jung, Min-A Kang, Kiwoong Kim, Sung-Jin Chang, Sun Sook Lee, Jongsun Lim, Jinha Hwang, Sung Myung, et al. Carbon nanotube and graphene hybrid thin film for transparent electrodes and field effect transistors. *Advanced Materials*, 26(25):4247–4252, 2014.

[82] MA Novotny, L Solomon, Chris Varghese, and Stefan Boettcher. Renormalization group calculation of electron transport through a fully connected blob. *Physics Procedia*, 4:85–88, 2010.

[83] Hideo Aoki. Decimation method of real-space renormalization for electron systems with application to random systems. *Physica A: Statistical Mechanics and its Applications*, 114(1-3):538–542, 1982.

APPENDIX A

DERIVATION OF TRANSMISSION PROBABILITY FOR DIMERIZED LEADS AND OTHER QUANTUM DRAGON SOLUTIONS FOR LINEAR NANODEVICES

This appendix has three separate parts. They are

- Appendix A.1: Transmission, $\mathcal{T}$ for dimerized leads derivation
- Appendix A.2: Quantum dragon solutions for $m = 1$ and $l = 2$
- Appendix A.3: Example numerical results for $m = 1$ with $l = 2, 4, 8, 16$

A.1 Transmission, $\mathcal{T}$ for dimerized leads, derivation

The derivation of the transmission for odd-even interactions and on-site energies in the semi-infinite leads, i.e., for dimerized leads as in Fig. A.1, is presented.

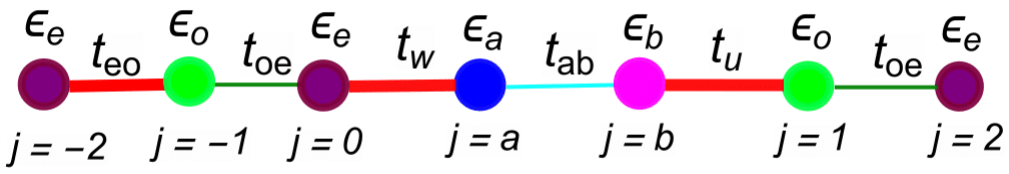

Figure A.1

A device connected to input (incoming) and output (outgoing) leads.

In Fig. A.1, the $m = 1, l = 2$ device is located between lead sites $j = 0$ and $j = 1$. The hopping strength between site $j = 0$ and site $j = a$ is denoted by t_w. The inter-slice hopping parameter between the site $j = 1$ and the site $j = b$ is denoted by t_u. The hopping

interactions between the even-to-odd sites and odd-to-even sites in the leads are denoted by t_{eo} and t_{oe}, respectively. The on-site energy for odd numbered lead sites is ϵ_o, and for the even lead sites ϵ_e. The device has on-site energies ϵ_a and ϵ_b, and hopping strength t_{ab} between the two leads.

The derivation of the transmission for odd-even interactions and on-site energies in the semi-infinite leads, i.e., for dimerized leads as in Fig. A.1, is presented. The matrix method is used throughout. The inter-slice hopping strengths between the even-to-odd lead sites are t_{eo}, and between the odd-to-even lead sites are t_{oe}. The negative signs for the hopping interactions are included explicitly, for instance, the hopping between lead sites labeled -1 and 0 is $-t_{oe}$ with $t_{oe} > 0$. The time-independent Schrödinger matrix equation to solve is

$$(\mathcal{H} - E\mathbf{I}_\infty)\,\vec{\Psi} = \vec{0}\,, \tag{A.1}$$

where $\mathcal{H}$ is the Hamiltonian of the incoming electron, E is the energy of the incoming electron, and $\vec{\Psi}$ the infinite vector containing as the elements the wavefunction ψ_j for site j. Assume lead sites have different on-site energies. The on-site energies for lead sites labeled even is ϵ_e and the on-site energies for lead sites labeled odd is ϵ_o. The form of the lattice, written for two sites (labeled a and b) in the nano-device which are placed between lead sites numbered 0 and 1 is shown in Fig. A.1. By multiplying the matrix and vector in

Eq. (A.1) to the sites that are not connected directly to the 2-site device, this results in the set of infinite equations expressed as

$$\begin{aligned}
-t_{oe}\psi_{j-1} + (\epsilon_e - E)\psi_j - t_{eo}\psi_{j+1} &= 0 \qquad j = \cdots, -6, -4, -2 \\
-t_{eo}\psi_{j-1} + (\epsilon_o - E)\psi_j - t_{oe}\psi_{j+1} &= 0 \qquad j = \cdots, -5, -3, -1 \\
-t_{oe}\psi_{j-1} + (\epsilon_e - E)\psi_j - t_{eo}\psi_{j+1} &= 0 \qquad j = 2, 4, 6, \cdots \\
-t_{eo}\psi_{j-1} + (\epsilon_o - E)\psi_j - t_{oe}\psi_{j+1} &= 0 \qquad j = 3, 5, 7, \cdots .
\end{aligned} \tag{A.2}$$

It should be noted that in Eq. (A.2), the sites numbered 0 and 1 are not included since they couple to the device sites. In this approach, an $ansatz$ is used which assumes Bloch wavefunctions for the lead. Let χ an undetermined parameter in the $ansatz$ for the lead wave functions which takes into account the nature of a Bloch wavefunction in the dimerized leads. Explicitly

$$\begin{aligned}
\psi_j &= \chi e^{iqj} + r\,\chi^* e^{-iqj} \qquad j = -\infty, \cdots, -4, -2, 0 \\
\psi_j &= e^{iqj} + r\, e^{-iqj} \qquad j = -\infty, \cdots, -5, -3, -1 \\
\psi_j &= t_T\, \chi e^{iq(j-1)} \qquad j = 2, 4, \cdots, +\infty \\
\psi_j &= t_T\, e^{iq(j-1)} \qquad j = 1, 3, 5, 7, 9 \cdots, +\infty
\end{aligned} \tag{A.3}$$

where the $ansatz$ is also valid for sites numbered 0 and 1 which connect to the device. The $ansatz$ is a traveling wave coming from $-\infty$, impinging on the device, and being partly reflected back to $-\infty$ and partly transmitted to ∞. Here, $|t_T|^2 + |r|^2 = \mathcal{T} + \mathcal{R} = 1$. Note

both leads are identical. Substitute the $ansatz$ in Eq. (A.3) back into Eq. (A.2). This gives the infinite sets of equations expressed as

$$\begin{aligned}
e^{iqj}[-t_{oe}e^{-iq} + (\epsilon_e - E)\chi - t_{eo}e^{iq}] + re^{-iqj}[-t_{oe}e^{iq} + (\epsilon_e - E)\chi^* - t_{eo}e^{-iq}] &= 0 \qquad j1 \\
e^{iqj}[-t_{eo}\chi e^{-iq} + (\epsilon_o - E) - t_{oe}\chi e^{iq}] + re^{-iqj}[-t_{eo}\chi^* e^{iq} + (\epsilon_o - E) - t_{oe}\chi^* e^{-iq}] &= 0 \qquad j2 \\
t_T e^{iq(j-1)}[-t_{oe}e^{-iq} + (\epsilon_e - E)\chi - t_{eo}e^{iq}] &= 0 \qquad j3 \\
t_T e^{iq(j-1)}[-t_{eo}\chi e^{-iq} + (\epsilon_o - E) - t_{oe}\chi e^{iq}] &= 0 \qquad j4\,.
\end{aligned} \tag{A.4}$$

where we have defined for convenience $j1$ as Eq. (2.10), $j2$ as Eq. (2.11), $j3$ as Eq. (2.12) and $j4$ as Eq. (2.13). The two equations for the outgoing lead in Eq. (A.4) can be manipulated to eliminate the phase factor χ. The Bloch structure of the even-odd dimerized leads is captured by χ. This gives

$$\chi = \frac{t_{eo}e^{iq} + t_{oe}e^{-iq}}{\epsilon_e - E} = \frac{\epsilon_o - E}{t_{eo}e^{-iq} + t_{oe}e^{iq}}\,. \tag{A.5}$$

Eq. (A.5) is satisfied provided

$$\cos(2q) = \frac{(\epsilon_e - E)(\epsilon_o - E) - t_{eo}^2 - t_{oe}^2}{2t_{eo}t_{oe}}\,, \tag{A.6}$$

or with the double-angle formula for $\cos(2q)$

$$\cos(q) = \pm\sqrt{\frac{(\epsilon_e - E)(\epsilon_o - E) - (t_{eo} - t_{oe})^2}{4t_{eo}t_{oe}}}\,. \tag{A.7}$$

From trigonometry, since $\cos(q)^2 + \sin(q)^2 = 1$, this means that from Eq. (A.7)

$$\sin q = \pm\sqrt{\frac{4t_{eo}t_{oe} - [(\epsilon_e - E)(\epsilon_o - E) - (t_{eo} - t_{oe})^2]}{4t_{eo}t_{oe}}}\,. \tag{A.8}$$

The quantity in the numerator under the square root in Eq. (A.8) can be simplified and hence, Eq. (A.8) can be re-expressed as

$$\sin q = \pm\sqrt{\frac{(t_{eo}+t_{oe})^2 - [(\epsilon_e - E)(\epsilon_o - E)]}{4t_{eo}t_{oe}}}\,. \tag{A.9}$$

In the case where $\epsilon_e = \epsilon_o = 0$, Eq. (A.7) reduces to

$$\cos(q) = \pm\sqrt{\frac{E^2 - (t_{eo}-t_{oe})^2}{4t_{eo}t_{oe}}} \tag{A.10}$$

which is the result in Appendix A of reference [18]. From Eq. (A.5), when $\epsilon_o = \epsilon_e = 0$, the expression for χ reduces to

$$\chi = -\frac{t_{eo}e^{iq} + t_{oe}e^{-iq}}{E} = -\frac{E}{t_{eo}e^{-iq} + t_{oe}e^{iq}}\,. \tag{A.11}$$

which is the also one of equations in Appendix A of reference [18]. The Schrödinger equation for the input lead terms are satisfied with these values of χ and q. Using Eq. (A.7), the energy range of propagation of propagating electrons can be calculated, since for traveling waves one requires

$$-1 \leq \cos q \leq 1. \tag{A.12}$$

Therefore

$$-1 \leq -\sqrt{\frac{(\epsilon_e - E)(\epsilon_o - E) - (t_{eo}-t_{oe})^2}{4t_{eo}t_{oe}}} \leq 0, \tag{A.13}$$

and the other sign in Eq. (A.7) gives

$$0 \leq \sqrt{\frac{(\epsilon_e - E)(\epsilon_o - E) - (t_{eo}-t_{oe})^2}{4t_{eo}t_{oe}}} \leq 1\,. \tag{A.14}$$

One has a complete freedom to set the zero of energy of the entire quantum system. A reasonable choice for the zero of energy is $\frac{\epsilon_e+\epsilon_o}{2}$. Setting the zero of energy at the midpoint

of ϵ_o and ϵ_e makes the subsequent algebra easier. Therefore the propagating waves for negative energies are

$$-\sqrt{\vartheta^2 + (t_{eo} + t_{oe})^2} \leq E \leq -\sqrt{\vartheta^2 + (t_{eo} - t_{oe})^2} \tag{A.15}$$

and

$$\sqrt{\vartheta^2 + (t_{eo} - t_{oe})^2} \leq E \leq \sqrt{\vartheta^2 + (t_{eo} + t_{oe})^2} \tag{A.16}$$

for positive energies where $\vartheta = \frac{\epsilon_e - \epsilon_o}{2}$. When $\epsilon_e = \epsilon_o = 0$ and $t_{eo} \neq t_{oe}$, Eq. (A.15) and Eq. (A.16) allows propagation modes in the leads for both negative and positive energies respectively expressed by [18]

$$-|t_{eo} + t_{oe}| \leq E \leq -|t_{eo} - t_{oe}| \qquad \text{and} \qquad |t_{eo} - t_{oe}| \leq E \leq |t_{eo} + t_{oe}| \ . \tag{A.17}$$

When $t_{oe} = t_{eo} = t_{lead}$ this further simplifies to the input lead terms with these values of

$$-2t_{lead} \leq E \leq 2t_{lead} \, . \tag{A.18}$$

The Schrödinger equation of Eq. (A.1) is satisfied for all sites, except so far for sites labeled 0, a, b, and 1. For the two device sites define $\kappa_a = \epsilon_a - E$ and $\kappa_b = \epsilon_b - E$. Using the *ansatz* of Eq. (A.3), there are four equations still to be solved. The part with the device and the connections between the leads and the device, from

$$(\mathcal{H} - E\mathbf{I})\, \vec{\Psi} = \vec{0} \, , \tag{A.19}$$

in Eq. (A.1) is

$$\begin{pmatrix} -t_{oe} & (\epsilon_e - E) & -t_w & 0 & 0 & 0 \\ 0 & -t_w & \kappa_a & -t_{ab} & 0 & 0 \\ 0 & 0 & -t_{ab} & \kappa_b & -t_u & 0 \\ 0 & 0 & 0 & -t_u & (\epsilon_o - E) & -t_{oe} \end{pmatrix} \begin{pmatrix} e^{-iq} + re^{iq} \\ \chi + r\chi^* \\ \psi_a \\ \psi_b \\ t_T \\ t_T \chi e^{iq} \end{pmatrix} = \begin{pmatrix} 0 \\ 0 \\ 0 \\ 0 \end{pmatrix}. \tag{A.20}$$

Multiplying through gives the four equations

$$\begin{pmatrix} -t_{oe}e^{-iq} - t_{oe}re^{iq} + (\epsilon_e - E)\chi + (\epsilon_e - E)r\chi^* - t_w\psi_a \\ -t_w\chi - t_w r\chi^* + \kappa_a\psi_a - t_{ab}\psi_b \\ -t_{ab}\psi_a + \kappa_b\psi_b - t_u t_T \\ -t_u\psi_b + (\epsilon_o - E)t_T - t_{oe}t_T\chi e^{iq} \end{pmatrix} = \begin{pmatrix} 0 \\ 0 \\ 0 \\ 0 \end{pmatrix}. \tag{A.21}$$

Eq. (A.21) can be rewritten as

$$\begin{pmatrix} -t_{oe}e^{-iq} - t_{oe}re^{iq} + (\epsilon_e - E)\chi + (\epsilon_e - E)r\chi^* - t_w\psi_a \\ -t_w\chi - t_w r\chi^* + \kappa_a\psi_a - t_{ab}\psi_b \\ -t_{ab}\psi_a + \kappa_b\psi_b - t_u t_T \\ -t_u\psi_b + t_T\xi_R(E) \end{pmatrix} = \begin{pmatrix} 0 \\ 0 \\ 0 \\ 0 \end{pmatrix} \tag{A.22}$$

where in the bottom equation we can define

$$\xi_R(E) = (\epsilon_o - E) - t_{oe}\chi e^{iq}. \tag{A.23}$$

Eq. (A.22) can be written in the matrix form

$$\begin{pmatrix} \xi_L(E) & -t_w & 0 & 0 \\ -t_w & \kappa_a & -t_{ab} & 0 \\ 0 & -t_{ab} & \kappa_b & -t_u \\ 0 & 0 & -t_u & \xi_R(E) \end{pmatrix} \begin{pmatrix} \chi + r\chi^* \\ \psi_a \\ \psi_b \\ t_T \end{pmatrix} = \begin{pmatrix} \Lambda(E) \\ 0 \\ 0 \\ 0 \end{pmatrix} . \tag{A.24}$$

From the first row of Eq. (A.24) by multiplying through, it can be seen that

$$\xi_L\chi - \Lambda + \xi_L r\chi^* - t_w\psi_a = 0 \, . \tag{A.25}$$

Similarly, from the first row of Eq. (A.22), by multiplying through it can be seen

$$-t_{oe}e^{-iq} + (\epsilon_e - E)\chi + r[\chi^*(\epsilon_e - E) - t_{oe}e^{iq}] - t_w\psi_a = 0 \, . \tag{A.26}$$

From Eq. (A.25) and Eq. (A.26), it can be seen that

$$\xi_L\chi - \Lambda = -t_{oe}e^{-iq} + (\epsilon_e - E)\chi \tag{A.27}$$

and

$$\xi_L\chi^* = \chi^*(\epsilon_e - E) - t_{oe}e^{iq} \, . \tag{A.28}$$

Solving for ξ_L from Eq. (A.28) gives

$$\xi_L(E) = \frac{\chi^*(\epsilon_e - E) - t_{oe}e^{iq}}{\chi^*}. \tag{A.29}$$

Substitute the expression of ξ_L in Eq. (A.29) back into Eq. (A.27) and then solve for Λ. Upon substitution and a little algebra this yields

$$\Lambda = \frac{-t_{oe}}{\chi^*}(\chi e^{iq} - \chi^* e^{-iq}). \tag{A.30}$$

Therefore solving the matrix equation in Eq. (A.24) means the Schrödinger equation is also satisfied for the device and the lead sites connected to the device. It should be noted that the matrix equation to solve can easily be extended to more than two sites in the device. By calculating the probability current of the *ansatz*, the transmission for any t_{eo} and t_{oe} and any ϵ_e and ϵ_o is given by

$$\mathcal{T} = |t_T|^2. \tag{A.31}$$

In the rest of the section, other simplified expressions of $\xi_L(E)$, $\xi_R(E)$ and Λ are derived. The goal is to aid in the transmission probability calculation when there are dimerized on-site energies, ϵ_e and ϵ_o in the leads as well as dimerized hopping strengths t_{eo} and t_{oe}. Substitute the definition of $\chi = \frac{(\epsilon_o - E)}{t_{eo}e^{-iq} + t_{oe}e^{iq}}$ from Eq. (A.5) into $\xi_R(E)$ in Eq. (A.23). This means that $\xi_R(E)$ can be reexpressed as

$$\xi_R(E) = (\epsilon_o - E) - t_{oe}\chi e^{iq} = (\epsilon_o - E)\left[1 - \frac{t_{oe}e^{iq}}{t_{eo}e^{-iq} + t_{oe}e^{iq}}\right]. \tag{A.32}$$

Eq. (A.32) can further be written as

$$\xi_R(E) = \frac{(\epsilon_o - E)t_{eo}e^{-iq}}{t_{eo}e^{-iq} + t_{oe}e^{iq}} \tag{A.33}$$

upon small algebra manipulations. Similarly, from Eq. (A.29) for $\xi_L(E)$ using the definition of $\chi^* = \frac{t_{eo}e^{iq} + t_{oe}e^{-iq}}{\epsilon_e - E}$ from Eq. (A.5) this means that

$$\xi_L(E) = (\epsilon_e - E) - \frac{t_{oe}e^{iq}}{\chi^*} = (\epsilon_e - E)\left[1 - \frac{t_{oe}e^{iq}}{t_{eo}e^{-iq} + t_{oe}e^{iq}}\right]. \tag{A.34}$$

Eq. (A.34) can be further be re-expressed as

$$\xi_L(E) = \frac{(\epsilon_e - E)t_{eo}e^{-iq}}{t_{eo}e^{-iq} + t_{oe}e^{iq}} \tag{A.35}$$

upon small algebra manipulations. Now from the definition of Λ in Eq. (A.30) let

$$\Upsilon = \chi e^{iq} - \chi^* e^{-iq}. \tag{A.36}$$

This means that the expression for Λ in Eq. (A.30) can be expresssed as

$$\Lambda = \frac{-t_{oe}}{\chi^*}\Upsilon. \tag{A.37}$$

Use the definition of χ and χ^* from Eq. (A.5), and a little algebra gives that Υ in Eq. (A.36) can be expressed as

$$\Upsilon = \frac{2it_{eo}(\epsilon_o - E)\sin 2q}{(t_{eo}e^{-iq} + t_{oe}e^{iq})(t_{eo}e^{iq} + t_{oe}e^{-iq})}. \tag{A.38}$$

Use the definition $\chi^* = \frac{t_{eo}e^{iq}+t_{oe}e^{-iq}}{(\epsilon_o - E)}$ from Eq. (A.5) this means that Λ can be rewritten as

$$\Lambda = \frac{-t_{oe}}{\chi^*}\Upsilon = \frac{-2it_{eo}t_{oe}\sin 2q}{t_{eo}e^{-iq} + t_{oe}e^{iq}}. \tag{A.39}$$

In the limiting case where, $t_{eo} = t_{oe} = 1$ for the uniform leads, the expression of Λ in Eq. (A.39) reduces to [18, 19]

$$\Lambda = -2i\sin q. \tag{A.40}$$

A.2 Quantum dragon solutions for $l = 2$ and $m = 1$

In chapter 2, it was shown that for a $m = 1$, $l = 2$ device, the matrix method, the matrix RG method, and the traditional Green's function method all give the same expression for the electron transmission probability. For simplicity, here we let $\epsilon_e = \epsilon_o = 0$, also setting our zero of energy. Thus also $\xi_L = \xi_R = \xi$. This also suggests that the atoms in the incoming as well the outgoing leads are the same. In this section, it will be shown mathematically how to find quantum dragon solutions for $l = 2$ and $m = 1$. The goal is to

show that quantum dragon solutions are ubiquitous. The electron transmission probability for $l = 2$ and $m = 1$ in chapter 2 was given in Eq. (2.26) as

$$\mathcal{T}(E) = \frac{t_w^2 t_u^2 t_{ab}^2 \Lambda^* \Lambda}{[(t_w^2 - \kappa_a \xi)(t_u^2 - \kappa_b \xi) - t_{ab}^2 \xi^2][(t_w^2 - \kappa_a \xi^*)(t_u^2 - \kappa_b \xi^*) - t_{ab}^2 \xi^{*2}]} \,. \tag{A.41}$$

The complex quantities ξ and Λ are different for both the non-dimerized leads and dimerized leads. They are expressed as Eq. (2.53) and Eq. (2.60). In the limiting case when $t_u = t_w$, this means that Eq. (A.41) can be re-expressed as:

$$\mathcal{T}(E) = \frac{t_w^4 t_{ab}^2 \Lambda^* \Lambda}{[(t_w^2 - \kappa_a \xi)(t_w^2 - \kappa_b \xi) - t_{ab}^2 \xi^2][(t_w^2 - \kappa_a \xi^*)(t_w^2 - \kappa_b \xi^*) - t_{ab}^2 \xi^{*2}]} \,. \tag{A.42}$$

From Eq. (A.42), lets assume further that, $t_w = t_{ab} = 1$ and $\kappa_a = \kappa_b$ which means that Eq. (A.42) can be expressed as

$$\mathcal{T}(E) = \frac{\Lambda^* \Lambda}{[(1 - \kappa_a \xi)^2 - \xi^2][(1 - \kappa_a \xi^*)^2 - \xi^{*2}]} \,. \tag{A.43}$$

Note that in the uniform case $\Lambda = -2i \sin q$ and $\xi = e^{-iq}$. Since $\kappa_a = \epsilon_a - E$, by setting $\epsilon_a = 0$, this means that Eq. (A.43) can be expressed as

$$\mathcal{T}(E) = \frac{4 \sin^2(q)}{[(1 + E\xi)^2 - \xi^2][(1 + E\xi^*)^2 - \xi^{*2}]} \,. \tag{A.44}$$

In the rest of the section, we perform calculations only for uniform leads. In the case of the uniform leads, $\sin q = \frac{\sqrt{4 - E^2}}{2}$ this means that Eq. (A.44) can be re-expressed as

$$\mathcal{T}(E) = \frac{4 - E^2}{[(1 + E\xi)^2 - \xi^2][(1 + E\xi^*)^2 - \xi^{*2}]} \,. \tag{A.45}$$

Using the definitions of $\xi = e^{-iq}$ and $\xi^* = e^{iq}$ this implies that Eq. (A.45) can be expressed as

$$\mathcal{T}(E) = \frac{4 - E^2}{[(1 + Ee^{-iq})^2 - e^{-2iq}][(1 + e^{iq})^2 - e^{2iq}]} \,. \tag{A.46}$$

Looking at the denominator of Eq. (A.46), for simplicity let

$$\alpha = (1 + Ee^{-iq})^2 - e^{-2iq} \tag{A.47}$$

and

$$\alpha^* = (1 + Ee^{iq})^2 - e^{2iq}\,. \tag{A.48}$$

This means that Eq. (A.46) can be rewritten as

$$\mathcal{T}(E) = \frac{4 - E^2}{\alpha\alpha^*}. \tag{A.49}$$

Simplify α and α^* and find $\alpha\alpha^*$ and put these results back into Eq. (A.49). Simplifying Eq. (A.47) further gives

$$\alpha = (1 + Ee^{-iq})^2 - e^{-2iq} = 1 + 2Ee^{-iq} + e^{-2iq}(E^2 - 1)\,. \tag{A.50}$$

Similarly, from Eq. (A.48)

$$\alpha^* = (1 + Ee^{iq})^2 - e^{2iq} = 1 + 2Ee^{iq} + e^{2iq}(E^2 - 1)\,. \tag{A.51}$$

Using the above definitions for α and α^* this means that $\alpha\alpha^*$

$$\alpha\alpha^* = 2 + 2E^2 + E^4 + 4E\cos(q) + 2(E^2 - 1)\cos(2q) + 4E(E^2 - 1)\cos(q)\,. \tag{A.52}$$

Using the double angle formula $\cos 2q = 2\cos^2 q - 1$, Eq. (A.52) can be expressed as

$$\alpha\alpha^* = 2+2E^2+E^4+4E\cos(q)+2(E^2-1)(2\cos q^2-1)+4E(E^2-1)\cos(q)\,. \tag{A.53}$$

Using the fact that for uniform leads $\cos(q) = \frac{-E}{2}$, this means that Eq. (A.53) can be expressed as

$$\alpha\alpha^* = 2 + 2E^2 + E^4 + 4E(-\frac{E}{2}) + 2(E^2 - 1)(\frac{2E^2}{4} - 1) + 4E(-\frac{E}{2})(E^2 - 1)\,. \tag{A.54}$$

Eq. (A.54) can also be rewritten as

$$\alpha\alpha^* = 2 + 2E^2 + E^4 - 2E^2 + 2(E^2-1)\frac{E^2}{2} - 2(E^2-1) - 2E^2(E^2-1)\,. \quad \text{(A.55)}$$

Upon multiplying through and doing a small simplification, Eq. (A.55) can be rewritten as

$$\alpha\alpha^* = 2 + E^4 + E^2(E^2-1) - 2(E^2-1) - 2E^2(E^2-1)\,. \quad \text{(A.56)}$$

Furthermore, Eq. (A.56) can be rewritten as

$$\alpha\alpha^* = 2 + 2 + E^4 + E^4 - 2E^4 - E^2 = 4 - E^2 + 2E^4 - 2E^4\,. \quad \text{(A.57)}$$

and therefore

$$\alpha\alpha^* = 4 - E^2\,. \quad \text{(A.58)}$$

Consequently, Eq. (A.49) can be expressed as

$$\mathcal{T}(E) = \frac{4-E^2}{\alpha\alpha^*} = \frac{4-E^2}{4-E^2} = 1\,. \quad \text{(A.59)}$$

Therefore we have shown mathematically how a quantum dragon solution comes from Eq. (A.43). Note that because in the non-dimerized case $\cos(q) = \frac{-E}{2}$, quantum dragon solutions only exist for the energy range

$$-2 \leq E \leq 2\,. \quad \text{(A.60)}$$

The analysis carried out here can be extended to the case for $m = 1$ and general l, but the algebra becomes much complex than for the uniform case. Similar analysis can also be done for the dimerized leads with $l = 2, m = 1$ but again the algebra becomes more complex. Therefore a numerical approach is beneficial. The plots of $\mathcal{T}(E)$ vs E for uniform and dimerized leads are shown in Fig. A.2 and Fig. A.3.

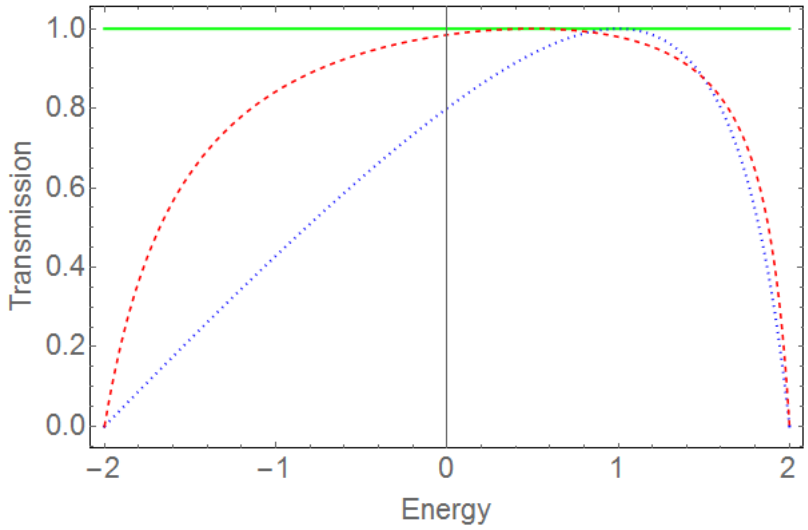

Figure A.2

$\mathcal{T}$ vs E for devices with $l = 2$ and $m = 1$ uniform leads and $\epsilon_e = \epsilon_o = 0$.

In Fig. A.2, the three cases are the quantum dragon solution $\epsilon_a = \epsilon_b = 0$ (green, solid) as well as the cases, $\epsilon_a = \epsilon_b = 0.5$ (red, dashed), $t_{eo} = t_{oe} = 1$, and $\epsilon_a = \epsilon_b = 1$ (blue, dotted).

Fig. A.3, is a plot of $\mathcal{T}$ vs E, for devices with $l = 2$ and $m = 1$ dimerized leads with $t_{eo} = 1$ and $t_{oe} = 3$ and all curves have $t_{oe} = t_{ab}$ and $\epsilon_e = \epsilon_o = 0$. The three cases are the quantum dragon solution $\epsilon_a = \epsilon_b = 0$ (green, solid) as well as the cases $\epsilon_a = \epsilon_b = 0.5$ (red, dashed) and $\epsilon_a = \epsilon_b = 1$ (blue, dotted).

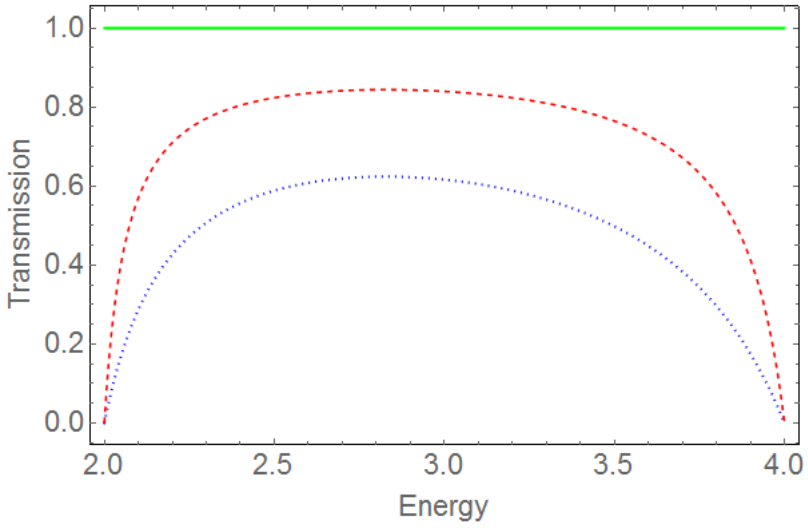

Figure A.3

$\mathcal{T}$ vs E for $l = 2$, $m = 1$ devices for dimerized leads.

A.3 Example numerical results for $m = 1$ and $l = 2, 4, 8, 16$ devices coupled to dimerized leads

In this section, the matrix method will be used to find quantum dragons for $m = 1$ with $l = 2, 4, 8, 16$ sites. In Eq. (2.20) of Chap 2, the matrix equation which was used to calculate $\mathcal{T}(E)$ through the nanodevice between site $j = 0$ and site $j = 1$ was given. This matrix expression can be generalized to any number of sites (atoms) in the linear chain so that the transmission probability as a function of E can be calculated. For instance, for 4 sites in the linear chain in the device which is coupled to single channel incoming and

outgoing dimerized leads, the matrix equation to solve to calculate $\mathcal{T}$ can be expressed as [18]

$$\begin{pmatrix} \xi_L(E) & -t_w & 0 & 0 & 0 & 0 \\ -t_w & \kappa_a & -t_{ab} & 0 & 0 & 0 \\ 0 & -t_{ab} & \kappa_b & -t_{bc} & 0 & 0 \\ 0 & 0 & -t_{bc} & \kappa_c & -t_{cd} & 0 \\ 0 & 0 & 0 & -t_{cd} & \kappa_d & -t_u \\ 0 & 0 & 0 & 0 & -t_u & \xi_R(E) \end{pmatrix} \begin{pmatrix} \chi + r\chi^* \\ \psi_a \\ \psi_b \\ \psi_c \\ \psi_d \\ t_T \end{pmatrix} = \begin{pmatrix} \Lambda \\ 0 \\ 0 \\ 0 \\ 0 \\ 0 \end{pmatrix}. \tag{A.61}$$

Using Eq. (A.61), the transmission probability can be calculated numerically by inverting the matrix, and solving for t_T to obtain the transmission $\mathcal{T} = |t_T|^2$. A plot of $\mathcal{T}$ as a function of E for $m = 1$ and $l = 2, 4, 8, 16$ in the device is shown in Fig. A.4. The dimension of the matrix to invert since $m = 1$ is $(2+l) \times (2+l)$. All couplings and on-site energies have been turned to the quantum dragon solutions.

Fig. A.4, shows a plot of the electron transmission probability vs E, for a linear chain of l sites in the device. The hopping strengths are $t_{eo} = t_w = t_u = 2$ and $t_{oe} = t_{ab} = 3$ and the on-site energy for the atom at site $j = a$ and $j = b$ is $\epsilon_a = \epsilon_b = 0.0$. Here, $l = 2, 4, 8, 16$ in the linear chain in the device. Thus there is full electron transmission provided, $t_{eo} = t_w = t_u$, $t_{oe} = t_{ab}$ and $\epsilon_a = \epsilon_b = \epsilon_L = 0$.

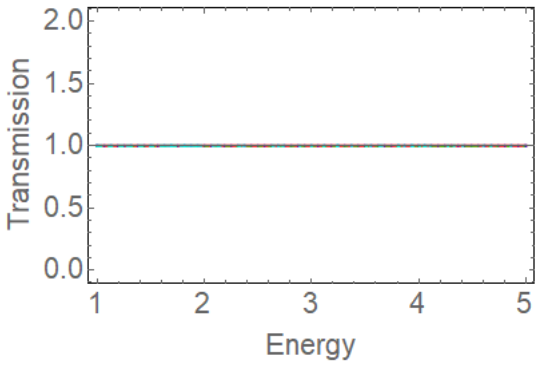

Figure A.4

$\mathcal{T}(E)$ is shown for a linear chain of l sites in the device, with $m = 1$ and $l = 2, 4, 8, 16$.

APPENDIX B

DECIMATION RENORMALIZATION GROUP (RG) CALCULATION

There is more than one way to perform a decimation RG on the transport problem. In section 2.3.1, the decimation RG followed [22, 26], while in this appendix the decimation RG follows [82]. Both methods are exact (no approximations), and are equivalent to each other.

B.1 Decimation Renormalization Group (RG) calculation

The renormalization group (RG) is a mathematical tool which enables one to make changes in a physical system as one views it at different distance scales. To perform RG, certain degrees of freedom corresponding to the original problem are eliminated in some

way. Here, the original problem is assumed to be a quantum system which consists of tight binding sites. In this way, one can then think about the new system as an assembly of the chosen sites which form a lattice which has a larger spacing [83]. The central equation which is used in the RG type of solution for a matrix $\mathbf{F}$ which has dimension of size $n \times n$ can be expressed as

$$\int_{-\infty}^{\infty} \cdots \int_{-\infty}^{\infty} d\vec{x} \exp\left[-\vec{x}^T \mathbf{F} \vec{x} + \vec{b}\vec{x}\right] = \frac{\pi^{\frac{n}{2}}}{\sqrt{\det \mathbf{F}}} \exp\left[\frac{1}{4}\vec{b}^T \mathbf{F}^{-1} \vec{b}\right]. \tag{B.1}$$

The matrix $\mathbf{F}$ is symmetric, where the determinant of the matrix $\det \mathbf{F}$ can be expressed as

$$\det \mathbf{F} = \frac{\pi^n \exp\left[\frac{1}{2}\vec{b}^T \mathbf{F}^{-1} \vec{b}\right]}{\left(\int_{-\infty}^{\infty} \cdots \int_{-\infty}^{\infty} d\vec{x} \exp\left[-\vec{x}^T \mathbf{F} \vec{x} + \vec{b}\vec{x}\right]\right)^2}. \tag{B.2}$$

B.1.1 Quantum transmission solution for 2 site device : RG method

Fig. B.1, shows a schematic representation of the decimation procedure. (a) 2 atom device before decimation. The device is located between site $j = 0$ and $j = 1$. Eliminating the atom at site $j = a$ we obtain the renormalized chain in (b).

By decimating one of the sites, the finite matrix equation to solve for a 2 site device can be expressed as

$$\begin{pmatrix} (\xi - t_w^2 \kappa_a^{-1}) & -t_w \kappa_a^{-1} t_{ab} & 0 \\ -t_{ab} \kappa_a^{-1} t_w & (\kappa_b - \kappa_a^{-1} t_{ab}^2) & -t_u \\ 0 & -t_u & \xi \end{pmatrix} \begin{pmatrix} \chi + r\chi^* \\ \psi_b \\ t_T \end{pmatrix} = \begin{pmatrix} \Lambda \\ 0 \\ 0 \end{pmatrix} \tag{B.3}$$

where the transmission probability, $\mathcal{T}(E) = |t_T(E)|^2$ and the reflection probability, $\mathcal{R}(E) = |r(E)|^2$ can be calculated. Eq. (B.3) is the same as Eq. (2.34) except that here, the wave-function for the device site $j = a$ has been decimated. Eq. (B.3) comes as a result when

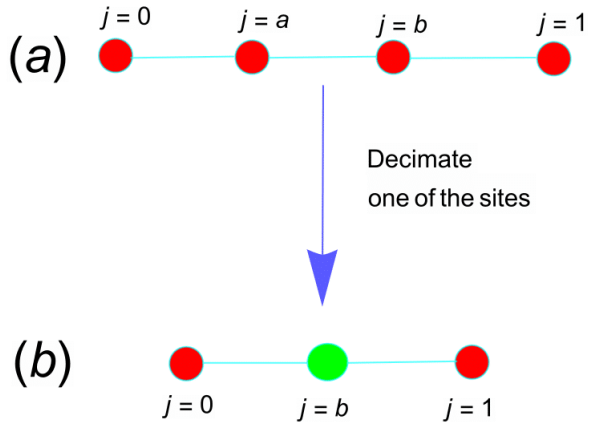

Figure B.1

Schematic representation of the decimation procedure for the atomic site labeled a.

one of the sites in the $l = 2$ linear chain is decimated, or in other words eliminated. In other words, we have used the RG of sec 2.3.1 to decimate the site $j = a$. The RG is shown schematically in Fig. B.1.

To demonstate the RG method of this appendix, we now decimate the site $j = b$. This is shown schematically in Fig. B.2. From Eq. (B.3), the matrix to find the inverse to calculate electron transmission probability is

$$\mathbf{M}_3 = \begin{pmatrix} (\xi - t_w^2 \kappa_a^{-1}) & -t_w \kappa_a^{-1} t_{ab} & 0 \\ -t_{ab} \kappa_a^{-1} t_w & (\kappa_b - \kappa_a^{-1} t_{ab}^2) & -t_u \\ 0 & -t_u & \xi \end{pmatrix} . \tag{B.4}$$

Then from Eq. (B.3) this means that

$$\chi + r\chi^* = (\mathbf{M}_3^{-1})_{(1,1)} \Lambda \, . \tag{B.5}$$

In Eq. (B.5), $(\mathbf{M}_3^{-1})_{(1,1)}$ is the $(1,1)$ element of the inverse of the matrix $\mathbf{M}_3$. To carry out the decimation renormalization group calculation for $\mathbf{M}_3$, number the site just before the blob as x_- and the site after the blob as x_+ and the site of the blob as x_1 and form the vector

$$\vec{x} = \begin{pmatrix} x_- \\ x_1 \\ x_+ \end{pmatrix} . \tag{B.6}$$

Fig. B.1 shows a typical setup of the problem. From Eq. (B.2), the determinant of the matrix can be expressed as

$$\det \mathbf{M}_3 = \frac{\pi^3}{\left(\int_{-\infty}^{\infty}\int_{-\infty}^{\infty}\int_{-\infty}^{\infty} d\vec{x} \exp\left[-\vec{x}^T \mathbf{M}_3 \vec{x}\right] \right)^2} . \tag{B.7}$$

Therefore using Cramer's rule to calculate the $(1,1)$ element of the inverse gives,

$$\chi + r\chi^* = \Lambda \frac{\eta}{\rho} \tag{B.8}$$

where $\eta = \begin{vmatrix} \kappa_b - \frac{t_{ab}^2}{\kappa_a} & -t_u \\ -t_u & \xi \end{vmatrix}$ and $\rho = \begin{vmatrix} \xi - \frac{t_w^2}{\kappa_a} & -\frac{t_w t_{ab}}{\kappa_a} & 0 \\ -\frac{t_w t_{ab}}{\kappa_a} & \kappa_b - \frac{t_{ab}^2}{\kappa_a} & -t_u \\ 0 & -t_u & \xi \end{vmatrix}$,

$$\chi + r\chi^* = \frac{\Lambda}{\pi}\left(\frac{I_3}{I_2}\right)^2 \tag{B.9}$$

where

$$I_3 = \int_{-\infty}^{\infty}\int_{-\infty}^{\infty}\int_{-\infty}^{\infty} dx_- dx_1 dx_+ \exp\left[-\vec{x}^T \mathbf{M}_3 \vec{x} \right] \tag{B.10}$$

and

$$I_2 = \int_{-\infty}^{\infty}\int_{-\infty}^{\infty} dx_1' dx_+' \exp\left[-\begin{pmatrix} x_1' & x_+' \end{pmatrix} \begin{pmatrix} \kappa_b - \frac{t_{ab}^2}{\kappa_a} & -t_u \\ -t_u & \xi \end{pmatrix} \begin{pmatrix} x_1' \\ x_+' \end{pmatrix} \right] . \tag{B.11}$$

From Eq. (B.11), let

$$\beta = \begin{pmatrix} x_1' & x_+' \end{pmatrix} \begin{pmatrix} \kappa_b - \frac{t_{ab}^2}{\kappa_a} & -t_u \\ -t_u & \xi \end{pmatrix} \begin{pmatrix} x_1' \\ x_+' \end{pmatrix} . \tag{B.12}$$

Multiplying through and re-arranging like terms, Eq. (B.12) can be expressed as

$$\beta = \Big(\kappa_b - \frac{t_{ab}^2}{\kappa_a}\Big) x_1'^2 - 2t_u x_+' x_1' + \xi x_+'^2 . \tag{B.13}$$

Put Eq. (B.13) back into Eq. (B.11), Eq. (B.11) can be expressed as

$$I_2 = \int_{-\infty}^{\infty}\int_{-\infty}^{\infty} dx_1' dx_+' \exp\Big[- \Big(\kappa_b - \frac{t_{ab}^2}{\kappa_a}\Big) x_1'^2 - 2t_u x_+' x_1' + \xi x_+'^2 \Big] . \tag{B.14}$$

Eq. (B.14) above can be re-expressed as

$$I_2 = \int_{-\infty}^{\infty} dx_1' \exp\Big[- \Big(\kappa_b - \frac{t_{ab}^2}{\kappa_a}\Big) x_1'^2 - 2t_u x_+' x_1' \Big] \int_{-\infty}^{\infty} dx_+' exp\Big[- \xi x_+'^2 \Big] . \tag{B.15}$$

For simplicity, in Eq. (B.15), let

$$\gamma_1 = \int_{-\infty}^{\infty} dx_1' \exp\Big[- \Big(\kappa_b - \frac{t_{ab}^2}{\kappa_a}\Big) x_1'^2 - 2t_u x_+' x_1' \Big] . \tag{B.16}$$

The above integral, γ_1 can easily be integrated since

$$\int_{-\infty}^{\infty} \exp\Big[- (ax^2 + 2bx) \Big] dx = \sqrt{\frac{\pi}{a}} \exp\Big(\frac{b^2}{a}\Big) \tag{B.17}$$

where ($a > 0$). Using the above standard integral, Eq. (B.16) can be calculated and this gives

$$\gamma_1 = \sqrt{\frac{\pi\kappa_a}{\kappa_a\kappa_b - t_{ab}^2}} \exp\Big[\frac{x_+'^2 t_u^2 \kappa_a}{\kappa_a\kappa_b - t_{ab}^2} \Big] . \tag{B.18}$$

Substitute Eq. (B.18) back into Eq. (B.15) and do some algebra manipulation. This gives

$$I_2 = \sqrt{\frac{\pi\kappa_a}{(\kappa_a\kappa_b - t_{ab}^2)}} \int_{-\infty}^{\infty} dx_+' \exp\Big[- (\xi - \frac{\kappa_a t_u^2}{(\kappa_a\kappa_b - t_{ab}^2)}) x_+'^2 \Big] . \tag{B.19}$$

Similarly, calculate I_3 by substituting Eq. (B.4) and Eq. (B.6) back into Eq. (B.10). Do some algebra manipulation and this gives

$$I_3 = \sqrt{\frac{\pi\kappa_a}{(\kappa_a\kappa_b - t_{ab}^2)}} I_2^* \tag{B.20}$$

where

$$I_2^* = \int_{-\infty}^{\infty}\int_{-\infty}^{\infty} dx_- dx_+ \exp\left[-\begin{pmatrix} x_- & x_+ \end{pmatrix}\begin{pmatrix} \xi - \frac{t_w^2}{\kappa_a} - \frac{t_w^2 t_{ab}^2}{\kappa_a(\kappa_a\kappa_b - t_{ab}^2)} & -\frac{t_w t_u t_{ab}}{(\kappa_b\kappa_a - t_{ab}^2)} \\ -\frac{t_w t_u t_{ab}}{(\kappa_b\kappa_a - t_{ab}^2)} & \xi - \frac{t_u^2\kappa_a}{(\kappa_a\kappa_b - t_{ab}^2)} \end{pmatrix}\begin{pmatrix} x_- \\ x_+ \end{pmatrix}\right]. \tag{B.21}$$

In calculating the integral I_3 in Eq. (B.20) make use of the standard integral in Eq. (B.17). Now collect all terms together and we have

$$\chi + r\chi^* = \Lambda\frac{\det\varphi}{\det\mu} \tag{B.22}$$

where $\varphi = \xi - \frac{\kappa_a t_u^2}{\kappa_a\kappa_b - t_{ab}^2}$ and $\mu = \begin{pmatrix} \xi - \frac{t_w^2}{\kappa_a} - \frac{t_w^2 t_{ab}^2}{\kappa_a(\kappa_a\kappa_b - t_{ab}^2)} & -\frac{t_w t_u t_{ab}}{(\kappa_b\kappa_a - t_{ab}^2)} \\ -\frac{t_w t_u t_{ab}}{(\kappa_b\kappa_a - t_{ab}^2)} & \xi - \frac{t_u^2\kappa_a}{(\kappa_a\kappa_b - t_{ab}^2)} \end{pmatrix}$ so

$$\chi + r\chi^* = \Lambda(\mathbf{M}_2^{-1})_{1,1} \tag{B.23}$$

where

$$\mathbf{M}_2 = \begin{pmatrix} \xi - \frac{t_w^2}{\kappa_a} - \frac{t_w^2 t_{ab}^2}{\kappa_a(\kappa_a\kappa_b - t_{ab}^2)} & -\frac{t_w t_u t_{ab}}{(\kappa_b\kappa_a - t_{ab}^2)} \\ -\frac{t_w t_u t_{ab}}{(\kappa_b\kappa_a - t_{ab}^2)} & \xi - \frac{t_u^2\kappa_a}{(\kappa_a\kappa_b - t_{ab}^2)} \end{pmatrix}. \tag{B.24}$$

Then

$$\mathbf{M}_2\begin{pmatrix} \chi + r\chi^* \\ t_T \end{pmatrix} = \begin{pmatrix} \xi - \frac{t_w^2}{\kappa_a} - \frac{t_w^2 t_{ab}^2}{\kappa_a(\kappa_a\kappa_b - t_{ab}^2)} & \frac{-t_w t_u t_{ab}}{(\kappa_a\kappa_b - t_{ab}^2)} \\ \frac{-t_w t_u t_{ab}}{(\kappa_a\kappa_b - t_{ab}^2)} & \xi - \frac{t_u^2\kappa_a}{(\kappa_a\kappa_b - t_{ab}^2)} \end{pmatrix}\begin{pmatrix} \chi + r\chi^* \\ t_T \end{pmatrix} = \begin{pmatrix} \Lambda \\ 0 \end{pmatrix}. \tag{B.25}$$

The above matrix equation can be solved by taking the inverse of $\mathbf{M}_2$. The decimation of the site $j = b$ has been accomplished. Using Eq. (B.25) and solving for t_T, the transmission probability as a function of energy, E, $\mathcal{T}(E)$ gives

$$\mathcal{T}(E) = \frac{t_w^2 t_u^2 t_{ab}^2 \Lambda^* \Lambda}{[(t_w^2 - \kappa_a \xi)(t_u^2 - \kappa_b \xi) - t_{ab}^2 \xi^2][(t_w^2 - \kappa_a \xi^*)(t_u^2 - \kappa_b \xi^*) - t_{ab}^2 \xi^* 2]}. \tag{B.26}$$

Fig. B.2 is a schematic representation of the decimation procedure. Here, one of the three

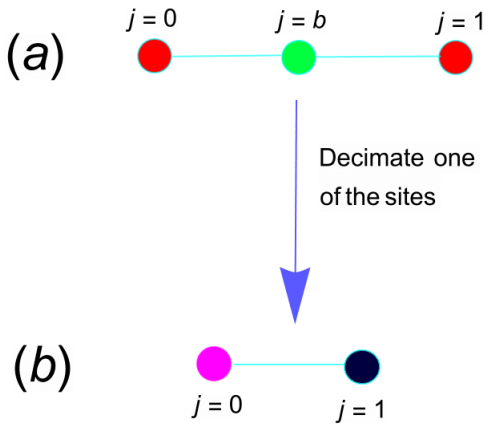

Figure B.2

Schematic representation of the decimation procedure for the atomic site labeled b.

sites is decimated and this gives two sites, both of which are lead sites.

This means that Eq. (B.26), Eq. (2.26), Eq. (2.49) and Eq. (2.59) are all the same. Thus both RG methods, the matrix method and the standard Green's function method all

give the same result for the transmission probability as a function of energy, E, $\mathcal{T}(E)$ for the 2 site device. Eq. (B.26) is one of the equations plotted in Fig. 2.6 and Fig. 2.7.